# REPORT DOCUMENTATION PAGE

Form Approved OMB NO. 0704-0188



| 1. REPORT DATE (DD-MM-YYYY) | 2. REPORT TYPE | 3. DATES COVERED (From - To) |
|---|---|---|
| 12-12-2013 | Final Report | 1-Jul-2007 - 30-Nov-2011 |

4. TITLE AND SUBTITLE
Ionic Liquids in Electro-active Devices (ILED)

5a. CONTRACT NUMBER
W911NF-07-1-0452

5b. GRANT NUMBER

5c. PROGRAM ELEMENT NUMBER
611103

6. AUTHORS
Timothy E. Long, Karen Winey, Brent C. Bowden

5d. PROJECT NUMBER

5e. TASK NUMBER

5f. WORK UNIT NUMBER

7. PERFORMING ORGANIZATION NAMES AND ADDRESSES
Virginia Polytechnic Institute & State Unive
North End Center, Suite 4200
300 Turner Street, NW
Blacksburg, VA 24061 -0001

8. PERFORMING ORGANIZATION REPORT NUMBER

9. SPONSORING/MONITORING AGENCY NAME(S) AND ADDRESS (ES)
U.S. Army Research Office
P.O. Box 12211
Research Triangle Park, NC 27709-2211

10. SPONSOR/MONITOR'S ACRONYM(S)
ARO

11. SPONSOR/MONITOR'S REPORT NUMBER(S)
52545-MS-MUR.165

12. DISTRIBUTION AVAILIBILITY STATEMENT
Approved for Public Release; Distribution Unlimited

13. SUPPLEMENTARY NOTES
The views, opinions and/or findings contained in this report are those of the author(s) and should not contrued as an official Department of the Army position, policy or decision, unless so designated by other documentation.

14. ABSTRACT
Multidisciplinary research focused on the systematic tuning of multiphase morphology on electro-active performance has served as the cornerstone of the fourth year ILEAD MURI program. This team-oriented focus provided collaborations among scientists and engineers with graduate student exchanges, real-time feedback, and multidisciplinary peer-reviewed publications. Synthetic chemists collaborated with morphologists to predict the design of novel electro-active materials. Unprecedented charged polymeric compositions have been prepared with attention to the correlation of charge density and chemical composition with morphological structure in both

15. SUBJECT TERMS
Ionic Liguids, Electromechanical Devices, Charged Polymers, Assembled Structures, Actuators, Electro-active Applications

| 16. SECURITY CLASSIFICATION OF: | | | 17. LIMITATION OF ABSTRACT | 15. NUMBER OF PAGES | 19a. NAME OF RESPONSIBLE PERSON |
|---|---|---|---|---|---|
| a. REPORT | b. ABSTRACT | c. THIS PAGE | | | Timothy Long |
| UU | UU | UU | UU | | 19b. TELEPHONE NUMBER 540-231-2480 |

## Report Title

Ionic Liquids in Electro-active Devices (ILED)

## ABSTRACT

Multidisciplinary research focused on the systematic tuning of multiphase morphology on electro-active performance has served as the cornerstone of the fourth year ILEAD MURI program. This team-oriented focus provided collaborations among scientists and engineers with graduate student exchanges, real-time feedback, and multidisciplinary peer-reviewed publications. Synthetic chemists collaborated with morphologists to predict the design of novel electro-active materials. Unprecedented charged polymeric compositions have been prepared with attention to the correlation of charge density and chemical composition with morphological structure in both solution and the solid state. Scattering studies revealed the importance of charge location on structure at the nanoscale and the correlation of structure with membrane performance. Novel families of electromechanical transducers were discovered with special attention to the design of assembled structures based on the tuning of electrostatic interactions; these novel transducers demonstrated unparalleled performance. Polymeric ionic liquids as mobile anion transducers were demonstrated for the first time. Characterization instrumentation for the electromechanical responses of conductive network/ionomer composites (CNIC) were developed. The overall research goal successfully developed a fundamental understanding of the design of charged polymers and interactions with ionic liquids. This program continues to discover new families of ionic liquid-based polymers and physical properties as a function of structure.

**Enter List of papers submitted or published that acknowledge ARO support from the start of the project to the date of this printing. List the papers, including journal references, in the following categories:**

**(a) Papers published in peer-reviewed journals (N/A for none)**

| Received | Paper |
|---|---|
| 01/24/2011 63.00 | M. Hunley, J. England, T. Long. Influence of Counteranion on the Thermal and Solution Behavior of Poly(2-(dimethylamino)ethyl methacrylate)-Based Polyelectrolytes, Macromolecules, (11 2010): . doi: |
| 02/02/2011 64.00 | R. Brown, M. Hunley, M. Allen, T. Long. Electrospinning zwitterion-containing nanoscale acrylic fibers, Polymer, (08 2009): . doi: |
| 02/03/2011 65.00 | M. Green, T. Long. Designing Imidazole-Based Ionic Liquids and Ionic Liquid Monomers for Emerging Technologies, Journal of Macromolecular Science, Polymer Review, (06 2009): . doi: |
| 02/03/2011 73.00 | S. Williams, D. Salas-de la Cruz, K. Winey, T. Long. Ionene segmented block copolymers containing imidazolium cations: Structure–property relationships as a function of hard segment content, Polymer, (06 2009): . doi: |
| 02/03/2011 72.00 | L. Gwee, J. Choi, K. Winey, Y. Elabd. Block copolymer/ionic liquid films: The effect of ionic liquid composition on morphology and ion conduction, Polymer, (09 2010): . doi: |
| 02/03/2011 71.00 | B. Dong, L. Gwee, D. Salas-de la Cruz, K. Winey, Y. Elabd. Super Proton Conductive High-Purity Nafion Nanofibers, Nano Letters, (08 2010): . doi: |
| 02/03/2011 70.00 | M. Lee, Z. Niu, D. Schoonover, C. Slebodnick, H. Gibson. 1,2-Bis[N-(N0-alkylimidazolium)]ethane salts as new guests for crown ethers and cryptands, Tetrahedron, (05 2010): . doi: |
| 02/03/2011 69.00 | M. Lee, Z. Niu, C. Slebodnick, H. Gibson. N,N-Alkylene Bis(N'-Alkylimidazolium) Salts, Journal of Physical Chemistry B, (03 2010): . doi: |
| 02/03/2011 68.00 | B. aitken, M. Lee, M. Hunley, H. Gibson, K. Wagener. Synthesis of Precision Ionic Polyolefins Derived from Ionic Liquids, Macromolecules, (01 2010): . doi: |
| 02/03/2011 67.00 | M. Lee, U. Choi, R. Colby, H. Gibson. Ion Conduction in Imidazolium Acrylate Ionic Liquids and their Polymers, Chemical Materials, (10 2010): . doi: |
| 02/03/2011 66.00 | M. Lee, U. Choi, D. Salas-de la Cruz, A. Mittal, K. Winey, R. Colby, H. Gibson. Imidazolium Polyesters: Structure-Property Relationships in Thermal Behavior, Ionic Conductivity, and Morphology , Advanced Functional Materials, (01 2010): . doi: |
| 02/06/2009 18.00 | A. Duncan, D. Leo, T. Long. Beyond Nafion: Charged Macromolecules Tailored for Performance as Ionic Polymer Transducers, Macromolecules, ( 2008): . doi: |

02/06/2009 20.00 J. Li, K. Wilmsmeyer, L. Madsen. Anisotropic Diffusion and Morphology in Perfluorosulfonate Ionomers Investigated by NMR,
Macromolecules, ( 2009): . doi:

02/06/2009 19.00 S. Williams, W. Wang, K. Winey, T. Long. Synthesis and Morphology of Segmented Poly (tetramethyleneoxide)-Based Polyurethanes Containing Phosphonium Salts,
Macromolecules, ( 2008): . doi:

03/09/2010 49.00 B. Aitken, M. Lee, M. Hunley, H. Gibson, K. Wagener. Synthesis of precision ionic polyolefins derived from ionic liquids,
Macromolecules, (03 2010): . doi:

03/09/2010 50.00 S. Liu, W. Liu, Y. Liu, J. Lin, X. Zhou, M. Janik, R. Colby, Q. Zhang. Influence of imidazolium-based ionic liquids on the performance of ionic polymer conductor network composite actuators,
Polymer International, (02 2010): . doi:

03/11/2009 22.00 S. Williams, Z. Barta, S. Ramirez, T. Long. Synthesis of 12,12-Ammonium Ionenes with Functionality for Chain Extension and Cross-Linking via UV Irradiation,
Macromolecular Chemistry and Physics, ( 2009): . doi:

04/14/2011 75.00 Y. Elabd, Y. Ye. Anion exchanged polymerized ionic liquids: High free volume single ion conductors,
Polymer, (01 2011): . doi:

04/14/2011 76.00 M. Green, M. Allen Jr., J. Dennis, D. Salas-de la Cruz, R. Gao, K. Winey, T. Long. Tailoring macromolecular architecture with imidazole functionality: A perspective for controlled polymerization processes,
European Polymer Journal, (10 2010): . doi:

05/17/2011 79.00 J. Hou, Z. Zhang, L. Madsen. Cation/Anion Associations in Ionic Liquids Modulated by Hydration and Ionic Medium,
Journal of Physical Chemistry B, (05 2011): . doi:

06/08/2010 57.00 Y. Liu, S. Liu, J. Lin, D. Wang, V. Jain, R. Montazami, J. Heflin, J. Li, L. Madsen, Q. Zhang. Ion transport and storage of ionic liquids in ionic polymer conductor
network composites,
Applied Physics Letters, (06 2010): . doi:

07/23/2008 2.00 J.M. Layman, E.M. Borgerding, S.R. Williams, W.H. Heath, T.E. Long. Synthesis and Characterization of Aliphatic Ammonium Ionenes: Aqueous Size Exclusion Chromatography for Absolute Molecular Weight Characterization,
Macromolecules, ( ): . doi:

07/28/2010 58.00 S. Liu, Y. Liu, H. Cebeci, R. de Villoria, J. Lin, B. Wardle, Q. Zhang. High electromechanical response of ionic polymer actuators with controlled-morphology aligned carbon nanotube/Nafion nanocomposite electrodes,
Advanced Functional Materials, (07 2010): . doi:

07/30/2009 27.00 J. Li, K. Wilmsmeyer, J. Hou, L. Madsen. The role of water in transport of ionic liquids in polymeric artificial muscle actuators,
Soft Matter, ( 2009): . doi:

08/09/2008 4.00 J. Li, K.G. Wilmsmeyer, L.A. Madsen. Hydrophilic Channel Alignment Modes in Perfluorosulfonate Ionomers: Implications for Proton Transport,
, ( ): . doi:

08/12/2009 28.00 S. Liu, R. Montazami, Y. Liu, V. Jain, M. Lin, J. Heflin, Q. M. Zhang. Layer-by-layer self-assembled conductor network composites in ionic polymer metal composite actuators with high strain response,
Applied Physics Letters, ( 2009): . doi:

08/12/2009 29.00 S. Williams, T. Long. Recent advances in the synthesis and structure–property relationships of ammonium ionenes,
Progress in Polymer Science, ( 2009): . doi:

08/27/2012 92.00 Matthew D. Green, Hiwote K. Getaneh, Michael H. Allen, Jr. , Timothy E. Long. Tailoring Charge Density and Hydrogen Bonding of Imidazolium Copolymers for Efficient Gene Delivery,
Biomacromolecules, (03 2011): 2243. doi:

08/27/2012 46.00 Michael H. Allen, Sean T. Hemp, Matthew D. Green, Timothy E. Long. Phosphonium-Containing Polyelectrolytes for Nonviral Gene Delivery,
Biomacromolecules, (01 2012): 231. doi: 10.1021/bm201503a

08/27/2012 44.00 Michael H. Allen, Sean T. Hemp, Adam E. Smith, Timothy E. Long. Controlled Radical Polymerization of 4-Vinylimidazole,
Macromolecules, (05 2012): 3669. doi: 10.1021/ma300543h

08/27/2012 43.00 Dong Wang, Sean T. Hemp, Jae-Hong Choi, Karen I. Winey, Matthew D. Green, James R. Heflin, Timothy E. Long. Synthesis of imidazolium ABA triblock copolymers for electromechanical transducers,
Polymer, (08 2012): 3677. doi: 10.1016/j.polymer.2012.06.023

08/27/2012 42.00 Matthew D. Green, Jae-Hong Choi, Karen I. Winey, Timothy E. Long. Synthesis of Imidazolium-Containing ABA Triblock Copolymers: Role of Charge Placement, Charge Density, and Ionic Liquid Incorporation,
Macromolecules, (06 2012): 4749. doi: 10.1021/ma300185b

08/27/2012 41.00 Jae-Hong Choi, Carl L. Willis, Karen I. Winey. Structure–property relationship in sulfonated pentablock copolymers,
Journal of Membrane Science, (03 2012): 169. doi: 10.1016/j.memsci.2011.12.036

08/27/2012 40.00 Q M Zhang, Gokhan Hatipoglu, Yang Liu, Ran Zhao, Mitra Yoonessi, Dean M Tigelaar, Srinivas Tadigadapa. A highly aromatic and sulfonated ionomer for high elastic modulus ionic polymer membrane micro-actuators,
Smart Materials and Structures, (05 2012): 0. doi: 10.1088/0964-1726/21/5/055015

08/27/2012 39.00 Jun-Hong Lin, Yang Liu, Q. M. Zhang. Influence of the Electrolyte Film Thickness on Charge Dynamics of Ionic Liquids in Ionic Electroactive Devices,
Macromolecules, (02 2012): 2050. doi: 10.1021/ma202165n

08/27/2012 38.00 Mehdi Ghaffari, Ran Zhao, Yang Liu, Jun-Hong Lin, Minren Lin, Q. M. Zhang. Enhanced Electromechanical Response of Ionic Polymer Actuators by Improving Mechanical Coupling between Ions and Polymer Matrix,
Macromolecules, (06 2012): 5128. doi: 10.1021/ma300591a

08/28/2012 49.00 Matthew D. Green, Yuesheng Ye, Yossef A. Elabd, Timothy E. Long, Karen I. Winey, David Salas-de la Cruz. Correlating backbone-to-backbone distance to ionic conductivity in amorphous polymerized ionic liquids,
Journal of Polymer Science Part B: Polymer Physics, (03 2012): 338. doi: 10.1002/polb.23019

08/28/2012 52.00 Reza Montazami, Dong Wang, James R. Heflin. Influence of conductive network composite structure on the electromechanical performance of ionic electroactive polymer actuators,
International Journal of Smart and Nano Materials, (01 2012): 0. doi: 10.1080/19475411.2011.650232

08/28/2012 51.00 Renlong Gao, Dong Wang, James R. Heflin, Timothy E. Long. Imidazolium sulfonate-containing pentablock copolymer–ionic liquid membranes for electroactive actuators,
Journal of Materials Chemistry, (07 2012): 13473. doi: 10.1039/c2jm16117f

08/29/2012 37.00 Q.M. Zhang, James R. Heflin, Yang Liu, Ran Zhao, Mehdi Ghaffari, Junhong Lin, Sheng Liu, Hülya Cebeci, Roberto Guzmán de Villoria, Reza Montazami, Dong Wang, Brian L. Wardle. Equivalent circuit modeling of ionomer and ionic polymer conductive network composite actuators containing ionic liquids,
Sensors and Actuators A: Physical, (07 2012): 70. doi: 10.1016/j.sna.2012.05.002

08/31/2012 14.00 Allen, Michael H., Jr., Green, Matthew D., Long, Timothy E. . Tailoring Charge Density and Hydrogen Bonding of Imidazolium Copolymers for Efficient Gene Delivery,
Biomacromolecules, (04 2011): 2243. doi:

08/31/2012 64.00 Sean T. Hemp, Timothy E. Long. DNA-Inspired Hierarchical Polymer Design: Electrostatics and Hydrogen Bonding in Concert,
Macromolecular Bioscience, (01 2012): 29. doi: 10.1002/mabi.201100355

08/31/2012 63.00 Jeremy N. Fowler, Tonomori Saito, Renlong Gao, Eric S. Fried, Timothy E. Long, David L. Green. Impact of Diblock Copolymers on Droplet Coalescence, Emulsification, and Aggregation in Immiscible Homopolymer Blends,
Langmuir, (02 2012): 2347. doi: 10.1021/la2037185

08/31/2012 62.00 C. Francisco Buitrago, Jason D. Heffley, Minjae Lee, Harry W. Gibson, Karen I. Winey, Brian S. Aitken, Kenneth B. Wagener. Precision Ionomers: Synthesis and Thermal/Mechanical Characterization,
Macromolecules, (01 2012): 681. doi: 10.1021/ma202304s

08/31/2012 61.00 Renlong Gao, Mingqiang Zhang, Ninad Dixit, Robert B. Moore, Timothy E. Long. Influence of ionic charge placement on performance of poly(ethylene glycol)-based sulfonated polyurethanes,
Polymer, (03 2012): 0. doi: 10.1016/j.polymer.2012.01.043

08/31/2012 60.00 Shijing Cheng, Mingqiang Zhang, Tianyu Wu, Sean T. Hemp, Brian D. Mather, Robert B. Moore, Timothy E. Long. Ionic aggregation in random copolymers containing phosphonium ionic liquid monomers,
Journal of Polymer Science Part A: Polymer Chemistry, (01 2012): 0. doi: 10.1002/pola.25022

08/31/2012 59.00 AKSHAY KOKIL, TOMONORI SAITO, WADE DEPOLO, CASEY L. ELKINS, GARTH L. WILKES, TIMOTHY E. LONG. Introduction of Multiple Hydrogen Bondingfor Enhanced Mechanical Performance of Polymer-CarbonNanotube Composites,
Journal of Macromolecular Science-Chemistry, (05 2011): 1016. doi:

08/31/2012 58.00 Wesley P. Hoffman, Dennis W. Smith Jr., Wenjin Deng, Alexander Lobovsky, Scott T. Iacono, Tianyu Wu, Neetu Tomar, Stephen M. Budy, Timothy Long. Poly (acrylonitrile – co -1-vinylimidazole): A new melt processable carbon fiber precursor,
Polymer, (02 2011): 0. doi: 10.1016/j.polymer.2010.11.054

08/31/2012 57.00 Gregory J. Tudryn, Ralph H. Colby, Wenqin Wang, Karen I. Winey. Thermally Driven Ionic Aggregation in Poly(ethylene oxide)-Based Sulfonate Ionomers,
Journal of the American Chemical Society, (07 2011): 0. doi: 10.1021/ja201405v

08/31/2012 56.00 Tianyu Wu, Frederick L. Beyer, Rebecca H. Brown, Robert B. Moore, Timothy E. Long. Influence of Zwitterions on Thermomechanical Properties and Morphology of Acrylic Copolymers: Implications for Electroactive Applications,
Macromolecules, (10 2011): 0. doi: 10.1021/ma201211j

10/09/2009 30.00 V. Jain, H. Yochum, R. Montazami, J. Heflin. Millisecond switching in solid state electrochromic polymer devices fabricated from ionic self-assembled multilayers,
Applied Physics Letters, (01 2008): . doi:

10/09/2009 31.00 H. Chen, J. Choi, D. Cruz, K. Winey, Y. Elabd. Polymerized ionic liquids: the effect of copolymer composition on ion conduction,
Macromolecules, (05 2009): . doi:

10/09/2009 35.00 H. Chen, Y. Elabd. Polymerized ionic liquids: solution properties and electrospinning,
Macromolecules, (04 2009): . doi:

10/09/2009 34.00 S. Williams, E. Borgerding, J. Layman, W. Wang, K. Winey, T. Long. Synthesis and characterization of well-defined 12,12-ammonium ionenes: evaluating mechanical properties as a function of molecular weight ,
Macromolecules, (06 2008): . doi:

10/15/2009 38.00 A. Duncan, B. Akle, T. Long, D. Leo. Ionomer design for augmented charge transport in novel ionic polymer transducers,
, (09 2009): . doi:

10/15/2009 37.00 M. Cashion, X. Li, Y. Geng, M. Hunley, T. Long. Gemini surfactant electrospun membranes,
, (10 2009): . doi:

| | | |
|---|---|---|
| 10/15/2009 | 39.00 | A. Duncan, J. Layman, M. Cashion, D. Leo, T. Long. Oligomeric A2 + B3 synthesis of highly branched polysulfone ionomers: novel candidates for ionic polymer transducers ,<br>, (01 2009): . doi: |
| 10/19/2009 | 41.00 | S. Ramiirez, J. Layman, P. Bissel, T. Long. Ring-Opening Polymerization of Imidazole Epoxides for the Synthesis of Imidazole-Substituted Poly(ethylene oxides),<br>, (10 2009): . doi: |
| 11/27/2009 | 47.00 | J. Hou, J. Li, L. Madsen. Anisotropy and Transport in Poly(arylene ether sulfone)Hydrophilic-Hydrophobic Block Copolymers,<br>Macromolecules, (11 2009): . doi: |
| 12/23/2010 | 62.00 | J. Lin, Y. Liu, Q. Zhang. Charge dynamics and bending actuation in Aquivion membrane swelled with ionic liquids,<br>Polymer, (12 2010): . doi: |
| **TOTAL:** | **60** | |

**Number of Papers published in peer-reviewed journals:**

## (b) Papers published in non-peer-reviewed journals (N/A for none)

| Received | | Paper |
|---|---|---|
| 04/03/2012 | 28.00 | M. Green, D. Salas-de la Cruz, Y. Ye, J. Layman, Y. Elabd, K. Winey, T. Long. Alkyl-Substituted N - Vinylimidazolium Polymerized Ionic Liquids: Thermal Properties and Ionic Conductivities, Macromolecular Chemistry and Physics, (10 2011): . doi: |
| 04/03/2012 | 27.00 | M. Green, C. Schreiner, T. Long. Thermal, Rheological, and Ion-Transport Properties of Phosphonium-Based Ionic Liquids, The Journal of Physical Chemistry A, (10 2011): . doi: |
| 04/04/2012 | 30.00 | b. Aitken, C. Buitrago, J. Heffley, M. Lee, H. Gibson, K. Winey, K. Wagener. Precision Ionomers: Synthesis and Thermal/MechanicalCharacterization, Macromolecules, (01 2012): . doi: |
| 04/04/2012 | 31.00 | J. Lin, Y. Liu, Q. Zhang. Charge dynamics and bending actuation in Aquivion membrane swelled with ionic liquids, Polymer, (11 2010): . doi: |
| 04/05/2012 | 32.00 | J. Lin, Y. Liu, Q. Zhang. Influence of the Electrolyte Film Thickness on Charge Dynamics of Ionic Liquids in Ionic Electroactive Devices, Macromolecules, (09 2011): . doi: |
| 07/19/2011 | 83.00 | J. Li, J. Park, R. Moore, L. Madsen. Linear coupling of alignment with transport in a polymer electrolyte membrane, Nature Materials, (06 2011): . doi: |
| 07/19/2011 | 84.00 | G. Tudryn, W. Liu, S. Wang, R. Colby. Counterion Dynamics in Polyester_Sulfonate Ionomers with Ionic Liquid Counterions, Macromolecules, (01 2011): . doi: |
| 08/27/2012 | 35.00 | and Sean Ramirez (editor), Harry Gibson, Timothy Long, Karen Winey, Ralph Colby, Yossef Elabd, Nakhiah Goulbourne, Louis Madsen, Garth Wilkes, Randy Heflin, Qiming Zhang. Ionic Conduction and Dielectric Response of Poly(imidazolium acrylate) Ionomers , Macromolecules, (04 2012): 3974. doi: |
| 08/27/2012 | 89.00 | Ye, Y., Elabd, Y.A. . Relative Chemical Stability of Alkaline Exchange Polymerized Ionic Liquids, Macromolecules, (08 2011): 0. doi: |
| **TOTAL:** | | **9** |

**Number of Papers published in non peer-reviewed journals:**

---

## (c) Presentations

1. D. Wang, R. Montazami, J.R. Heflin; "The Effect of Ionic Liquid Uptake and Self-Assembled Conductive Network Composite Layers on Nafion-Based Ionic Polymer Metal Composite Electromechanical Bending Actuators," 2013 Materials Research Society Spring Meeting (San Francisco, CA, 4 April, 2013).

2. Winey, K.I.; Materials Science and Engineering, University of Michigan (March, 2013) Ann Arbor, MI "Recent Progress in the Morphology of Precise Copolymers, Ionic Conductivity in Ionomers, and Electrical Conductivity in Polymer Nanocomposites"

3. Wang, S.; Ye, Y.; Elabd, Y.A.; Winey, K.I. Morphologies and Ionic Conductivity in Polymerized Ionic Liquid Block Copolymers. Materials Research Society Meeting, San Francisco, CA, April 2013.

4. Elabd, Y.A. Fuel Cell Membranes. Short course on Membranes for Clean Water and Energy. American Physical Society Meeting, Baltimore, MD, March 2013. Invited Speaker

5. Beyer, F.L.; Price, S.; Jackson, A.; Ren, X.; Chu, D.; Ye, Y.; Elabd, Y.A. Anion Exchange Membranes Based on Reactive Block Copolymers. American Physical Society Meeting, Baltimore, MD, March 2013.

6. Wang, S.; Ye, Y.; Elabd, Y.A.; Winey, K.I. Ordered and Disordered Polymerized Ionic Liquid Block Copolymers: Morphology and Ion Conductivity. American Physical Society Meeting, Baltimore, MD, March 2013.

7. Choi, J.-H.; Ye, Y.; Elabd, Y.A.; Winey, K.I. Effect of Morphology on Ion Transport in Polymerized Ionic Liquid Block Copolymers. American Physical Society Meeting, Baltimore, MD, March 2013.

8. Elabd, Y.A. Block Copolymers in Fuel Cells. Advanced in Materials for Proton Exchange Membrane Fuel Cells Systems Meeting, sponsored by The Division of Polymer Chemistry (POLY) of the American Chemical Society, Asilomar, CA, February 2013. Invited Speaker

9. Ye, Y.; Choi, J.; Wang, S.; Winey, K.I.; Elabd, Y.A. Hydroxide Conducting Polymerized Ionic Liquid Block Copolymers for Alkaline Fuel Cells. Annual Meeting of the American Institute of Chemical Engineers, Pittsburgh, PA October 2012. Invited Speaker

10. Ionically Conductive Polymers Incorporating Imidazolium Moieties, H. W. Gibson, M. Lee, A. Mittal, D. V. Schoonover, T. L. Price, Jr., A. Murugan, U-H. Choi, D. Salas-de la Cruz, R. H. Colby and K. I. Winey, XXI International Materials Research Congress, Cancun, Mexico, August 12-17, 2012. (Invited)

11. Design, Synthesis and Evaluation of Ion Conducting Imidazolium Polymers for Use as Actuators, H. W. Gibson, M. Lee, A. Mittal, T. L. Price, Jr., A. Murugan, D. V. Schoonover, U-H. Choi, R. H. Colby, D. Salas de la Cruz, K. I. Winey, Materials Engineering and Science Department, Penn State University, University Park, PA, March 12, 2013. (Invited)

12. Transport Dynamics in a Bis-Imidazolium-Based Organic Ionic Plastic Crystal, B. E. Kidd, M. D. Lingwood, M. Lee, H. W. Gibson, L. A. Madsen, 245th National Meeting of the American Chemical Society, New Orleans, LA, April 9, 2013.

13. Design and Synthesis of ROMP Imidazolium Polymers for Use as Actuators, T. L. Price, Jr.; U H. Choi, D. Wang, A. Murugan, D. V. Schoonover, M. Zhang, R. H. Colby, J. R. Heflin, R. B. Moore, H. W. Gibson, 245th National Meeting of the American Chemical Society, New Orleans, LA, April 11, 2013.

14. Design and Synthesis of ROMP Imidazolium Polymers for Use as Actuators, T. L. Price, Jr.; U H. Choi, D. Wang, A. Murugan, D. V. Schoonover, M. Zhang, R. H. Colby, J. R. Heflin, R. B. Moore, H. W. Gibson, Virginia Academy of Sciences 91st Annual Meeting, Virginia Tech, Blacksburg, VA, May 23, 2013.

15. Long, T. E. Gordon Research Conference, Adhesives, Charged Polymers as Interfacial Adhesives, July 2013.

16. Long, T.E. ACS Polymer Division Workshop, Polycondensation 2012, Engineering Thermoplastics Containing Charged Units, September 2012.

17. Long, T.E. BASF Research Seminar (invited), Germany, New Directions in Polymer Synthesis: Strategies and Structure, September 2012.

18. Long, T.E. SABIC Corporation (invited), Charged Polymers Enabling New Technologies, October 2012.

19. Long, T.E. LORD Corporation (invited), Block Copolymer Design, April 2013.

**Number of Presentations:** 19.00

## Non Peer-Reviewed Conference Proceeding publications (other than abstracts):

| Received | Paper |
|---|---|
| 08/28/2012 53.00 | Taylor T. Young, Stephen A. Sarles, Tianyu Wu, Matthew Green, Timothy E. Long, Donald J. Leo . Study of the effects of ionic liquids on lipid bilayers, SPIE . 11-MAR-12, . : , |
| **TOTAL:** | **1** |

**Number of Non Peer-Reviewed Conference Proceeding publications (other than abstracts):**

## Peer-Reviewed Conference Proceeding publications (other than abstracts):

| Received | Paper |
|---|---|
| 08/27/2012 48.00 | Ye, Y., Elabd, Y.A. Chemical Stability of Anion Exchange Membranes for Alkaline Fuel Cells, American Chemical Society. 27-MAR-12, . : , |
| **TOTAL:** | **1** |

**Number of Peer-Reviewed Conference Proceeding publications (other than abstracts):**

## (d) Manuscripts

| Received | Paper |
|---|---|
| 02/03/2011 74.00 | J. Hou, Z. Zhang, L. Madsen. Cation/Anion Associations in Ionic Liquids Modulated by Hydration and Ionic Medium,<br>Polymer (02 2011) |
| 02/06/2009 21.00 | J. Davidson, N. Goulbourne. A MODIFIED MICROMECHANICAL MODEL OF IONIC POLYMER-METAL COMPOSITE ACTUATION,<br>( ) |
| 03/09/2010 51.00 | M. Lee, Z. Niu, D. Schoonover, C. Slebodnick, H. Gibson. 1,2-Bis[N-(N'-alkylimidazolium)]ethane Salts as New Guests for Crown Ethers and Cryptands,<br>(03 2010) |
| 03/09/2010 48.00 | B. Aitken, M. Lee, M. Hunley, H. Gibson, K. Wagener. SYNTHESIS OF PRECISION IONIC POLYOLEFINS DERIVED FROM IONIC LIQUIDS,<br>(03 2010) |
| 03/09/2010 52.00 | Y. Liu, S. Liu, J. Lin, D. Wang, V. Jain, R. Montazami, J. Heflin, J. Li, L. Madsen, Q. Zhang. Ion Transport and Storage of Ionic Liquids In<br>Ionic Polymer Conductor Network Composite Actuators,<br>(03 2010) |
| 03/11/2009 25.00 | A. Duncan, J. Layman, M. Cashion, D. Leo, T. Long. Oligomeric A2 + B3 synthesis of highly branched polysulfone ionomers: novel candidates for ionic polymer transducers,<br>( ) |
| 03/18/2009 26.00 | J. Li, K. Wilmsmeyer, J. Hou, L. Madsen. The Role of Water in Transport of Ionic Liquids in Polymeric Artificial Muscle Actuators,<br>( ) |
| 04/04/2012 29.00 | M. Green, D. Wang, S. Hemp, J. Randy Heflin, T. Long. Imidazolium ABA Triblock Copolymers as Electroactive Devices,<br>( ) |
| 04/05/2012 33.00 | M. Green, K. Winey, T. Long. Synthesis of Imidazolium-Containing ABA Triblock Copolymers: Role of Charge Placement, Charge Density, and Ionic Liquid Incorporation,<br>( ) |
| 04/14/2011 77.00 | J. Lin, Y. Liu, Q. Zhang. Influence of the Ionic Polymer Membrane Thickness on Charge dynamics of Ionic Liquids in Ionic Polymer Actuators<br>,<br>(04 2011) |
| 05/17/2011 78.00 | J. Li, J. Park, L. Madsen, R. Moore. Linear coupling of alignment with transport in a polymer electrolyte membrane,<br>(05 2011) |
| 05/17/2011 80.00 | R. Montazami, S. Liu, Y. Liu, D. Wang, Q. Zhang, J. Heflin. THICKNESS DEPENDENCE OF CURVATURE, STRAIN, AND<br>RESPONSE TIME IN IONIC ELECTROACTIVE POLYMER<br>ACTUATORS FABRICATED VIA LAYER-BY-LAYER ASSEMBLY,<br>(05 2011) |

06/08/2010 56.00 M. lee, U. Choi, R. Colby, H. Gibson. Ion Conduction in Imidazolium Acrylate Ionic Liquids and their Polymers,
(06 2010)

07/19/2011 82.00 S. Cheng, F. Beyer, B. Mather, R. Moore, T. Long. Phosphonium-Containing ABA Triblock Copolymers: Controlled Free Radical Polymerization of Phosphonium Ionic Liquids,
(07 2011)

07/19/2011 81.00 M. Green, C. Schreiner, T. Long. Thermal, Rheological, and Ion-Transport Properties of Phosphonium-Based Ionic Liquids,
(07 2011)

07/23/2008 1.00 S.R. Williams, E.M. Borgerding, J.M. Layman, W. Wang, K.I. Winey, T.E. Long. Synthesis and Characterization of Well Defined 12,12-Ammonium Ionenes: Evaluating Mechanical Properties as a Function of Molecular Weight,
Macromolecules ( )

07/28/2010 59.00 M. Green, M. Allen, J. Dennis, D. Salas-de la Cruz, K. Winey, T. Long. Tailoring macromolecular architecture with imidazole functionality: a perspective for controlled polymerization processes,
(07 2010)

08/02/2010 60.00 J. Hou, Z. Zhang, L. Madsen. Cation/Anion Associations in Ionic Liquids,
(08 2010)

08/09/2008 3.00 S.R. Williams, E.M. Borgerding, J.M. Layman, W. Wang, K.I. Winey, T.E. Long. Ionic Liquid Polymers: Electrospinning and Solution Properties,
( )

08/09/2008 5.00 H.Chen, J-H. Choi, D.S. Cruz, K.I. Winey, Y.A. Elabd. Ionic Liquid Polymers: The Effect of Copolymer Composition on Structure and Ion Conduction,
( )

08/09/2008 6.00 A.J. Duncan, S. A. Sarles, D. Griffiths, D.J. Leo, others, see report. Influence of Topology and Morphology in Sulfonated Polysulfone Transducers,
( )

08/09/2008 7.00 A.J. Duncan, D.J. Leo, B.J. Akle, S.A. Sarles, T.E. Long. Ionomer Design for Augmented Charge Transport in Novel Ionic Polymer Transducers,
( )

08/09/2008 8.00 A.J. Duncan, D.J. Leo, T.E. Long, J.F. Snyder. Synthesis of Long Chain Branched Polysulfones for Multifunctional Transport Membranes,
( )

08/09/2008 9.00 A.J. Duncan, D.J. Leo, T.E. Long. Beyond Nafion: Charged Macromolecules Tailored for Performance as Ionic Polymer Transducers,
( )

08/09/2008 10.00 Wenqin Wang, T.E. Long, S.R. Williams, R.H. Colby, K.I. Winey. Nanoscale Superstructures in Copolymers with Evenly Spaced Charged Groups,
( )

08/09/2008 11.00 W. Wang, S.R. williams, T.E. Long, K.I. Winey. TopCon: New Approaches in Polymer Characterization: Nanocomposites, Block Copolymers, and Other Nanostructured Materials ,
( )

08/09/2008 12.00 R. Montazami, V. Jain, S. Liu, J.R. Heflin, Qiming Zhang. Ionic Self-Assembled Multilayers in Electroactive-Polymer Actuators,
( )

08/09/2008 13.00 R. Montazami, V. Jain, J.R. Heflin. High Contrast and Fast Switching Polymer Electrochromic Devices Fabricated From Ionic Self-Assembled Multilayers,
( )

08/09/2008 14.00 S.R. Williams, E.M. Borgerding, J.M. Layman, T.E. Long. Synthesis and Mechanical Property Characterization of Novel Ionenes for Biomedical Applications,
( )

08/09/2008 15.00 K.G. Wilmsmeyer, L.A. Madsen. Hydrophilic Channel Alignment in Ionomers Measured by 2H NMR,
( )

08/09/2008 16.00 K.G. Wilmsmeyer, L.A. Madsen. Shear and Field Alignment of Cetyl Trimethylammonium Bromide (CTAB) Wormlike Micelles Observed Using Rheo-NMR,
( )

08/09/2008 17.00 A.J. Duncan, S.A. Sarles, D.J. Leo, T.E. Long, B.J. Akle, M.D. Bennett. Optimization of Active Electrodes for Novel Ionomer Based Ionic Polymer Transducers,
( )

08/27/2012 36.00 Yang Liua, Caiyan Lub, Stephen Twiggc, Mehdi Ghaffarid, Junhong Lind, Nicholas Winogradb, Q. M. Zhang. Direct Observation of Ion Distributions near Electrodes in Ionic Polymer Actuators Containing Ionic Liquids,
Scientific Reports (06 2012)

08/27/2012 47.00 Yuesheng Ye, Jae-Hong Choi, Karen I. Winey, Yossef A. Elabd. Polymerized Ionic Liquid Block and Random Copolymers: Effect of Weak Microphase Separation on Ion Transport,
Macromolecules (05 2012)

08/27/2012 45.00 Sean T. Hemp, Adam E. Smith, Joshua M. Bryson, Michael H. Allen, Jr., Timothy E. Long. Phosphonium-Containing Diblock Copolymers for Enhanced Colloidal Stability and Efficient Nucleic Acid Delivery,
Biomacromolecules (05 2012)

08/31/2012 55.00 Jianbo Hou, Louis A. Madsen. New Insights into High Gradient Calibration using Low and High Gamma Nuclei,
Journal of Magnetic Resonance (06 2012)

10/09/2009 32.00 J. Hou, J. Li, L. Madsen. Anisotropy and transport in poly(arylene ether sulfone) hydrophilic-hydrophobic block copolymers,
(10 2009)

10/09/2009 33.00 S. Ramirez, J. Layman, P. Bissel, T. Long. Ring-Opening Polymerization of Imidazole Epoxides for the Synthesis of Imidazole-Substituted Poly(ethylene oxides),
(10 2009)

10/15/2009 40.00 S. Williams, D. Cruz, K. Winey, T. Long. Ionene segmented block copolymers containing imidazolium cations: structure-property relationships as a function of hard segment content,
(10 2009)

10/19/2009 42.00 S. Liu, Y. Liu, H. Cebeci, R. Guzman, J.Lin, B. Wardle, Q. Zhang. Electroactive polymer actuators based on ultra-high volume fraction vertically aligned carbon nanotube/Nafion nanocomposites,
(10 2009)

10/19/2009 44.00 S. Liu, W. Liu, Y. Liu, J. Lin, X. Zhou, M. Janiik, R. Colby, Q. Zhang. Influence of Imidazolium-based Ionic liquids on the Performance of Ionic Polymer Conductor Network Composite Actuators,
(10 2009)

10/19/2009 43.00 S. Liu, Y. Liu, M. Lin, X. Zhou, Q. Zhang, R. Montazami, V. Jain, J. Heflin. Influence of the conductor network composites on the electromechanical performance of ionic polymer conductor network composite actuators ,
(10 2009)

10/26/2009 45.00 S. Das, J. Goff, S. Williams, D. Salas-de la Cruz, J. riffle, T. Long, K. Winey, G. Wilkes. SYNTHESIS AND CHARACTERIZATION OF NOVEL SEGMENTED POLYIONENES BASED ON POLYDIMETHYLSILOXANE SOFT SEGMENTS ,
(10 2009)

| | | |
|---|---|---|
| 11/10/2009 | 46.00 | M. Green, T. Long. Designing imidazole-based ionic liquids and ionic liquid monomers for emerging technologies,<br>Journal of Macromolecular Science, Polymer Review (10 2009) |
| 12/23/2010 | 61.00 | S. Wang, W. Liu, R. Colby. Counterion Dynamics in Polyurethane-Carboxylate Ionomers with Ionic Liquid Counterions,<br>(12 2010) |

**TOTAL:** **45**

**Number of Manuscripts:**

## Books

| Received | Paper |
|---|---|

**TOTAL:**

## Patents Submitted

Elabd, Y.A.; Winey, K.I.; Ye, Yuesheng, Choi, J.-H. Sherick, T.-S. S. Polymerized Ionic Liquid Block Copolymers As Battery, U.S. Patent Application, filed September 12, 2013, Appl. No.: 14/024,734

## Patents Awarded

## Awards

Faculty Awards:

Timothy Long, VA Tech:
1. Regional Chair, IUPAC World Polymer Congress, MACRO 2012 at Virginia Tech, June 2012
2. Inducted into the ACS Polymer Division Fellows program in 2012
3. ACS PMSE Cooperative Research Award (shared w/ Kraton Polymers)
4. ACS Division of Polymer Chemistry, 2011 Mark Scholar Award
5. Pressure Sensitive Tape Council (PSTC) 2011 Carl Dahlquist Award

Karen Winey, UPenn:
1. Towerbrook Foundation Faculty Fellow, started in Nov. 2013 (endowed position)
2. Fellow, Materials Research Society, 2013
3. George H. Heilmeier Faculty Award for Excellence in Research, 2012
4. National Science Foundation, 2009-2011 Special Creativity Award
5. Chair, 2010 Polymer Physics Gordon Research Conference
6. Chair Elect, Vice Chair, Chair, Division of Polymer Physics, American Physical Society, 2011-2014

## Graduate Students

| NAME | PERCENT_SUPPORTED | Discipline |
|---|---|---|
| Michael Allen | 1.00 | |
| Matthew Green | 1.00 | |
| Klye Wilmsmyer | 1.00 | |
| Collin Smith | 1.00 | |
| Reza Montazema | 1.00 | |
| Yang Liu | 1.00 | |
| Gregory Tudryn | 1.00 | |
| David Salas-de la Cruz | 1.00 | |
| Dong Wang | 1.00 | |
| Yuesheng Ye | 1.00 | |
| Jae Hong Choi | 1.00 | |
| U Hyeok Choi | 1.00 | |
| Zhiyang Zhang | 1.00 | |
| Jun-Hong Lin | 1.00 | |
| Shin-Wa Wang | 1.00 | |
| Jing Han Wang | 1.00 | |
| Matthew Hunley | 0.50 | |
| **FTE Equivalent:** | **16.50** | |
| **Total Number:** | **17** | |

## Names of Post Doctorates

| NAME | PERCENT_SUPPORTED |
|---|---|
| Philippe Bissel | 0.50 |
| Anjul Mittal | 0.75 |
| Hong Chen | 1.00 |
| Yuesheng Ye | 1.00 |
| **FTE Equivalent:** | **3.25** |
| **Total Number:** | **4** |

## Names of Faculty Supported

| NAME | PERCENT_SUPPORTED | National Academy Member |
|---|---|---|
| Timothy Long | 0.08 | |
| Karen Winey | 0.06 | |
| Ralph Colby | 0.08 | |
| Yossef Elabd | 0.08 | |
| Qiming Zhang | 0.05 | |
| Randy Heflin | 0.08 | |
| Harry Gibson | 0.06 | |
| Louis Madsen | 0.00 | |
| **FTE Equivalent:** | **0.49** | |
| **Total Number:** | **8** | |

## Names of Under Graduate students supported

| NAME | PERCENT_SUPPORTED |
|---|---|
| **FTE Equivalent:** | |
| **Total Number:** | |

## Student Metrics

This section only applies to graduating undergraduates supported by this agreement in this reporting period

The number of undergraduates funded by this agreement who graduated during this period: ..... 0.00

The number of undergraduates funded by this agreement who graduated during this period with a degree in science, mathematics, engineering, or technology fields:..... 0.00

The number of undergraduates funded by your agreement who graduated during this period and will continue to pursue a graduate or Ph.D. degree in science, mathematics, engineering, or technology fields:..... 0.00

Number of graduating undergraduates who achieved a 3.5 GPA to 4.0 (4.0 max scale):..... 0.00

Number of graduating undergraduates funded by a DoD funded Center of Excellence grant for Education, Research and Engineering:..... 0.00

The number of undergraduates funded by your agreement who graduated during this period and intend to work for the Department of Defense ..... 0.00

The number of undergraduates funded by your agreement who graduated during this period and will receive scholarships or fellowships for further studies in science, mathematics, engineering or technology fields: ..... 0.00

## Names of Personnel receiving masters degrees

| NAME | |
|---|---|
| Jing-Han Wang | |
| Reuben Bushnell | |
| **Total Number:** | **2** |

## Names of personnel receiving PHDs

| NAME | |
|---|---|
| Shin-Wa Wang | |
| Jing Han Wang | |
| David Salas-de la Cruz | |
| Reza Montazami | |
| Matthew Hunley | |
| Junhong Lin | |
| Jae Hong Choi | |
| Matthew Green | |
| Yang Liu | |
| Michael Allen | |
| **Total Number:** | **10** |

## Names of other research staff

| NAME | PERCENT_SUPPORTED |
|---|---|
| Victoria K Long | 0.06 |
| **FTE Equivalent:** | **0.06** |
| **Total Number:** | **1** |

## Sub Contractors (DD882)

## Inventions (DD882)

## Scientific Progress

See Attachment

# Technology Transfer

**Ionic Liquids for Electro-Active Devices (ILEAD)**

**TABLE OF CONTENTS**

## SCIENTIFIC PROGRESS AND ACCOMPLISHMENTS

The ILEAD MURI research program involves an integrated and interdisciplinary strategy for the discovery of both low molar mass ionic liquid (IL) solvents and high molar mass polymers containing novel charged monomers based on IL building blocks. Our overarching scientific objective is the fundamental correlation of macromolecular chemistry and architecture with fundamental physical properties and device performance. Areas of potential Army impact range broadly from electromechanical transducers and electrochromic devices to selective membranes for chemical and biological protection as well as fuel cells. **Specific technical accomplishments are listed below for the three Materials Platforms.**

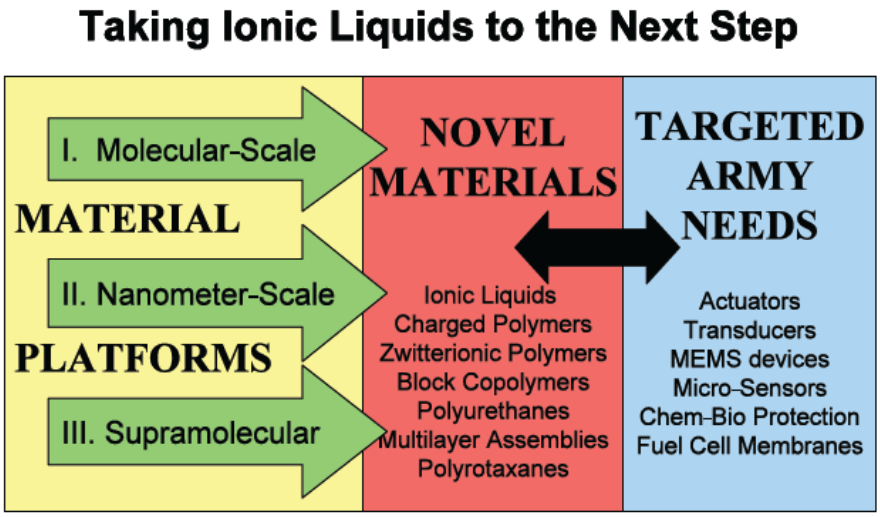


### Materials Platform I Highlights: Molecular-Scale Design

- ABA triblock copolymers are reported for the first time where a co-continuous morphology permits optimization of mechanical performance utilizing a reinforcing outer block with a low glass transition temperature-conducting central block.
- Controlled radical polymerization strategies with ionic liquid monomers enabled a new class of ductile polymeric membranes with ionic liquid localization at the nanoscale with precise, tunable placement within the center of the multiblock copolymer.
- Characterization of membrane and actuator performance and correlation to molecular structure and dynamics.
- Investigate and quantify the chemical stability of an imidazolium-based alkaline anion exchange polymerized ionic liquid (PIL), poly(1-[(2- methacryloyloxy)ethyl]-3-butylimidazolium hydroxide) (poly(MEBIm-OH), over a broad range of humidities, temperatures, and alkaline concentrations using the combined techniques of electrochemical impedance spectroscopy and nuclear magnetic resonance spectroscopy.
- Observe high chemical stability under dry conditions (10% RH) at 30 °C, humid and saturated conditions up to 80 °C, and even in mild alkaline conditions ([KOH] < 1 M) at 25 °C. Degradation occurred only under more vigorous conditions: dry conditions (10% RH) at 80 °C or at higher alkaline concentrations ([KOH] > 1 M).

- Discovery of metathesis strategies to prepare novel ion-conducting block copolymers.
- Recent efforts utilize Ring Opening Metathesis Polymerization (ROMP) to prepare triblock copolymers as microphase separated systems for ion conductive membranes as actuator components. The efforts build on the success of previous work in designing and studying polyacrylates and polymethacrylates with pendant imidazolium moieties as ion conductors; this work generated polymers with low glass transition temperatures and high room temperature ionic conductivities

**Materials Platform II Highlights: Nanometer-Scale Design**

- Fundamental studies have provided important and new insights into the design of polymeric materials for higher conductivity.
- Morphology and ion conductivity have been studied in a comprehensive series of model poly(vinyl imidazolium) homopolymers as a function of alkyl chain length (n = 2, 4, 8, 12) and anion type (M- = Br-, BF4-, TfO-,Tf2N-). All these polymers show modest levels of interdigitation (10 – 40. The conductivity nearly collapses into a common response (conductivity vs. T/Tg).
- A novel class of imidazolium-based homopolymers (poly(MEBIm) place the imidizolium group further from the backbone. These next generation polymeric materials produce a nearly fully interdigitated morphology (~ 100% interdigitation) and the ion conductivity normalized is higher by a factor of 10.
- Synthesis and characterization of block and segmented copolymers containing charged monomeric units and modified with IL solvents that have structures at the 1-50 nm scale.
- Identification of structure-property relationships for actuation performance, ensuring rapid ionic transport, high water and proton conductivity, high selectivity, and a high concentration of mobile ions.
- Ion-containing segmented block polyurethanes as templates for Nanoscale ordering of ionic liquids.

**Materials Platform III Highlights: Supramolecular Design**

- Direct characterization for the first time of the excess charge profile at ionomer membrane/metal electrode interfaces using unique SIMS instrumentation. This is unprecedented for fundamental understanding of ion transport and storage in ionic electro-active polymers.
- The direct measured charge profile confirms the large capacitance measured from time domain I-V curves, suggesting that the image forces at the metal electrodes can significantly enhance the charge storage.
- Established direct experimental evidence showing that one main reason for the slow response in the electroactive polymer devices is due to the slow diffusion current. By reducing the contribution of this slow diffusion current using the approaches such as porous electrodes with nano-pore size, the response time was improved.
- The formation of multilayered, supramolecular structures using electrostatic interactions in self-assembly for the formation of novel electrochromic devices.

- To increase efficiency, preparation of ROMP monomers with the same or similar pendant group structures to provide novel shelf-stable, room temperature storable monomers. These will comprise the center blocks of triblock copolymers subsequently built up through both ROMP and free radical protocols.

These Materials Platforms enable the ILEAD MURI team to design, build, and evaluate innovative electro-active systems with improved device performance. Furthermore, this multidisciplinary team will enable electro-active polymer devices for future Army technologies by developing processing and fabrication means that are cost-effective and exploit the inherent advantages of the proposed novel ILs and unique charged polymers. The following recent student monthly reports highlight research activities. **A complete collection of all student reports can be found in the ILEAD MURI scholar website (https://scholar.vt.edu/portal).**

## I. THRUST 1: Macromolecular-Scale Design (Leader: Prof. T.E. Long)

Supporting faculty: Karen Winey, Yossef Elabd, and Harry Gibson

### 1. Synthesis of novel imidazolium monomers and polymers and incorporation of 4-vinylimidazole into triblock copolymers for electroactive materials (M. Allen and T. Long)

As the MURI project has developed, we found that lower $T_g$ polymers are more effective for ion conduction applications. This discovery led to the synthesis of either a low $T_g$ homopolymer or the incorporation of a low $T_g$ comonomer into various copolymers. The large drawback of a low $T_g$ system is the lack of mechanical strength necessary for an electroactive material; therefore, the recent goal of this project is to synthesize ABA triblock copolymers to incorporate polystyrene A-blocks or other monomers to increase mechanical strength. The B-block will consist of a low $T_g$ conductive phase. The monomer previously targeted was 3-ethyl-1-vinylimidazolium bromide because of its facile synthesis. It was found the radical instability of 1-vinylimidazole or 1-vinylimidazolium monomers will undergo chain transfer with the diethylene glycol sidechain resulting in crosslinking. This suggested copolymerizations or controlled radical polymerizations with 1-vinylimidazole would exhibit difficult obstacles to overcome; therefore, studies with a more radically stable isomer were performed. Due to the radical stability of 4-vinylimidazole (**Figure 1**), it was believed that 4-vinylimidazole exhibited the potential to undergo polymerization using controlled radical techniques. The discovery opened the possibility for controlled radical polymerization of 4-vinylimidazole due to its improved radical stability compared to 1-vinylimidazole. This is advantageous as it would allow the imidazole ring to be adjacent to the polymer backbone, as well as provide hydrogen bonding sites throughout the polymer. Previously, 1-vinylimidazole failed to polymerize utilizing nitroxide-mediated polymerization (NMP) due to the radical instability of the propagating radical. As shown in **Figure 2**, 4-vinylimidazole was polymerized using NMP in DMSO. The kinetics of the reaction were monitored and after six hours of reaction time conversion remained less than 20%. Molecular weight determined using size exclusion chromatography

demonstrated an increase in molecular weight as the reaction progressed, suggesting control of the reaction is occurring using this method.

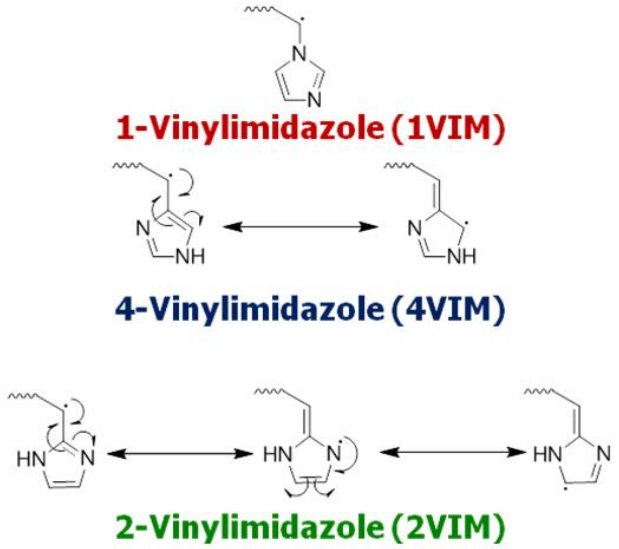


**Figure 1.** Resonance structures of the propagating radical for various vinylimidazole regioisomers.

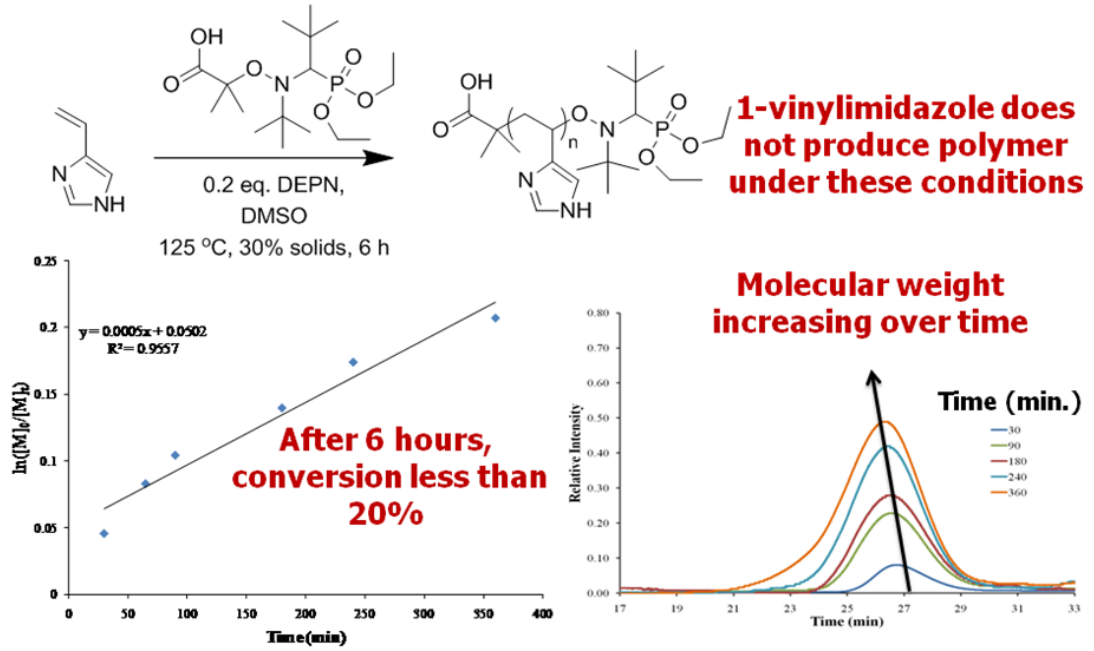


**Figure 2.** Controlled radical polymerization of 4-vinylimidazole monitoring reaction kinetics and molecular weight during the course of the polymerization. Over the same period of time 1-vinylimidazole did not polymerize.

However, upon further analyzing the data in **Figure 3**, molecular weight versus conversion failed to match theoretical calculations. In fact, the polydispersities reported remain broad and more typical of a conventional polymerization. This lead to the investigation of a chain transfer study shown in **Figure 4**.

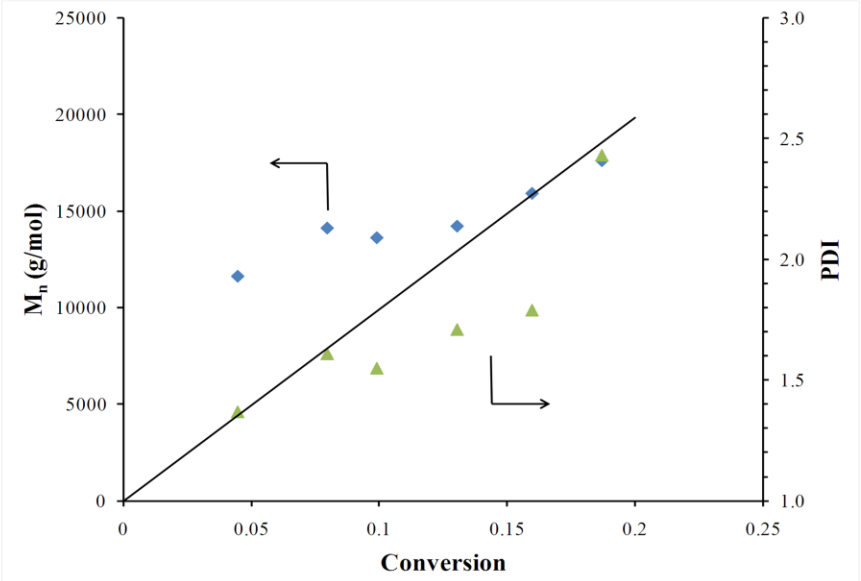


**Figure 3.** Molecular weight and PDI versus conversion of a controlled radical polymerization of 4-vinylimidazole

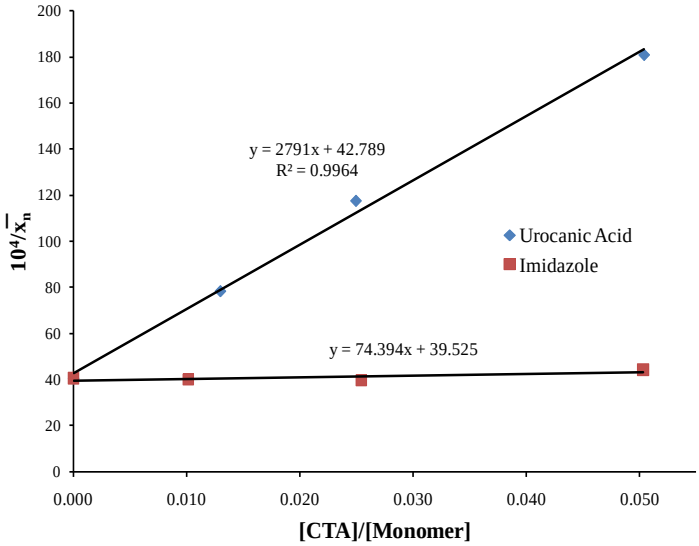


**Figure 4.** Chain transfer study using urocanic acid and imidazole in a 1-vinylimidazole homopolymerization.

Figure 4 shows a chain transfer study using both urocanic acid and imidazole in a 1-vinylimidazole polymerization. This study was preformed to better understand the lack of control in the 4-vinylimidazole polymerization. We found imidazole does not chain transfer, but urocanic acid, the precursor the 4-vinylimidazole did result in chain transfer. Therefore, contaminant of this material would reduce control in a living polymerization. Upon further analysis, urocanic acid is not the direct chain transfer agent. There is a triethylamine contaminant in urocanic acid which distills during 4-vinylimidazole synthesis. Due to this contamination a more rigorous purifcation of 4-vinylimidazole was required. First, urocanic acid was recrystallized from water, prior to

the decarboxylation/distillation of 4-vinylimidazole. After distillation, 4-vinylimidazole was further purified through sublimation. The $^{1}$H NMR shown in **Figure 5** confirmed purity of the monomer as well as mass spectroscopy. In the distilled 4-vinylimidazole, a contaminant at approximately 1.8 ppm that is also seen more clearly in the remaining solid from the sublimation. The absence of this peak in the sublimed 4-vinylimidazole confirms the purification of this monomer was successful.

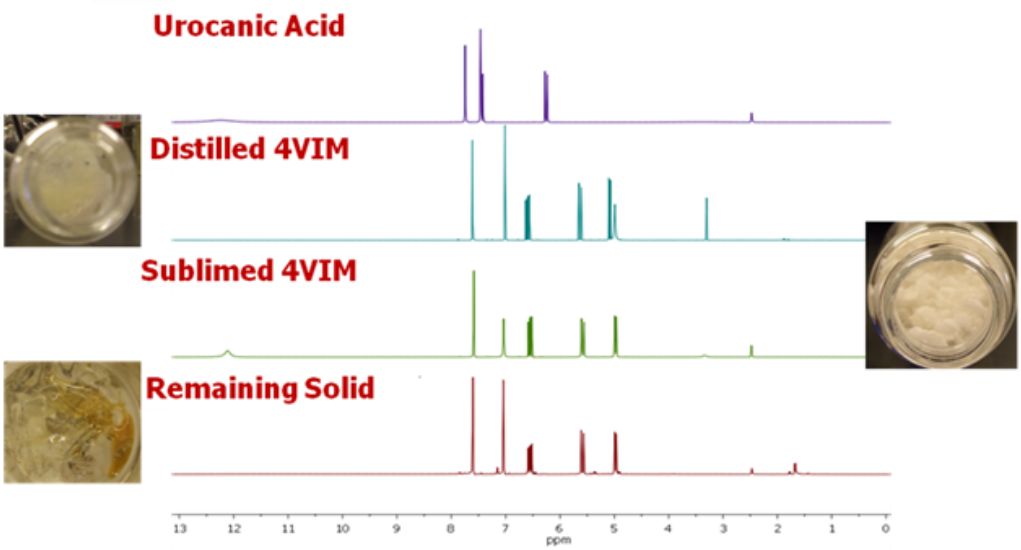


**Figure 5.** $^{1}$H NMR of urocanic acid and subsequent purification of 4-vinylimidazole for use in nitroxide-mediated polymerization.

Upon polymerization of the purified sample with the same reaction conditions as previously reported, the conversion obtained after 4 h remained relatively low (< 20%) as shown in **Figure 6**. Additionally, the molecular weight did not match the predicted/targeted molecular weight. The size exclusion chromatography trace showed bi-modality suggesting that a low concentration high molecular weight polymers were being formed while other polymer chains were growing in a more "living" fashion.

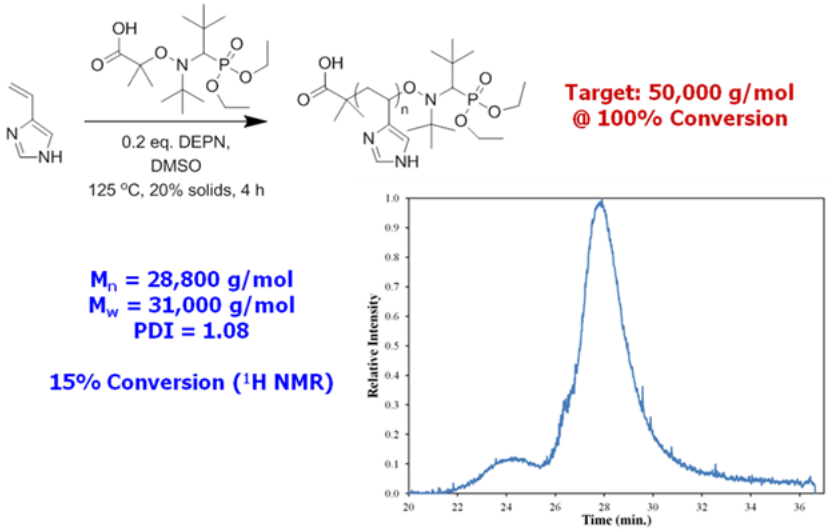


**Figure 6.** Nitroxide-mediated polymerization of 4-vinylimidazole with molecular weight analysis using size exclusion chromatography.

In addition, we also measured the reaction kinetics of the polymerization to better understand how to improve the control of 4-vinylimidazole. As shown below in Figure 7, in the first 100 min. the rate of conversion is extremely fast and after that length of time, the reaction kinects begin to slow. These kinetics do not fit a controlled polymerization as growth should be linear over time. Further investigation of molecular weight, show molecular weights continue to deviate from the theoretical prediction. The one improvement made through purification was the molecular weight distribution of these polymers became extremely narrow, but obtaining linear kinetics remained problematic. After performing *in situ* infrared spectroscopy, we found that during the polymerization, although not visible to the naked eye, polymer was precipitating during the reaction leading to heterogeneous reaction conditions. This would certainly prevent obtaining high molecular weight polymers and limit the reaction kinetics of the polymerization. Realizing DMSO as a solvent was not ideal, we added 50 v/v % MeOH to facilitate polymer solubility. At a temperature of 110 °C methanol was refluxing, which led to unreproducible and inconsistent results. The concentration variation of the reaction solution as methanol boiled was responsible for the inconsistent molecular weights.

Due to the refluxing conditions of methanol, a higher boiling point solvent was required for the nitroxide-mediated polymerization of 4-vinylimidazole. We found that glacial acetic acid exhibited a high boiling point and dissolved both monomer and polymer. All other high boiling point solvents did not dissolve 4-vinylimidazole as they failed to disrupt the inter- and intra-molecular hydrogen bonds between 4-vinylimidazole repeat units. Before attempting a controlled polymerization in acetic acid, as there is no literature precedent, a conventional free radical polymerization was performed using both 1- and 4-vinylimidazole. Polymer was obtained and size exclusion chromatography was performed. As shown in **Figure 7**, the light scattering detector shows a higher molecular weight polymer for 4-vinylimidazole. Using off-line *dn/dc* values, we found poly(4-vinylimidazole)'s absolute $M_n$ was 1,094,000 g/mol while poly(1-vinylimidazole)'s $M_n$ was much lower, 50,200 g/mol.

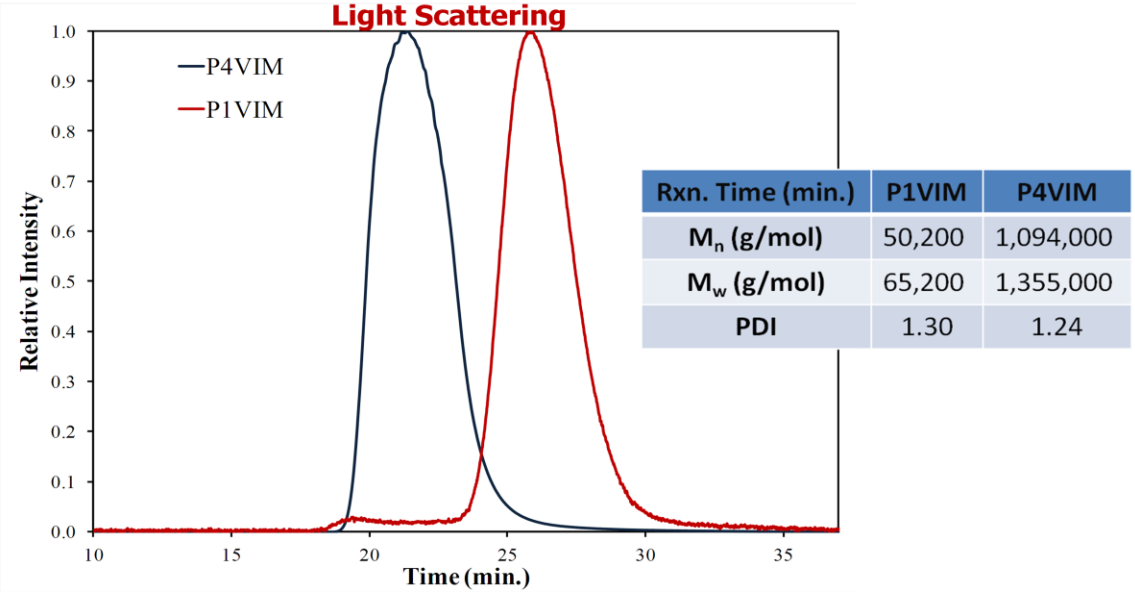


| Rxn. Time (min.) | P1VIM | P4VIM |
|---|---|---|
| $M_n$ (g/mol) | 50,200 | 1,094,000 |
| $M_w$ (g/mol) | 65,200 | 1,355,000 |
| PDI | 1.30 | 1.24 |

**Figure 7.** Size exclusion chromatogram of poly(1-vinylimidazole) and poly(4-vinylimidazole) polymerized using conventional free radical polymerization techniques in glacial acetic acid.

## 2. Creation and Characterization of Lipid Bilayer Interfaces in an Ionic Liquid Solution (T. Young and D. Leo)

Your body is made up of billions of cells, many of which are replicating constantly and replacing those that have been damaged or died. The walls of your cells are made of lipids assembled into a membrane two layers thick, a lipid bilayer. Our research is centered around testing the effects ionic liquids have on different properties of lipid bilayers. The bilayers we test are droplet interface bilayers (DIB), titled so because they are formed at the interface of two aqueous volumes[1]. The aqueous volumes are suspended in a solvent, which in our case is hexadecane. The lipids are in solution in the aqueous solution and when added to the solvent self-assemble into a monolayer membrane at the boundary between the oil and solution. When the volumes are brought together, the solvent between the monolayers is expelled and the monolayers fuse into a bilayer.

For our experiments a substrate that uses the Regulated Attachment Method (RAM) [2] was designed and fabricated to allow for consistency in the measurements; a diagram is shown in Figure 1. The substrate consists of a base tray to hold the solvent and two inserts that support and align the droplets of solution. This substrate utilizes hydrogel pads attached to divots in the inserts to attach the aqueous droplets to the substrate and suspend them in the oil. The aqueous solution is manually pipetted onto the hydrogel pads for each experiment.

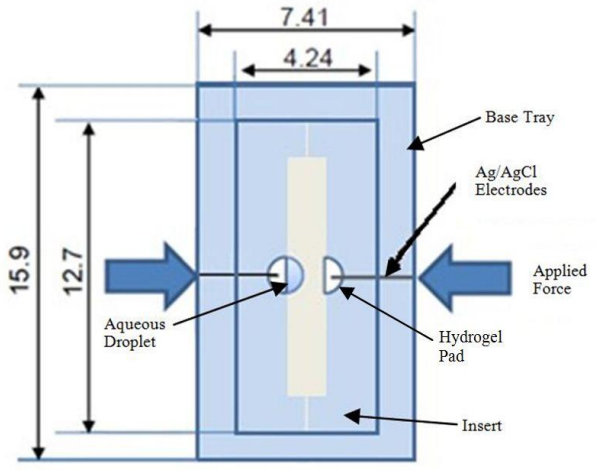


Figure 1: RAM substrate used to form and support bilayers

Once the solution has been added to the hydrogels and the monolayers have formed on the surface of the droplets, force is applied to the substrate as shown and the droplets are brought into contact. The image in Figure 2 shows the hydrogel pads with droplets attached before and after force is applied.

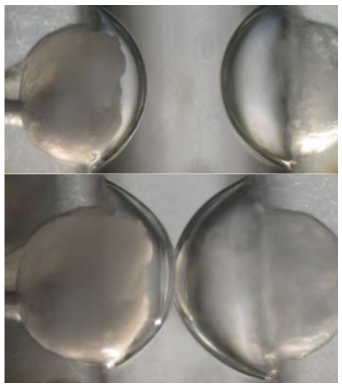

Figure 2: (a) Aqueous droplets before force is applied (b) Aqueous droplets with lipid bilayer formed in between

Recent experiments have centered on the incorporation of Ionic Liquids (IL) into the lipid solution and the characterization of the bilayer in this solution. Experiments measuring the time of formation and stability of the bilayer were initially conducted. Table 1 shows some of the data collected in those tests and Figure 3 gives a graphic depiction of the effect the ionic liquid had on the stability of the bilayer.

Table 1: Data from study bilayer stability

| Time allowed to for monolayer | | 10 sec | 1 min | 5 min | 10 min |
|---|---|---|---|---|---|
| Time to form bilayer | Trial 1 | 100 | 70 | 54 | 33 |
| | Trial 2 | 80 | 175 | 47 | 40 |
| | Trial 3 | 70 | 110 | 52 | 32 |
| | Trial 4 | 124 | 142 | 139 | 114 |
| | Trial 5 | 30 | 73 | 48 | 52 |
| Level off value | Trial 1 | 59 | 130 | 65 | 170 |
| | Trial 2 | 61 | 90 | 60 | 162 |
| | Trial 3 | 68 | 95 | 64 | 168 |
| | Trial 4 | 70 | 83 | 92 | 65 |
| | Trial 5 | 50 | 97 | 76 | 83 |
| Rupture time | Trial 1 | 200 | 380 | 600 | 175 |
| | Trial | 77 | 600 | 600 | 600 |

| | | | | | |
|---|---|---|---|---|---|
| | 2 | | | | |
| | Trial 3 | 175 | 600 | 463 | 212 |
| | Trial 4 | 600 | 163 | 216 | 600 |
| | Trial 5 | 145 | 600 | 600 | 600 |
| Time of stable bilayer | Trial 1 | 100 | 310 | 546 | 142 |
| | Trial 2 | 0 | 425 | 553 | 560 |
| | Trial 3 | 105 | 490 | 411 | 180 |
| | Trial 4 | 476 | 21 | 77 | 486 |
| | Trial 5 | 115 | 527 | 552 | 548 |

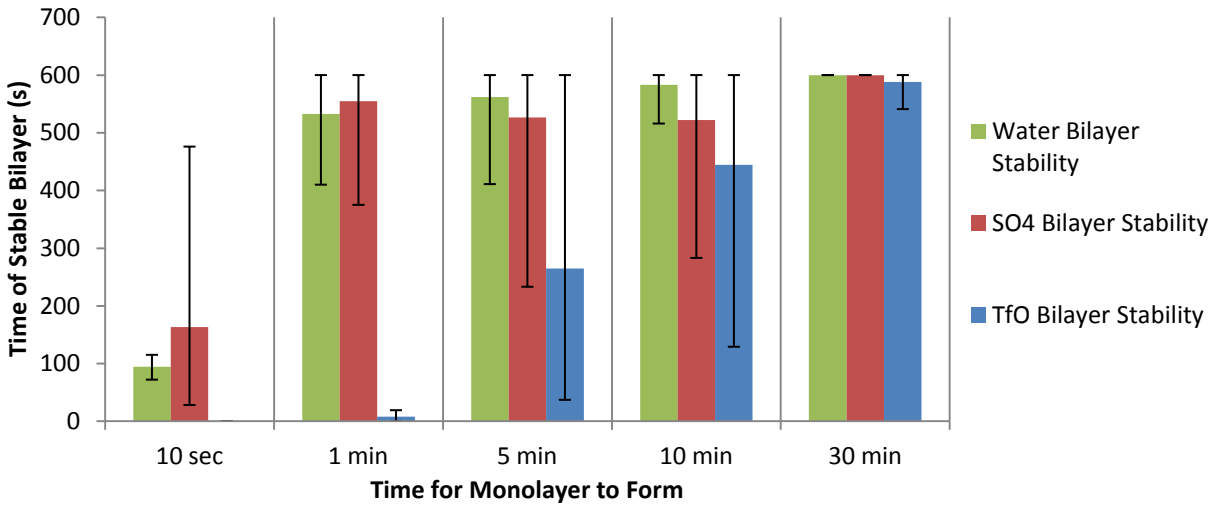


**Figure 3:** A plot of the amount of time a bilayer was stable as a function of the amount of time the monolayer was allowed to form.

The bilayer may sometimes experience a buildup of voltage potential either through discharge from the electrodes or applied during an experiment. The effect of the ILs on the voltage resistance of the bilayer was also tested. The tests showed that the [EMIm] [SO4] (SO4) did not have a significant effect on the voltage resilience of the bilayer; however the [EMIm] [TfO] (TfO) reduced the resilience significantly. A bilayer formed between droplets of TfO typically could not withstand more than 200 mV without rupturing while bilayer between water and SO4 droplets could typically survive more than 350 mV.

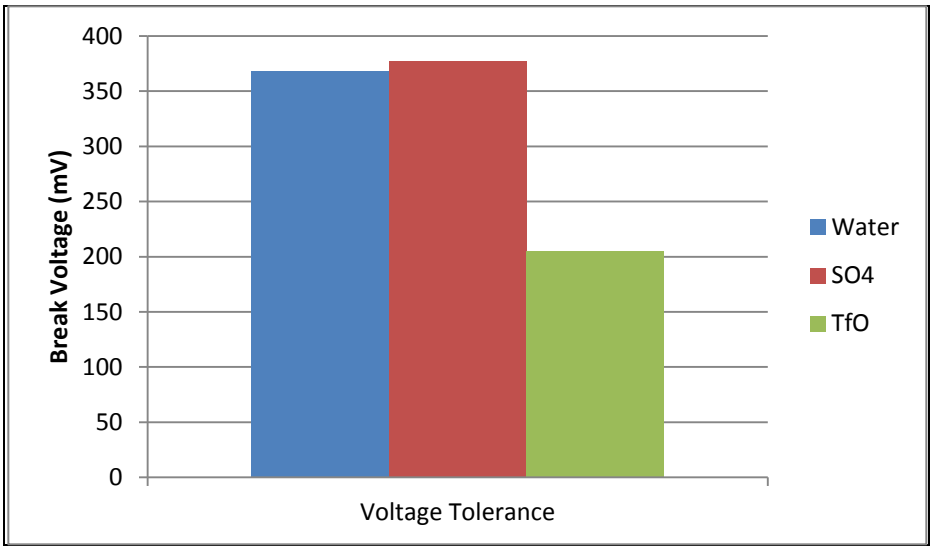


**Figure 4:** Plot of the voltage tolerance of bilayers formed between a water control and the two ionic liquids.

These experiments showed [EMIm] [SO4] did not have a discernibly negative effect on the properties of the bilayer. [EMIm] [TfO] did have a negative impact on bilayers it was in contact with. It lower the voltage resilience and stability of the bilayers significantly.
Alamethicin peptide transport experiments have been conducted on the SO4 and TfO solutions and compared to previous findings. Alamethicin self-inserts into the bilayer when an electrical potential is applied across said bilayer. The peptide the opens pores in the membrane which allows current to flow from one side to the other. These pores are typically only open for a few fractions of a second and the current measurements look similar to a step signal. An example of the signal we usually see in Figure 5 at three different magnitudes of applied voltage.

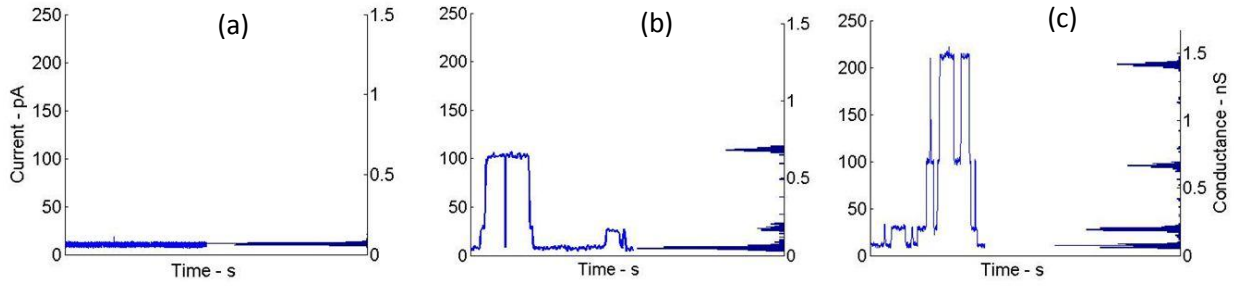


Figure 5: Gating events from tests with Alamethicin peptides in solution with TfO ionic liquid at an applied voltage of (a) 0 mV, (b) 80 mV and (c)150 mV

To the right of each plot in Figure 5 is a histogram showing the times spent at particular magnitudes of conductance which are categorized as conductance levels. According to literature and previous experiments conducted without ionic liquids, the first four conductance levels should have average magnitudes around, 0.12, 0.48, 0.92, and 1.5 nS [3]. As can be seen in Figure 5, in the TfO tests the third conductance level is at a much higher magnitude than what would be expected. In fact it is much closer to the

value recognized as the fourth conductance level in literature. Analysis is currently being done to determine what is causing this increase in conductance.
It is not clear if it is the ionic liquid ions that are being transported or the ions of the KCL in the lipid buffer solution. Future test will attempt to determine which additive is contributing ions. Experiments will be done where the KCL will be replaced with the same concentration of ionic liquid and transport test conducted. Also the data that has already been taken will be compared to data without ionic liquid and property differences will be analyzed.

### 3. Synthesis and Characterization of Imidazole Containing Copolymers for Electroactive Devices (C. Jangu and T. E. Long)

The polymerization of VBIm was successfully controlled by nitroxide–mediated polymerization. There is a linear increase in molecular weight with conversion and PDIs are narrow even as high conversions. The polymer was then quaternized with methyl iodide and exchanged with TFSI anion to improve thermal stability and decrease Tg of the middle block to finally make the soft middle block and introduce charged block in the triblock system using the conditions shown in scheme 2.

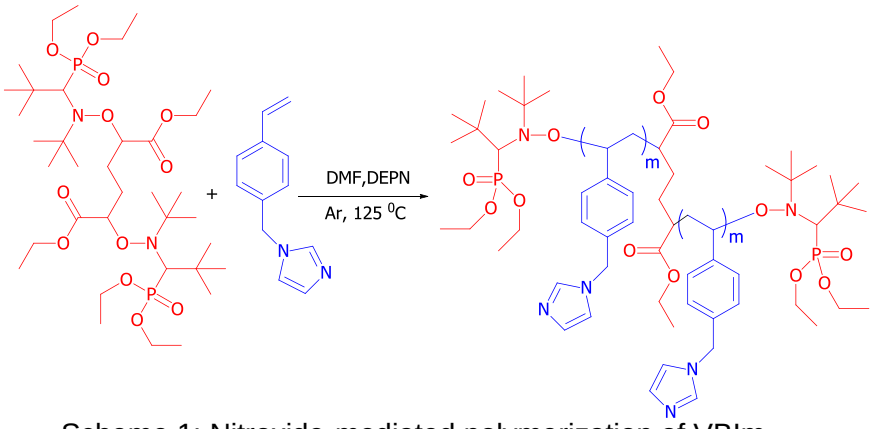


Scheme 1: Nitroxide-mediated polymerization of VBIm

.

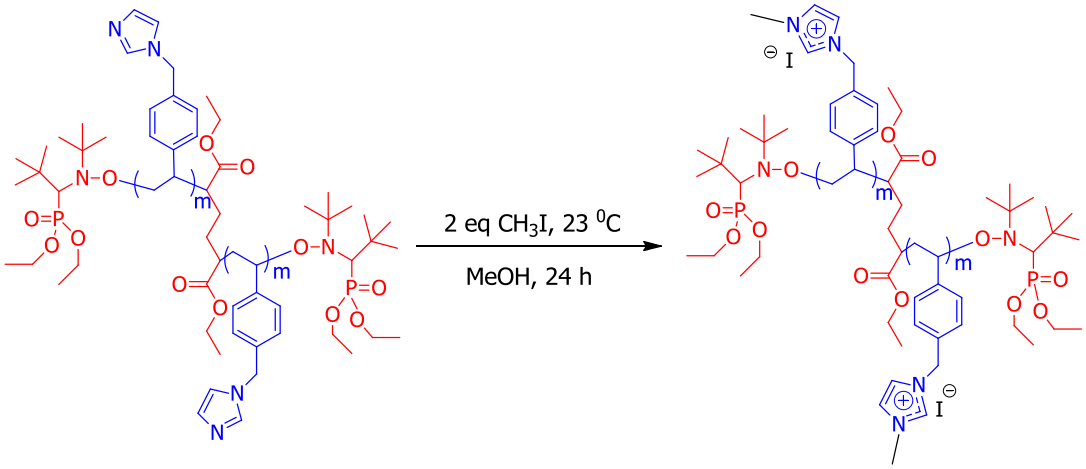

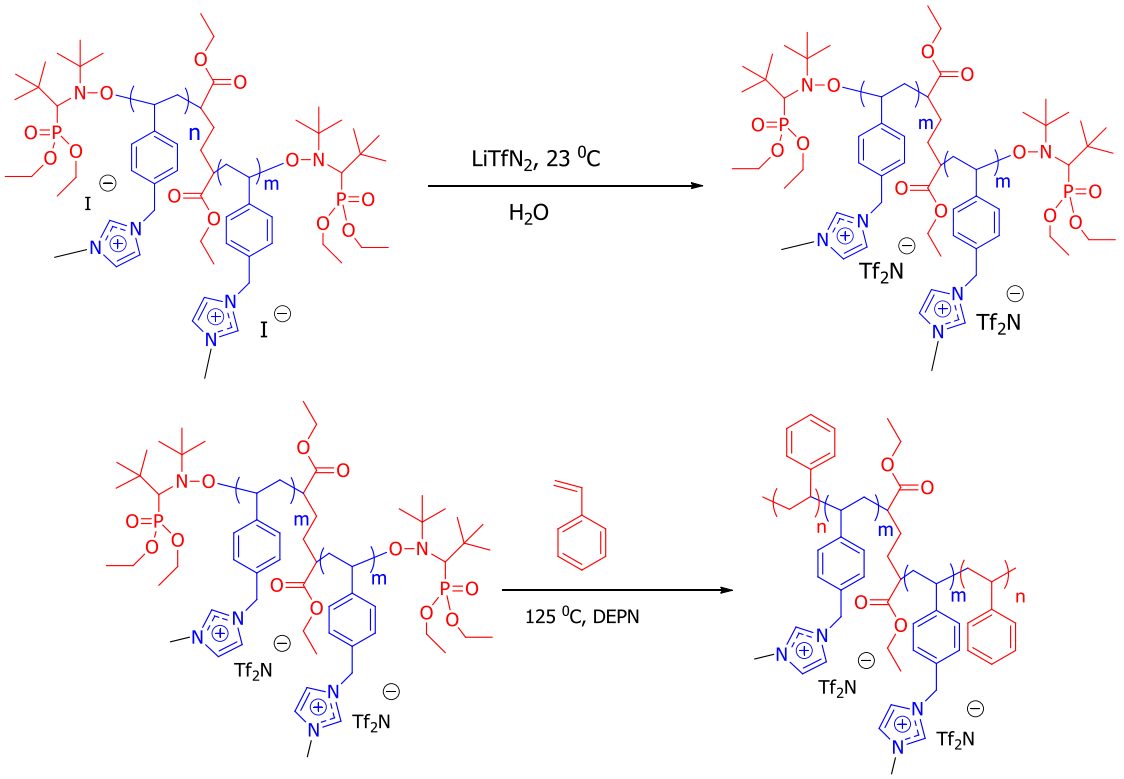


Scheme 2: Anion exchange and chain extension of poly(VBIm) with styrene to make triblock copolymer

The poly(VBIm) quaternized with TFSI is then chain extended with styrene as outer blocks to synthesize triblock copolymers with styrene as outer blocks providing mechanical stability to the system and VBIm as middle block giving thermal stability and ionic conductivity. Table 1 shows the molecular weight analysis of the triblock copolymers with increasing molecular wight of outer blocks.

**Table 1:** Molecular Weight Analysis of Triblock Copolymers

| **Polymer** | **$M_n$ (g/mol)** | **$M_w$ (g/mol)** | **PDI** |
|---|---|---|---|
| PVBIm | 73,200 | 72,500 | 1.13 |
| PMVBIm-I | 76,500 | 94,200 | 1.16 |
| PMVBIm-$TF_2N$ | 80,200 | 98,700 | 1.17 |
| Poly($Sty_{10}$-MVBIm-$TF_2N_{80}$-$Sty_{10}$) | 100,200 | - | - |
| Poly($Sty_{35}$-MVBIm-$TF_2N_{80}$-$Sty_{35}$) | 150,200 | - | - |
| Poly($Sty_{60}$-MVBIm-$TF_2N_{80}$-$Sty_{60}$) | 200,200 | - | - |

The thermal transitions of these triblock copolymers. Tg increases after quaternization which decreases after anion exchange to TFSI.

**Table 2:** Thermal Characterization of Triblock Copolymers

| **Polymer** | **$T_{g1}$ C** | **$T_{g2}$ C** | **$T_{D,5\%}$ C** |
|---|---|---|---|
| PVBIm | 105 | - | 348 |
| PMVBIm-I | 126 | - | 251 |
| PMVBIm-$TF_2N$ | 22 | - | 339 |
| Poly($Sty_{10}$-MVBIm-$TF_2N_{80}$-$Sty_{10}$) | 22 | - | 323 |
| Poly($Sty_{35}$-MVBIm-$TF_2N_{80}$-$Sty_{35}$) | 46 | 106 | 329 |
| Poly($Sty_{60}$-MVBIm-$TF_2N_{80}$-$Sty_{60}$) | 26 | 110 | 334 |

All the triblock copolymers show two transitions one for styrene and other for charged middle block. The storage modulus for these polymers is higher at room temperature. The rubbery plateau increases with increase in weight fraction of styrene as shown in Figure 1.

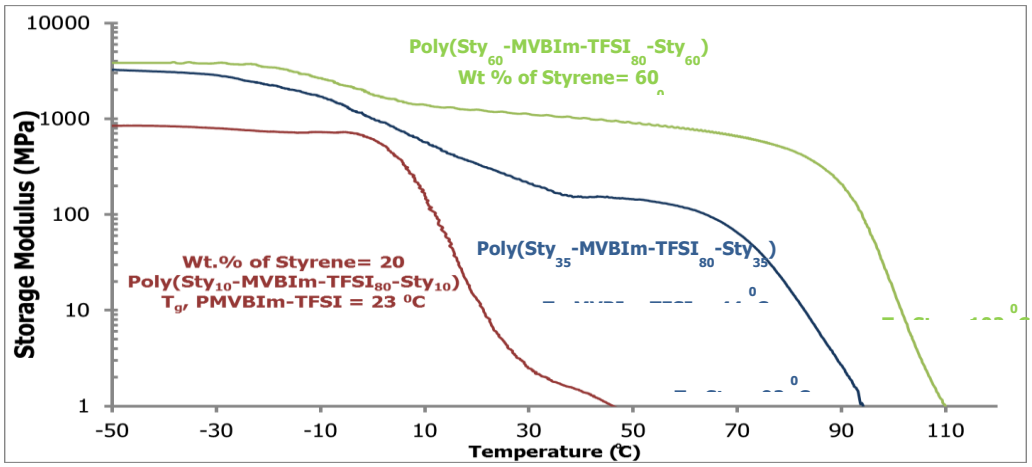


**Fig 1**: Dynamic Mechanical Analysis of triblock copolymers

To confirm the morphology of the triblock copolymer small angle light scattering was performing.The samples were prepared by annealing the films casted with methanol/water for 4-5 days.The SAXS shown in Figure 2 shows peaks at positions showing lamellar morphology.

These triblock copolymers show microphase separation proving the triblock copolymers are controlled.

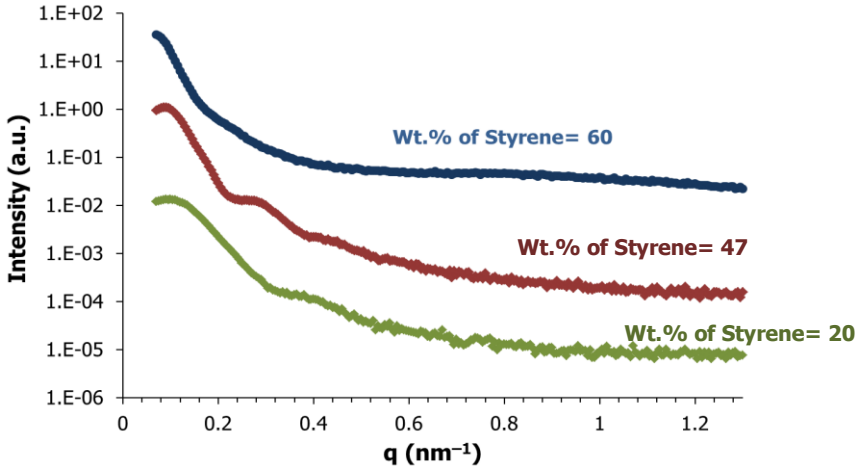


**Fig 2:** Small-angle X-Ray scattering of Triblock Copolymer

## II. THRUST 2: Nanometer-Scale Design (Leader: Prof. K. I. Winey)

Supporting faculty: Karen Winey, Yossef Elabd, and Harry Gibson

### 1. Effect of Nanostructured Morphology on Ion Transport in Polymerized Ionic Liquid Block Copolymers (Y. Ye, Y. A. Elabd, J.-H. Choi, and K. I. Winey)

This project is to study nanostructured morphology on ion transport in styrene- and MMA-containing PIL diblock copolymers. In this work, we not only investigate the various type of morphology as a function of composition and the influence of morphology on ion conduction in one type of PIL block copolymers, but also study morphology effect across different types of block copolymers at a similar PIL compositions.

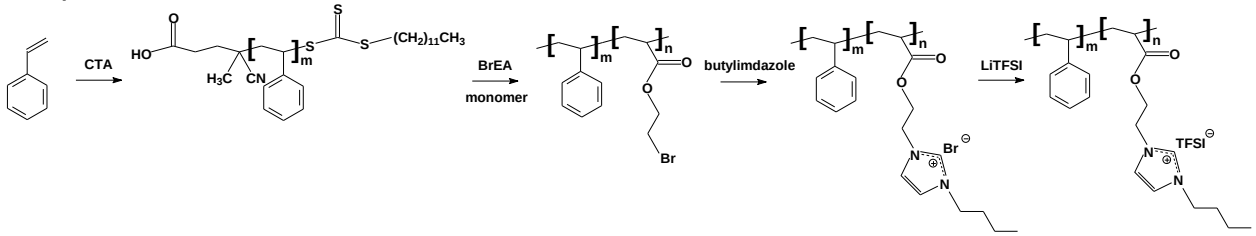


Scheme 1. Synthesis of styrene-containing and acrylate-based PIL block copolymers.

First, we synthesized a series of styrene-containing and acrylate-based PIL block copolymers at PIL compositions ranging from 6.6 to 23.6 ml% using the sequential RAFT polymerization technique (Scheme 1). Different from our previous work (Project 1 and Project 2), the quaternization reaction was performed on neutral block copolymers to introduce the charged imidazolium moieties after polymerization. The chemical structures, purity, and molecular weight of final products were investigated by $^{1}$H NMR, elemental analysis, and size exclusion chromatography, respectively.

Figure 1a shows the X-ray scattering profiles of PIL block copolymers with various PIL compositions, indicating different types of morphologies as a function of composition. TEM results show that block copolymers with 23.6, 17.0, 12.2 and 6.6 mol% PIL composition exhibit the mixed (lamellar and gyroid), lamellar, cylindrical and cylindrical morphologies, which agree with the X-ray scattering results. Figure 1b shows the morphological factors of PIL block copolymers, indicating that morphology type has significant effect on ion conduction. Specifically, the three-dimensional connected

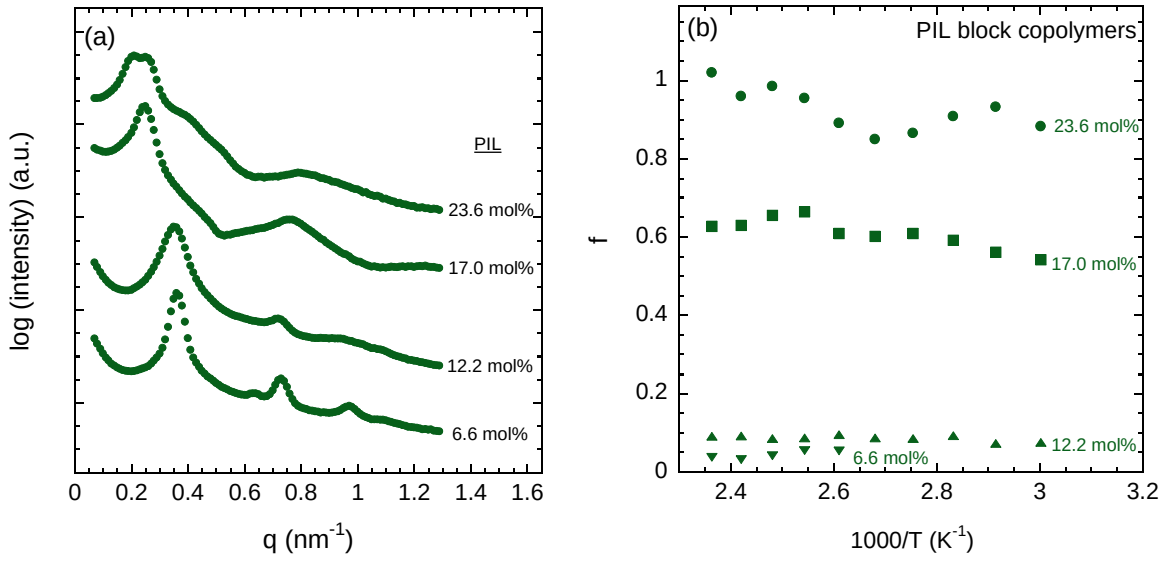


Figure 1. (a) X-ray scattering and (b) morphological factors of PIL block copolymers at various PIL compositions.

morphology of the sample with 23.6 mol% PIL composition is highly beneficial to the ion transport. In comparison, the poor conductivity of the sample with 6.6 mol% can be attributed to a relatively low concentration of conducting ions and the poorly connected conductive domains in the cylindrical morphology.

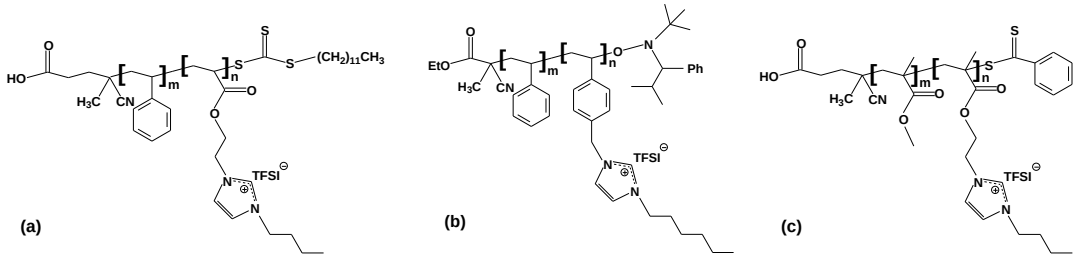


Scheme 2. Chemical structures of PIL block copolymers.

To better understand the effect of morphology on ion transport, we investigated different types of block copolymers at similar PIL compositions. We compared the morphology and ionic conductive properties of our styrene-containing and acrylate-based PIL block copolymer (Scheme 2, Sample a) with another styrene-containing but vinylbenzyl-based PIL block copolymer (Sample b), and MMA-containing block copolymer (Sample c) at a similar PIL composition (~ 42 vol%).

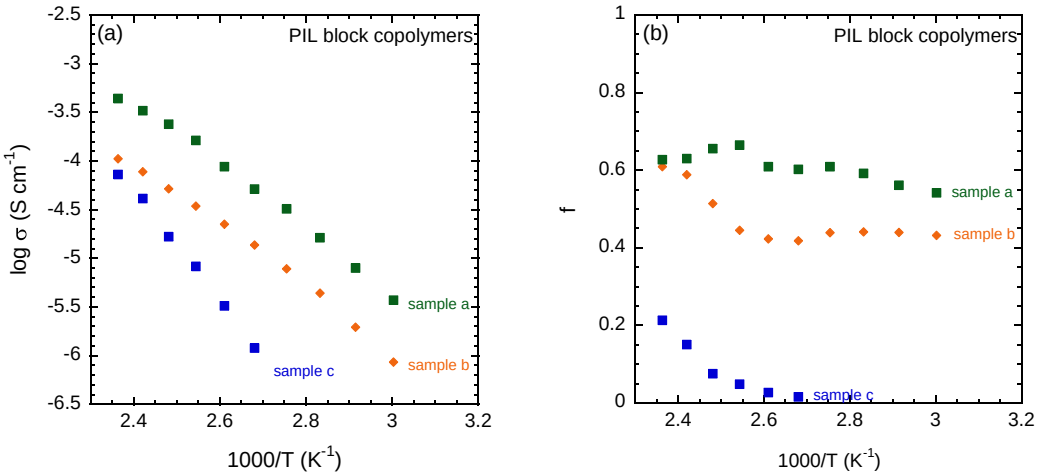


Figure 2. (a) Ionic conductivities and (b) morphological factors of three PIL block copolymers at a similar PIL composition (~ 42 vol%).

Studies of X-ray scattering and TEM show that Samples a-c have lamellar, lamellar, and microphase separated (without periodic structures) morphology, respectively. Figure 2 shows the corresponding ionic conductivities and morphology factors of 3 samples. Obviously, Sample a and Sample b show higher ionic conductivity than Sample c. This is largely attributed to the difference in morphology and glass transition temperature of the PIL block. Interestingly, both Sample a and Sample b have a lamellar morphology. However, Sample a shows a half order higher ionic conductivity than Sample b (Figure 2a). This may be related with the difference in the conductivity of the homopolymer (data not shown) and the connectivity of conducting domains of lamellar nanostructures (Figure 2b).

This work experimentally demonstrates that nanostructured morphology is a significant contribution to ion transport. This not only includes the type of morphology, but also includes the domain orientation, size, and connectivity as well. This fundamental study will be beneficial to design highly conductive polymer electrolytes that can significantly enhance the performance of energy conversion devices, such as fuel cells, batteries, and solar cells.

## 2. Morphology and Ion Transport in Charged Polymers with IL Moieties (T.-S. Wang and K. I. Winey)

Hydroxyalkyl imidazolium TFSI polymerized ionic liquids with different side chain lengths (n = 2, 3, 6, 8; chemical structure shown in 6b(vi)) were studied by room temperature SAXS and compared with their alkyl counterparts to investigate the effect of adding OH functional groups to the side chains. Another goal was to observe possible hydrogen-bonding between OH functional groups and imidazolium cations. Three peaks are seen in the X-ray scattering patterns, shown in Figure 5. The peak at 3 nm–1 < qb < 5 nm–1 corresponds to the backbone-to-backbone correlation distance, the peak at qi ~ 9 nm–1 corresponds to anion-to-anion correlation distance, and the peak at qp ~ 14 nm–1 corresponds to the pendant-to-pendant distance (or distance between side chains). For both the alkyl and hydroxyalkyl materials, qb decreases and the backbone-backbone spacing increases as pendant length n increases. The intensity of the peak at qb also increases noticeably because the microphase separation of polar (ionic and OH) and nonpolar (carbon) entities increases with pendant length. qi does not change with n for the alkyl materials and decreases slightly with increasing n for the hydroxyalkyls. qp remains approximately the same as a function of n for both the alkyl and hydroxyalkyl materials. The scattering intensity from qp increases as n increases; this is because as the pendant length increases, there is more of the pendant contributing to scattering.

When comparing alkyl and hydroxyalkyl materials with the same n, the backbone-backbone peak is stronger and sharper in the alkyl versions. This is because the addition of OH diminishes the electron density contrast between nonpolar and polar entities in the sample, which decreases the electron density contrast between the peaks at qb and qi and the peaks at qb and qp. For n = 6, 8, the peak at qb is lower intensity and broader for the hydroxyalkyls than for the alkyls. The anion-anion and pendant-pendant correlation peaks are more discernible. For n = 2, 3, there is less contrast between ions and pendants because of the OH groups and smaller separation distance between backbones. As a result, for n = 2, 3, the peaks at qi and qp are less resolved than for the alkyls, and the peak at qb is barely visible for the hydroxyalkyl materials. qb is slightly greater for the hydroxyalkyl materials than for alkyl materials, indicating that the backbone-backbone spacings are smaller for the hydroxyalkyls, despite them having longer pendants than the alkyls. The fact that the qb positions are higher for the hydroxyalkyl materials than the alkyls might suggest additional bonding between the OH groups and the imidazolium rings.

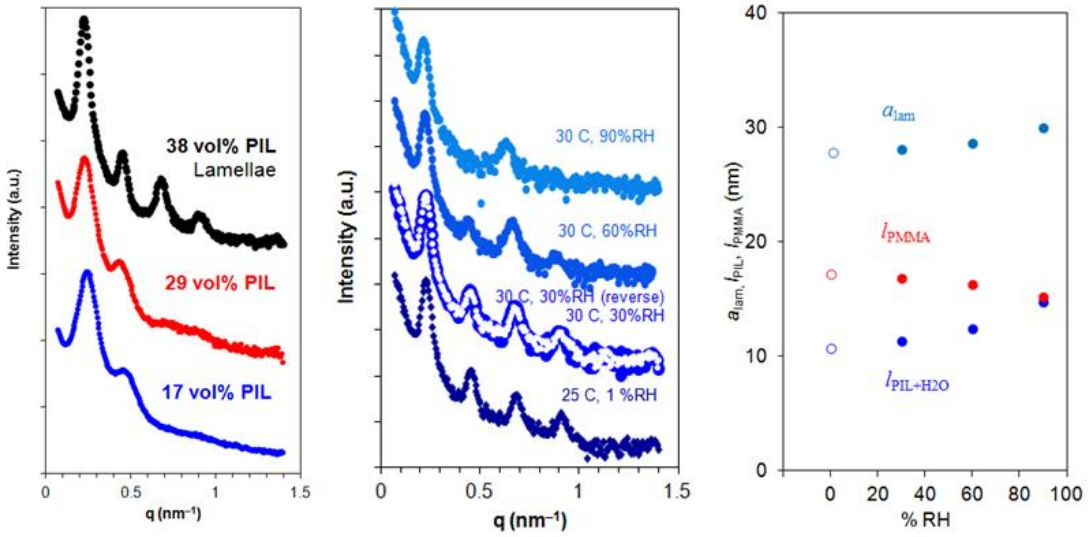


**Figure 1.** Morphology data for PMMA-*b*-PMEBIm-Br diblock copolymers. Left: Room-temperature SAXS data for PMMA-*b*-PMEBIm-Br as a function of PIL content. Center: SAXS data as a function of relative humidity (RH) for PMMA-*b*-PMEBIm-Br, 38 vol% PIL. The change in intensity of the second and fourth correlation peaks shows the sample's responsiveness to changes in RH. Right: Humidity-dependent lattice parameter ($a_{lam}$), PMMA domain thickness ($l_{PMMA}$), and PIL domain thickness ($l_{PIL}$) for PMMA-*b*-PMEBIm-Br, 38 vol% PIL.

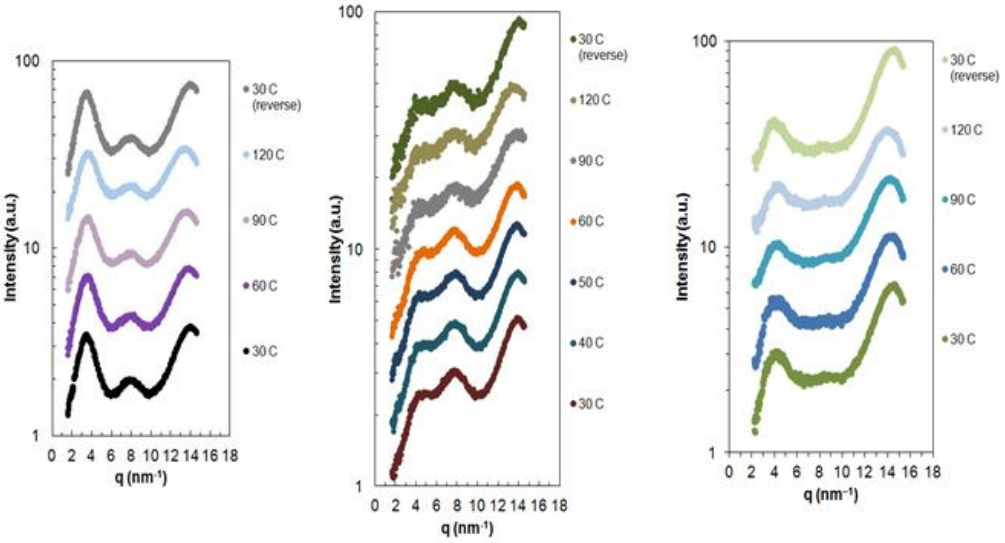


**Figure 2.** X-ray scattering results for $C_{12}$ $TFSI^-$ (left), $C_4$ $TFSI^-$ (center), and $C_4$ $PF_6^-$ (right) acrylate polymerized ionic liquids as a function of temperature.

**Figure 3.** X-ray scattering data as a function of temperature. Top: $(EO)_4C_{10}C_4$ TFSI methacrylate (a) monomer and (b) polymer. Bottom: $(EO)_4C_{10}C_4$ TFSI acrylate (a) monomer and (b) polymer.

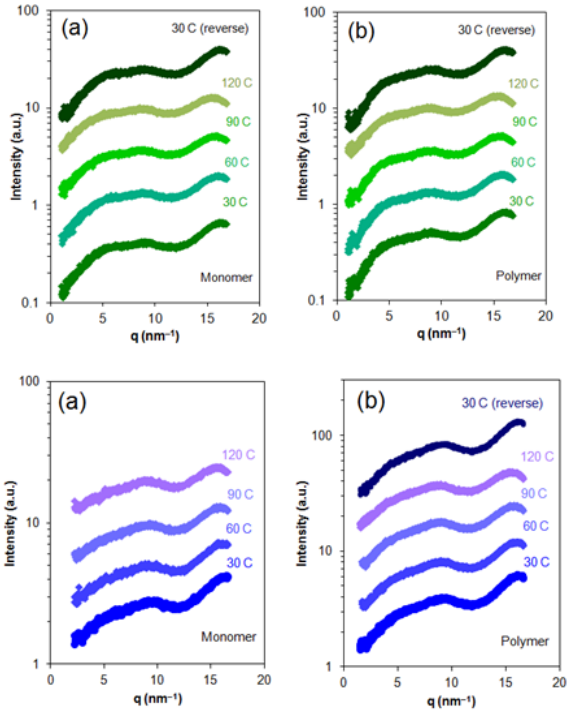


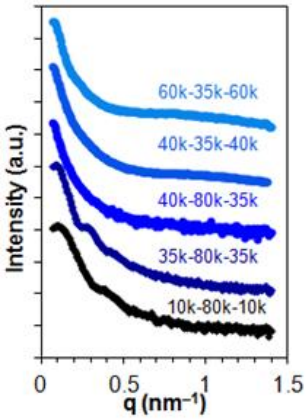


**Figure 4.** SAXS data at room temperature for PS-*b*-PVBIm-*b*-PS triblock copolymers with various molecular weights of the inner PVBIm and outer PS blocks.

**Figure 5.** SAXS data at room temperature for hydroxyalkyl and alkyl imidazolium TFSI polymerized ionic liquids with different side chain lengths ($n$ = 2, 3, 6, 8). For each side chain length $n$, the alkyl imidazolium PIL data is on top (pink/purple) and the hydroxyalkyl imidazolium PIL data is on the bottom (blue/green).

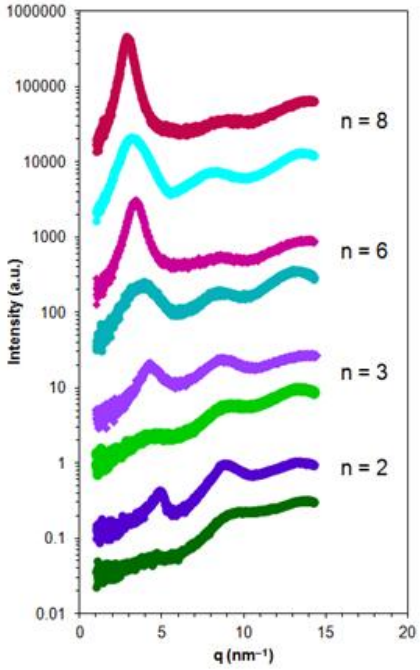

## Thrust 3: Macromolecular Design

### 1. Ionomeric Polymer/Conductor Network Composite Transducers with Ionic Liquids (Y. Liu and Q. Zhang)

#### Polymer in Ionic Polymer Actuators

#### 1.1 Materials

Since the polymer matrix in ionic polymer actuators play an important role in the electromechanical coupling process, the selection of polymer materials is crucial to the device performance. In this report, polymer matrices are intensively studied for improving the electromechanical energy efficiency of ionic polymer actuators.

Nafion®, which is a perfluorosulfonic acid ionomer membrane, exhibits high ionic conductivity, good mechanical strength, and high chemical resistance and therefore has been widely used as a benchmark material in fabricating IPCNC actuators. As shown in Figure 1(a), the molecular structure of Nafion® consists of polytetrafluoroethylene (PTFE) backbones, which serve as the high elastic modulus phase, and a double ether perfluoro side chains terminating in a sulfonic acid group. These sulfonic acid groups form a separated cluster phase with a lower glass transition temperature (Tg) than that of the backbone. With the presence of electrolytes, such as a polar solvent or a hydrophilic ionic liquid, the electrolyte molecules are exclusively contained in the clustered network, i.e. the ionic channels that are displayed in Figure 1(b). Although the ion channels are plasticized by the electrolyte molecules, which facilitate fast ion transport, their effect on the mechanical coupling between stored excess ions near electrodes and the polymer backbone (high modulus phase) may be negative.

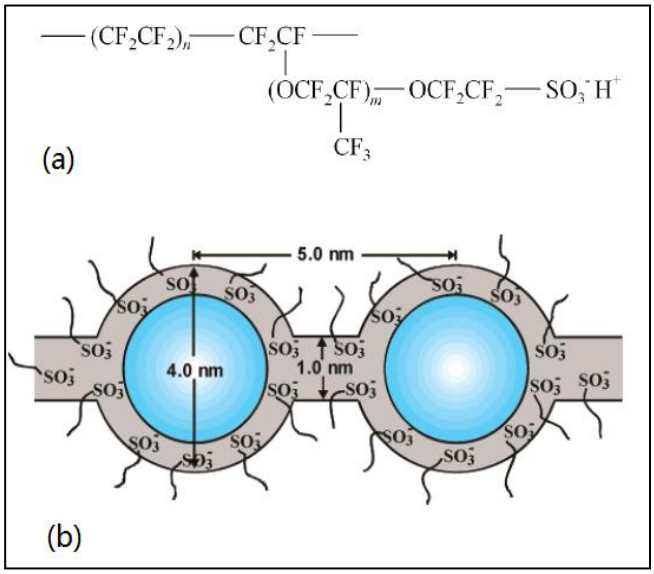


Figure 1: (a) Molecular structure of Nafion®
(b) Representation of ionic domain channels

In principle, under an electric field, the accumulation or depletion of ions with different sizes causes volume changes near electrodes, and consequently generate actuation. As illustrated in Figure 2, the flexible side chains of perfluorosulfonate ionomers may act as soft buffer layers between the PTFE backbones and the excess ions near the electrodes which damp the strain generated in the backbone by the excess ions. Because these flexible side chains are elastically much softer than the backbones, with the presence of large ion molecules, segmental motions of side chains within the backbone framework were observed by dynamic mechanical response which is a sign of an ineffective electromechanical transduction. An effective elastic coupling

of the stored ions with the high modulus phase of the polymer matrices is desired in achieving a high electromechanical transduction efficiency.

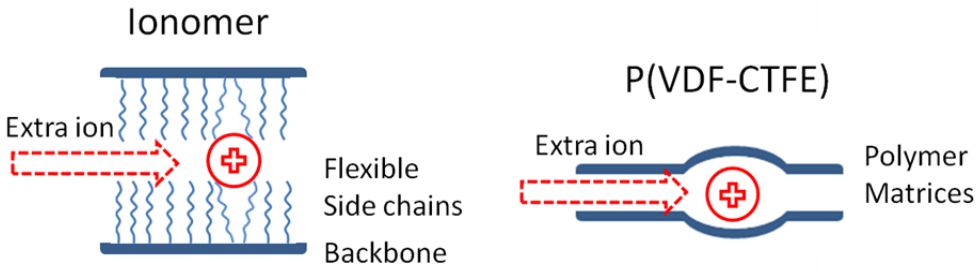


Figure 2: Effects of flexible side chains of perfluorosulfonate ionomers on electromechanical transduction efficiency

We investigated PVDF based polymer matrices, which do not have side groups in structures, such as fluoropolymer Poly[(vinylidene difluoride)-co-(chlorotrifluoroethylene)] (P(VDF-CTFE)) and poly(vinylidene fluoride-trifluoroethylene-chlorofluoroethylene) (P(VDF-TrFE-CFE), for ionic polymer actuators. P(VDF-CTFE) and (P(VDF-TrFE-CFE) are known as ferroelectric EAPs that can be operated under high voltage. Since Poly(methyl methacrylate) (PMMA) has a Young's modulus as high as ~3GPa, blending it with P(VDF-CTFE) will increase the stiffness of the polymer. Therefore, besides P(VDF-CTFE) and (P(VDF-TrFE-CFE), the cross-linked P(VDF-CTFE)/PMMA blends are also studied and compared with those of the perfluorosulfonate ionomers. Figure 3 shows the schematic of an ionic polymer membrane actuator with planar electrodes used in this study, which is a simple configuration that has a well controlled device structure and allows in-depth polymer material analysis.

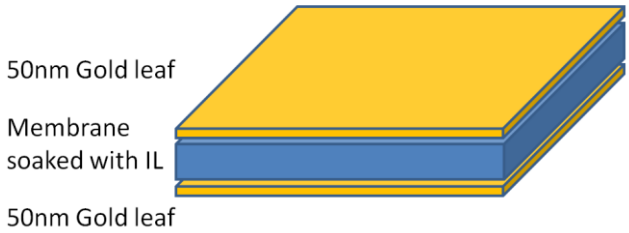


Figure 3: schematic of an ionic polymer membrane actuator with planar electrodes

## 2.1 Mechanical properties

**Table 1** Moduli of polymers without and with 40 wt% of EMI-Tf uptake

| Polymer Composition | Young's Modulus at 25°C (MPa) | |
|---|---|---|
| | Neat membrane | Membrane with 40 wt% EMITf |
| Nafion® | 550 | 50 |
| Aquivion® | 410 | 50 |
| P(VDF-CTFE) | 480 | 70 |
| P(VDF-CTFE)/PMMA blends* | 880 | 110 |
| Crosslinked P(VDF-CTFE)/PMMA | 1100 | 150 |
| P(VDF-TrFE-CFE)* | 175 | N/A |
| Crosslinked P(VDF-TrFE-CFE) | 470 | 50 |

* not characterized for actuator performance.

The moduli of the polymer membranes with and without EMI-Tf are summarized in Table 1. It is found that Nafion®, Aquivion® and P(VDF-CTFE) dry membranes have similar moduli, and by blending PMMA with P(VDF-CTFE), the young's modulus of the membrane is almost doubled from pure P(VDF-CTFE). To further increase the elastic modulus, 2wt% of an initiator (Bicumene) was added to P(VDF-CTFE)/PMMA blends in the fabrication process to create crosslinks in the blends. After melting molding into a film at 240°C, the modulus of the P(VDF-CTFE)/PMMA film is increased 25% compared to the pure blend which is an indication of some degree of crosslinking in the blends. Pure P(VDF-TrFE-CFE) has a very low Young's modulus and dissolves in ionic liquids. To improve its Young's modulus and chemical stability, both 2wt% of an initiator (Bicumene) and 2wt% of a crosslink agent (TAIC) were added to P(VDF-TrFE-CFE) in the fabrication process to create crosslinks in the polymer. After melting molding into a film at 240°C, the modulus of the P(VDF-TrFE-CFE) film is increased ~150% compared to the pure polymer film, which shows a high crosslink density. This finding agrees with the high gel content value of the crosslinking 63.5%. Different from pure P(VDF-TrFE-CFE), after crosslinking, this polymer membrane no longer dissolves in ionic liquid electrolytes.

Nafion® and Aquivion® are perfluorosulfonate ionomers that share the similar nano-structure, in which Aquivion® has a shorter side chain length than Nafion® does. As shown in Table 1, after swelling with 40 wt% of EMI-Tf, the moduli of Nafion® and Aquivion® membranes reduced significantly, from more than 400MPa to 50MPa due to the plasticizing effect of the ionic liquid molecules. Analogously, with 40 wt% EMI-Tf, the moduli of PVDF based materials are also reduced. However, with the same amount of

IL uptake, the moduli of all these PVDF based membranes are still higher than or equal to that of Nafion® and Aquivion®.

Actuator performance from three new materials, P(VDF-CTFE), crosslinked P(VDF-CTFE)/PMMA and crosslinked P(VDF-TrFE-CFE), is characterized and compared with that from the tradition ionomers, namely Nafion® and Aquivion®. The blend of P(VDF-CTFE) and PMMA without crosslinking is characterized for the purpose of investigating the crosslinking density, and thus is not further studied for the electromechanical responses.

### 1.3 Electrical properties

The frequency-dependent conductivity of five ionic polymer membrane actuators is presented in Figure 4, where the plateau region at high frequencies corresponds to the dc conductivity $\sigma_0$ of the material system. With 40 wt% uptake of EMI-Tf, Nafion® and Aquivion® exhibit a relatively higher $\sigma_0$ ($1.9\times10^{-4}$ S/cm and $1.3\times10^{-4}$ S/cm, respectively), which is due to the percolated ion channels and presence of flexible side chains, than those of P(VDF-CTFE) ($1.4\times10^{-5}$ S/cm), P(VDF-CTFE)/PMMA ($0.7\times10^{-4}$ S/cm), and P(VDF-TrFE-CFE) ($2.5\times10^{-5}$ S/cm). Interestingly, the data also show that adding PMMA not only increases the elastic modulus but also improves the ionic conductivity. This implies that the presence of PMMA provides some degree of "ion channels" which facilitate the ion transport. It is well known that PMMA is miscible with P(VDF-CTFE) in amorphous phase which may create nano-inter-phase regions between the two polymers, facilitating ion transport.

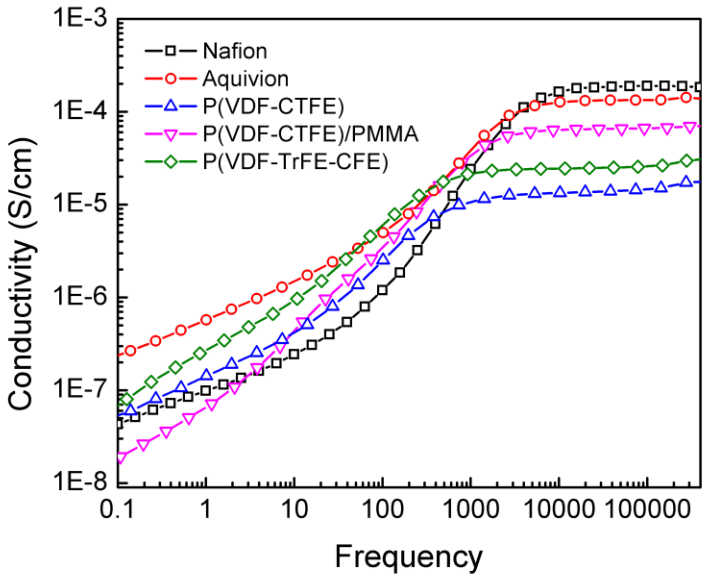


Figure 4: frequency-dependent conductivity of five ionic polymer membrane actuators

Presented in Figure 5 is the charge responses of five ionic polymer membrane actuators made with Nafion®, Aquivion®, P(VDF-CTFE), cross-linked P(VDF-CTFE)/PMMA, and P(VDF-TrFE-CFE) under a 4V step voltage. With the same weight

percentages (40 wt%) of EMI-Tf uptake, Nafion® and Aquivion® membranes consume ~70-100% more charge than those of PVDF based membranes. The higher charge densities and conductivities of Nafion® and Aquivion® with ionic liquids could be attributed to the ion channels that facilitate the ion transport and accommodate more ions.

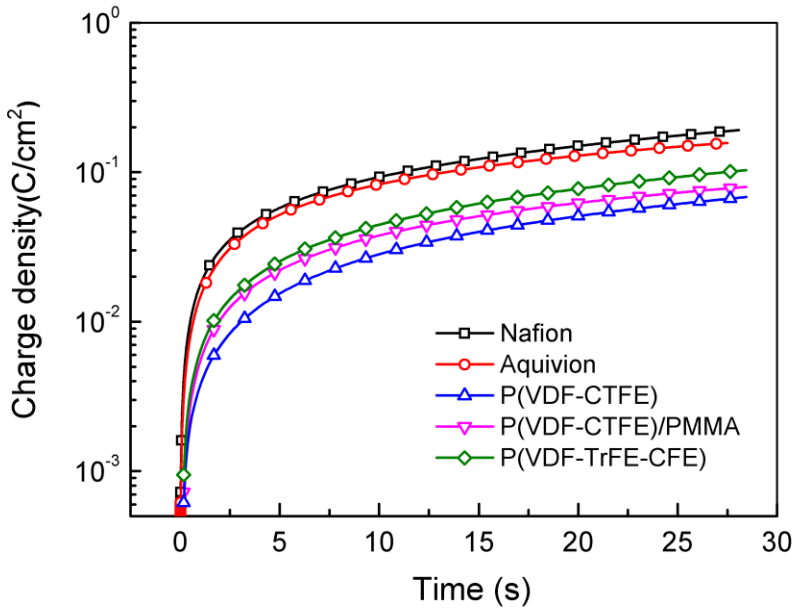


Figure 5: charge responses of five ionic polymer membrane actuators

It is noticed that due to the difference in polymer density, the corresponding volume percentages of the EMI-Tf content in the films vary slightly, which may affect the electrical performances of the devices. However, since the observed difference in EMI-Tf volume percentage in different films is within 5%, it is unlikely to be responsible for the observed large difference (more than 100%) in charge stored at the electrodes between the ionomers and PVDF-based polymers.

### 1.4 Electromechanical coupling

Figure 6 shows the evolution of the bending actuation of the five ionic polymer membrane actuators under a 4 V step voltage. The actuator initially bends towards the anode, and as the time progresses, it reverses the actuation direction and bends towards the cathode. This is an intrinsic properties of the ionic polymer actuators that caused by the two mobile ions in the actuation process. As shown figure 6, P(VDF-CTFE), P(VDF-CTFE)/PMMA, and P(VDF-TrFE-CFE) all possess enhanced electromechanical responses compared to Aquivion® and Nafion®. P(VDF-CTFE) exhibits bending magnitude of 0.45 mm$^{-1}$ and a relatively faster initial strain (<10 s) response, which is an indication of better AC actuation for this materials which will be discussed in the next section. P(VDF-CTFE)/PMMA displayed a even higher strain response (0.75 mm$^{-1}$) at longer actuation time scale (>12 s). P(VDF-TrFE-CFE) showed

the highest strain response (0.87 $mm^{-1}$) and the fastest initial strain response. The later stage strain response is mainly determined the by diffusion process of anions near the electrodes (due to the ion concentration gradient). All PVDF polymers bend back at larger time scales, which follows the 2-carrier model developed earlier.

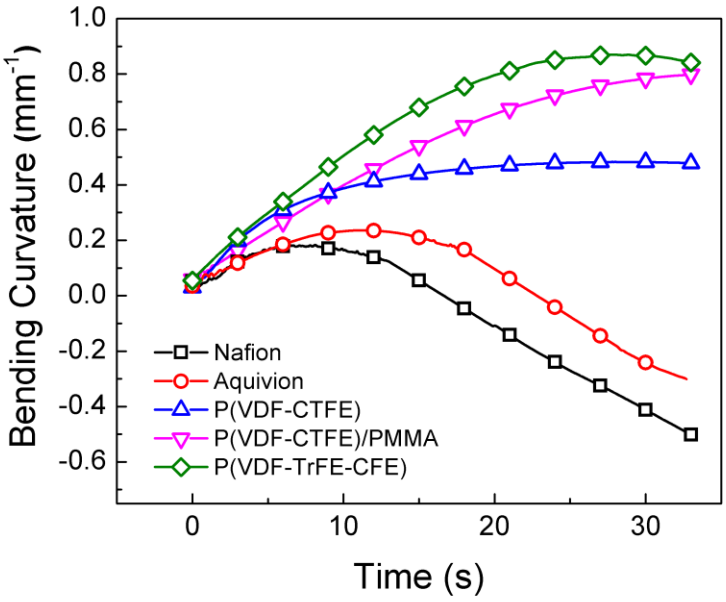


Figure 6: bending actuation of the five ionic polymer membrane actuators under a 4 V step voltage

The mechanical energy density of the five *i*-EAP membrane actuators can be calculated from the bending curvature $\kappa$ and the Young's moduli of the ionic polymer layer $Y_i$ and the Au layer $Y_m$ by the equation below,

$$u_m = \frac{1}{t_i + 2t_m}\left[\int_0^{\frac{t_i}{2}} Y_i(\kappa y)^2 dy + \int_{\frac{t_i}{2}}^{\frac{t_i}{2}+t_m} Y_m(\kappa y)^2 dy\right] \quad (6.2)$$

where $y$ is the distance from the middle plane of the actuator.

Meanwhile, the electrical energy density $u_e$ could be calculated as follows,

$$u_e = QV/At \quad (6.3)$$

where $Q/A$ is the charge density, $V$ is the applied voltage, and $t$ is the total sample thickness. Hence, the electromechanical energy efficiency of the actuators can be deduced by the following relation.

$$\eta = u_m/u_e \times 100\% \quad (6.4)$$

As illustrated in Figure 7, P(VDF-CTFE), P(VDF-CTFE)/PMMA and P(VDF-TRFE-CFE) has achieved an order of magnitude higher energy efficiencies than Nafion® and Aquivion®, which makes them preferred materials for i-EAP actuators.

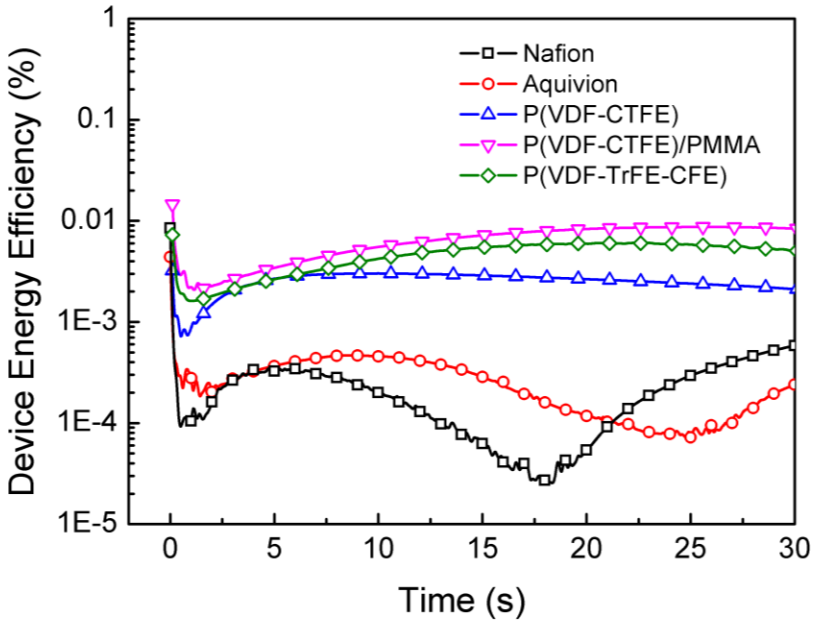


Figure 7: Device energy efficiency (%) vs. time (s)

Although the electromechanical coupling and efficiency is significantly improved by utilizing P(VDF-CTFE) based materials, it is found that the efficiencies of these membrane actuators are still very low (<0.1%), since their device configuration is not optimized for applications. *i*-EAP actuators (e.g. IPCNCs) are complex systems that are featured by many components, such as the electrolyte, polymer matrix and composite electrode. By adding conductor network composite (CNC) and varying the electrolyte, the electromechanical transduction efficiency, as well as the actuation speed, can be improved.

**1.5 Energy efficiency under alternating current (AC) stimulus**

Since the electromechanical coupling between ionic liquids and the polymer matrix is stronger at a short charging time (t< 10 s) than a long time, a comparison of the five ionic polymer membrane actuators under AC stimulus is performed. An example of the AC response of ionic polymer membrane actuators under 4V 0.1Hz triangle wave is presented in Figure 8 and a comparison of the five membrane actuators studied is displayed in Figure 9.

Again, despite their large Young's moduli, PVDF based *i*-EAP membrane actuators have larger bending curvatures, while consuming less driving current than Nafion® and Aquivion® perfluorosulfonate ionomers, which confirmed that P(VDF-CTFE), P(VDF-CTFE)/PMMA and P(VDF-TRFE-CFE) are superior *i*-EAP actuator material candidates in effectively generating strain.

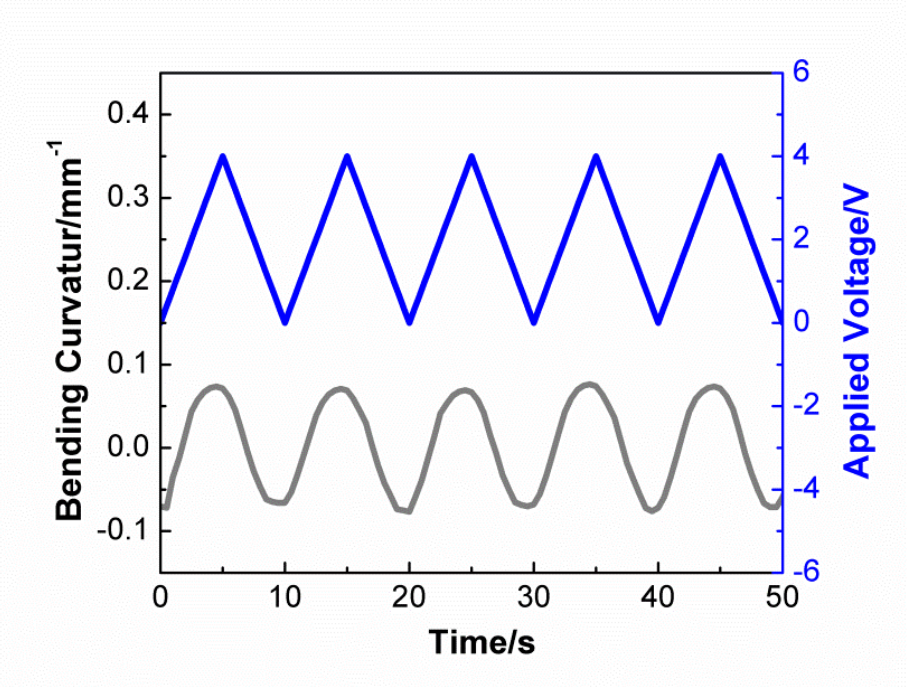


Figure 8: Triangle wave representation of AC response of ionic polymer membrane actuators under 4V 0.1Hz

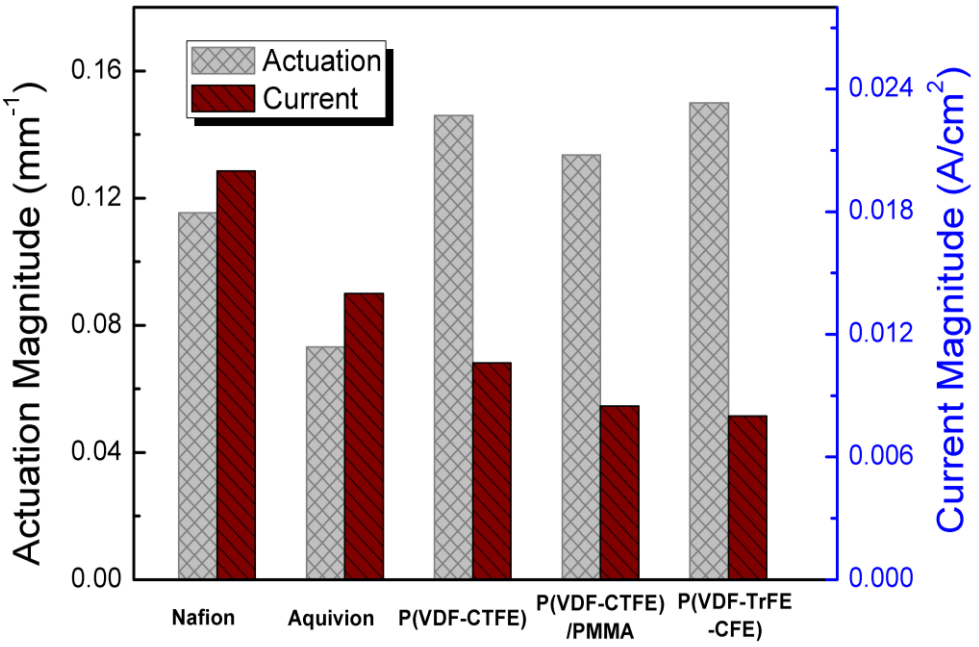


Figure 9: comparison of the five ionic polymer membrane actuators under AC stimulus

In conclusion, ionic polymer membrane actuators based on P(VDF-CTFE), P(VDF-CTFE)/PMMA and P(VDF-TrFE-CFE) polymers with 40 wt% of EMI-Tf are investigated.

These actuators exhibit great electromechanical responses in comparison with Nafion® and Aquivion® perfluorosulfonate ionomers. The improvement in bending actuation and energy efficiency illustrates that the electromechanical coupling between the ionic liquids and the polymer matrix is enhanced by selecting *i*-EAP polymers without flexible side chains or clustered ion channels. Under both DC and AC stimulus, the reduction in charge consumption and the increase in mechanical energy output of the PVDF based membrane actuators lead to order-of-magnitude higher electromechanical energy efficiencies, which indicates that they are valuable *i*-EAP actuator materials.

## 2. Fundamentals of Ion Transport (U. H. Choi and R. Colby)

### Morphology and Dielectric Properties of Poly(imidazolium acrylate) Ionomers

In collaboration with Minjae Lee from Dr. Gibson group and Sharon Wang form Dr. Winey group, I am studying the physical properties of imidazolium-based polymers with counterions as $PF_6^-$ vs $Tf_2N^-$ and with different imidazolium pendent tail length as *n*-butyl vs *n*-dodecyl, using dielectric relaxation spectroscopy (DRS). In this report, a physical model of electrode polarization (EP) is used to separate ionic conductivity of the ionomers into number density of conducting ions and their mobility. $Tf_2N^-$ counterions display higher ionic conductivity and mobility than $PF_6^-$ counterions, as anticipated by ab initio calculations. Ion mobility is coupled to polymer segmental motion, as there are observed to share the same Vogel temperature. Ionomers with the *n*-butyl tail impart much larger static dielectric constant than those with the n-dodecyl tail. From the analysis of the static dielectric constant using Onsager theory, there is more ionic aggregation in ionomers with the *n*-dodecyl tails than in those with the *n*-butyl tails, consistent with X-ray scattering, which shows a much stronger ionic aggregate peak for the ionomers with dodecyl tails on their imidazolium side-chains.

### A. X-Ray Scattering

Figure 1a compares the room temperature X-ray scattering profiles for the four imidazolium-acrylate ionomers with different side chain tail lengths and counterions, measured by David Salas-de la Cruz from Dr. Winey group. Three distinct peaks are observed: the higher-angle peak at $q_I \approx 14\,\mathrm{nm}^{-1}$ corresponds to the amorphous halo, the more subtle intermediate-angle peak at $q_{II} \approx 8\,\mathrm{nm}^{-1}$ is attributed to correlation between the anions, and the lower-angle peak at $q_{III} \approx 2\,\mathrm{nm}^{-1}$ for the ionomers with *n*-dodecyl tails and $q_{III} \approx 4\,\mathrm{nm}^{-1}$ for the ionomers with *n*-butyl tails indicates the spacing between ion aggregates. The intensity of the ionic aggregation scattering peak at $q_{III}$ increases

significantly, as the tail length increases from *n*-butyl to *n*-dodecyl. The ionomer peak ($q_{III}$) intensity arises from both the uniformity of the interaggregate spacing and the electron density difference between the matrix and the ionic aggregates. Both the peak positions and peak intensities remain nearly the same with increasing temperature as shown in Figures 1b, c, and d, measured by Sharon Wang from Dr. Winey group. Morphology studies of 1-alkyl-3-methylimidazolium $PF_6^-$ or $Tf_2N^-$ ionic liquids as a function of the alkyl chain length by means of neutron scattering and molecular dynamics simulation observed quite similar ion aggregation: ionic liquids with long side chains exhibit a bicontinuous morphology, one region consisting of polar moieties (anion / cation pairs and aggregates) and the other consisting of non-polar alkyl tails.

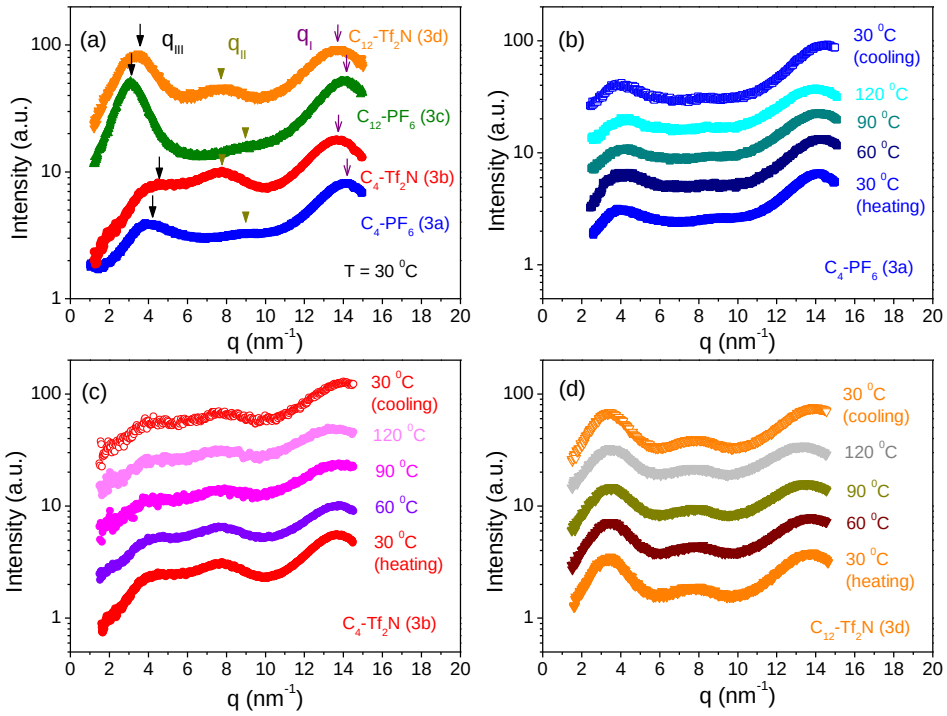


**Figure 1**| X-ray scattering intensity as a function of scattering wavevector $q$ for (a) the imidazolium-based ionomers at room temperature and (b) **$C_4$-$PF_6$ (3a)**, (c) **$C_4$-$Tf_2N$ (3b)** and (d) **$C_{12}$-$Tf_2N$ (3d)**, each at four temperatures (30, 60, 90 and 120 °C). The arrows indicate peaks that correspond to the amorphous halo ($q_I$), anion-anion correlations ($q_{II}$), and separation between ionic aggregates ($q_{III}$). The intensity of the ionic aggregation spacing peak ($q_{III}$) increases enormously as the tail length increases from *n*-butyl to *n*-dodecyl, which we interpret to signify that dodecyl tails favor ion aggregation. The data were shifted on the log intensity scale for clarity.

## B. Conducting Ion Content

The temperature dependence of the number density of simultaneously conducting ions $p$ calculated from EP model is plotted in Figure 2 and the fraction of ions participating in conduction ($p/p_0$ wherein $p_0$ is the total anion number density) is shown in the Figure 2 inset. The temperature dependence of simultaneously conducting ion concentration for these imidazolium-based ionomers is well described by an Arrhenius equation

$$p = p_\infty \exp\left(-\frac{E_a}{RT}\right) \qquad (1)$$

wherein $p_\infty$ and $E_a$ are the conducting ion concentration as $T \to \infty$ and the activation energy for conducting ions, respectively. The fact that for some ionomers $p_\infty$ is smaller than $p_0$ indicates some of the counterions are too strongly aggregated to participate in ionic conduction, and $1 - p_\infty / p_0$ tells us the fraction of counterions that are trapped and are unable to participate in conduction. The observation that ionomers with *n*-dodecyl tails have much higher fraction of trapped ions than ionomers with *n*-butyl tails suggests **$C_{12}$-$PF_6$ (3c)** and **$C_{12}$-$Tf_2N$ (3d)** exhibit stronger ionic aggregation than **$C_4$-$PF_6$ (3a)** and **$C_4$-$Tf_2N$ (3b)**, consistent with the stronger $q_{III}$ peak in X-ray scattering in previous section and the analysis of the static dielectric constant in next section. The activation energies for the $PF_6^-$ ionomers (**$C_4$-$PF_6$ (3a)** and **$C_{12}$-$PF_6$ (3c)**) are higher than those for $Tf_2N^-$ ionomers (**$C_4$-$Tf_2N$ (3b)** and **$C_{12}$-$Tf_2N$ (3d)**), indicating a lower binding energy for the imidazolium ions with the larger $Tf_2N^-$ ions than for the $PF_6^-$ ions as anticipated by the *ab initio* calculations.

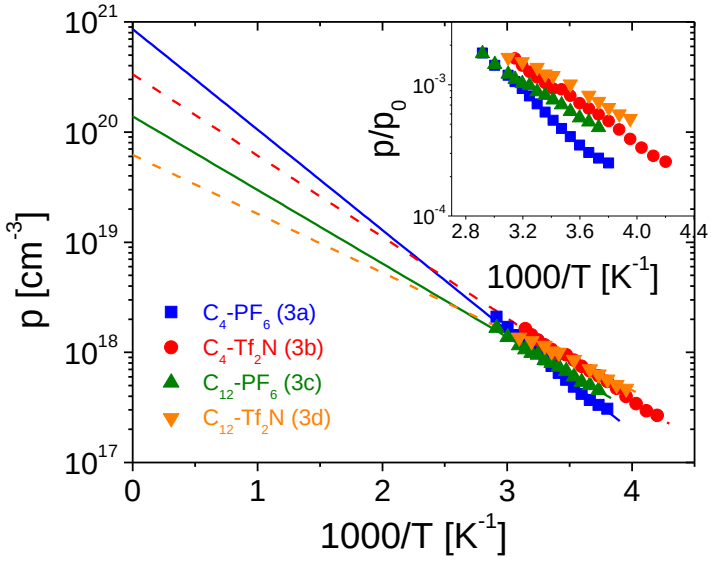

**Figure 2**| Temperature dependence of simultaneously conducting ion concentration $p$. Solid ($PF_6^-$ ionomers) and dashed ($Tf_2N^-$ ionomers) lines are Arrhenius fits to Eq. 1 with two fitting parameters ($E_a$ and $p_\infty$). The observation that ionomers with the *n*-dodecyl tails have much lower $p_\infty$ than ionomers with the *n*-butyl tails suggests that the former contain more aggregated ions than the latter. The inset displays the fraction of anions simultaneously participating in conduction ($p$ divided by the total anion concentration $p_0$).

The inset in Figure 2 indicates that the fraction of counterions simultaneously participating in conduction ($p/p_0$) in these single-ion conductors is quite low, < 0.1% of the total number of counterions, except at the highest temperatures studied. The conducting ion content evaluated from the EP model is the number density of ions in a conducting state in any snapshot, which sets the boundary condition for the solution of the Poisson-Boltzmann equation. Only a small fraction of total ions is in a conducting state at any given instant in time, similar to observations on other single-ion conducting ionomers with alkali metal counterions or ionic liquid counterions.

### C. Static Dielectric Constant

The static dielectric constant $\varepsilon_s$ is defined as the low frequency plateau of $\varepsilon'(\omega)$ before EP begins and calculated using EP model from the measured $\sigma_{DC}$ and $\tau_\sigma$ obtained from fitting EP Figure 3 displays the static dielectric constant for these imidazolium-based ionomers and the non-ionic polymer **5** vs. inverse temperature. The non-ionic polymer **5** having no imidazolium cation nor anion exhibits $\varepsilon_s = 8$ at room temperature. $\varepsilon_s$ for the ionomers with imidazolium cation and either $PF_6^-$ or $Tf_2N^-$ anion is much larger, especially for those with *n*-butyl tails (**$C_4$-$PF_6$ (3a)** and **$C_4$-$Tf_2N$** (**3b)**) with $\varepsilon_s \approx 80$ at the lowest temperatures studied. As the tail length increases from butyl to dodecyl, $\varepsilon_s$ in **$C_{12}$-$PF_6$ (3c)** and **$C_{12}$-$Tf_2N$ (3d)** significantly decreases. Singh and Kumar developed a simple predictive model for the estimation of dielectric constants of imidazolium-based ionic liquids with $PF_6^-$ or $Tf_2N^-$ as a counterion, based on internal pressure and a cohesive energy density approach. They showed that the dielectric constant of the ionic liquids also decreases with the increase in alkyl chain length of the imidazolium moiety.

The temperature dependence of $\varepsilon_s$ for the non-ionic polymer can be understood through the Onsager equation

$$\left[ \frac{\varepsilon_s - \varepsilon_\infty \quad 2\varepsilon_s + \varepsilon_\infty}{\varepsilon_s \quad \varepsilon_\infty + 2^{\,2}} \right]_{nonionic} = \frac{1}{9\varepsilon_0 kT} \sum_i \nu_i m_i^{\,2} \qquad (2)$$

wherein $\nu_i$ is the number density of dipoles, $m_i$ is their dipole moment, and $\varepsilon_\infty$ is the high-frequency limit of the dielectric constant (here taken to be an approximate value of $\varepsilon_\infty = n^2$, where $n$ is the refractive index). The purple dotted line in Figure 3 is fit to Eq. 2 with the $\sum_i \nu_i m_i^2$ term as the sole fitting parameter, showing that $\varepsilon_s$ of the non-ionic polymer **5** is well described by the Onsager equation. The polymerized ionic liquids have an imidazolium cation attached to each side chain with the associated anion ($PF_6^-$ or $Tf_2N^-$) and for such ionomers the contribution of the ions to the static dielectric constant can be analyzed by simply adding the effect of ion pairs to Eq. 2:

$$\left[\frac{\varepsilon_s - \varepsilon_\infty}{\varepsilon_s}\frac{2\varepsilon_s + \varepsilon_\infty}{\varepsilon_\infty + 2}^2\right]_{ionomer} = \frac{\nu_{pair} m_{pair}^2}{9\varepsilon_0 kT} + \left[\frac{\varepsilon_s - \varepsilon_\infty}{\varepsilon_s}\frac{2\varepsilon_s + \varepsilon_\infty}{\varepsilon_\infty + 2}^2\right]_{nonionic} \quad (3)$$

wherein $\nu_{pair}$ is the number density of ion pairs and $m_{pair}$ is their dipole moment. The solid and dashed lines in Figure 3 are the Onsager predictions of Eq. 3 for each ionomer, assuming all ions are in the isolated ion pair state ($\nu_{pair} = p_0$) with the contact pair dipole from *ab initio*. Starting at the top of Figure 3 the Onsager predication for the ionomers with *n*-butyl tails, **$C_4$-$PF_6$ (3a)** and **$C_4$-$Tf_2N$** (**3b)** agree reasonably with their measured $\varepsilon_s$. The Onsager equation predicts that the dielectric constant decreases as temperature increases (as 1/T) from thermal randomization. The Onsager prediction for **$C_4$-$PF_6$ (3a)** is ~13% above the measured dielectric constant, presumably indicating that the dipole of the ion pairs for imidazolium-$PF_6$ is overestimated by ~7% in our *ab initio* calculations. Although the ionomers with *n*-dodecyl tails exhibit dielectric constants that parallel the Onsager prediction of Eq. 3, **$C_{12}$-$PF_6$ (3c)** and **$C_{12}$-$Tf_2N$ (3d)** show nearly identical dielectric constants across the entire temperature range, that are more than a factor of 2 below the Onsager prediction of Eq. 3. Those ionomers with *n*-dodecyl tails are still significantly more polar than the non-ionic polymer **5** but many of their ions are aggregated, analogous to lithium sulfonate-PEO ionomers.[54]

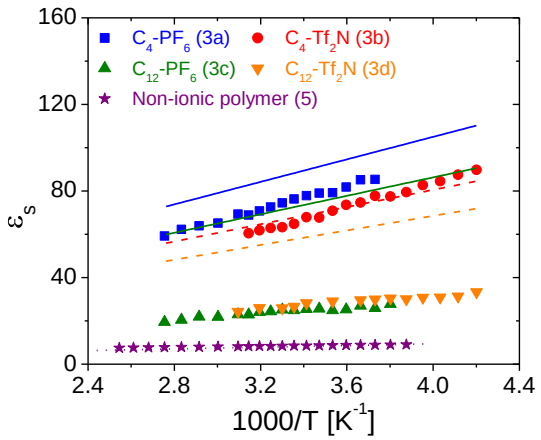

**Figure 3**| Temperature dependence of static dielectric constant $\varepsilon_s$ for imidazolium-based ionomers and a non-ionic polymer. The lines are predictions of the Onsager equation with fixed concentration and strength of dipoles: the purple dotted line is Eq. 2 for non-ionic polymer **5** with $\sum_i \nu_i m_i^2 / \ 9\varepsilon_0 k \ = 249\mathrm{K}$ as the sole fitting parameter and the colored solid and dashed lines are Eq. 3 for the four imidazolium-based ionomers, assuming all ions exist as isolated contact pairs ($\nu_{pair} = p_0$) with dipoles given by the *ab initio* estimates and assuming the Kirkwood correlation factor $g = 1$.

Another way to view ion aggregation is that this effectively correlates neighboring dipoles of ion pairs. Correlation of neighboring dipoles was considered by Kirkwood and Fröhlich by introducing a prefactor $g$ into Eq. 3 and this idea is extensively utilized.

$$g = \frac{9\varepsilon_0 kT}{\nu_{pair} m_{pair}^2} \left\{ \frac{\varepsilon_s - \varepsilon_\infty \quad 2\varepsilon_s + \varepsilon_\infty}{\varepsilon_s \quad \varepsilon_\infty + 2^{\ 2}} - \left[ \frac{\varepsilon_s - \varepsilon_\infty \quad 2\varepsilon_s + \varepsilon_\infty}{\varepsilon_s \quad \varepsilon_\infty + 2^{\ 2}} \right]_{nonionic} \right\} \quad (4)$$

If there are no specific correlations, $g = 1$ and the Kirkwood-Fröhlich equation reduces to the Onsager equation. For polar liquids in which dipoles tend to orient with parallel dipole alignments, $g > 1$. For example, hydrogen bonding in water makes *g* = 2.9 at 0 $^{o}$C, decreasing steadily as temperature is increased, to *g* = 2.3 at 100 $^{o}$C. When dipoles either prefer antiparallel alignment or a significant fraction of dipoles are unable to move in response to the field, $g < 1$. Our imidazolium ionomers exhibit apparent Kirkwood correlation factors $0.8 < g < 1.1$ for ionomers with *n*-butyl tails and $0.2 < g < 0.4$ for ionomers with *n*-dodecyl tails, over the whole temperature range studied. This can explain the strong increase in intensity of the ionic aggregate scattering peak in the X-ray data of Figure 1, as the tail length increases from *n*-butyl to *n*-dodecyl. Ionic aggregation makes $g << 1$ for the ionomers with *n*-dodecyl tails while $g \cong 1$ for the ionomers with *n*-butyl tails

- Comparison of Dielectric Constant of Imidazolium-based Monomers and Their Ionomers

In collaboration with Anuj Mittal from Dr. Gibson group, I am studying the physical properties of imidazolium-based monomers and their polymers with $Tf_2N^-$ counterion, using dielectric relaxation spectroscopy (DRS).

Figure 4 displays the frequency dependence of the dielectric constant $\varepsilon'(\omega)$ for two ILs (1-butyl-3-methylimidazolium bis((trifluoromethyl)sulfonyl)imide ([**$C_4$MIM][$Tf_2$N]**) and 1-[2'-tri(ethylene glycol)oxyethyl]-3-butylimidazolium bis((trifluoromethyl)sulfonyl)imide (**RTIL71**)), one IL monomer (**2b**) and its PIL (**4b**). The static dielectric constant $\varepsilon_s$ is

defined as the low frequency plateau of $\varepsilon'(\omega)$ before the onset of electrode polarization (EP) starts. However, $\varepsilon'(\omega)$ was not observed to clearly plateau before EP, but to gradually decrease with increasing frequency, indicating underlying relaxations. To display the $\varepsilon_s$ difference between the ionic liquids (ILs), the IL monomer and the polymerized ionic liquid (PIL), the dielectric constant spectra in the inset of Figure 4 were horizontally shifted. Interestingly, the PIL exhibits *higher* static dielectric constant than either its IL monomer or the smaller ILs. In contrast with this ionic polymer, the non-ionic polymers, after polymerized, exhibit the decrease of their static dielectric constant due to the increase in the hindrance to the orientation of polar groups.

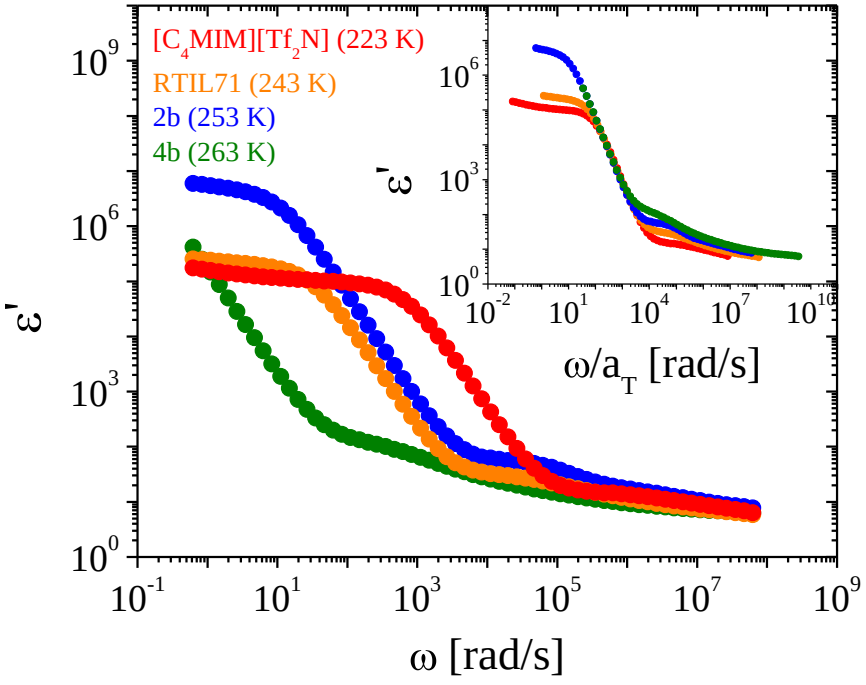


**Figure 4**| Dielectric dispersion spectra of the ILs ([$C_4$MIM][$Tf_2$N] at 223 K and RTIL71 at 243 K), IL monomer (2b at 253 K) and PIL (4b at 263 K), showing electrode polarization at lower $\omega$ and ion rearrangement at higher $\omega$. The inset shows the dielectric spectra shifted horizontally to superimpose the electrode polarization build-up and hence compare the static dielectric constant between the ILs, the IL monomer and the PIL. The static dielectric constant is usually the value of $\varepsilon'$ before electrode polarization starts but in these ionic liquid materials the ion rearrangements are not complete before EP starts, making $\varepsilon_s$ somewhat higher than the value of $\varepsilon'$ before EP starts.

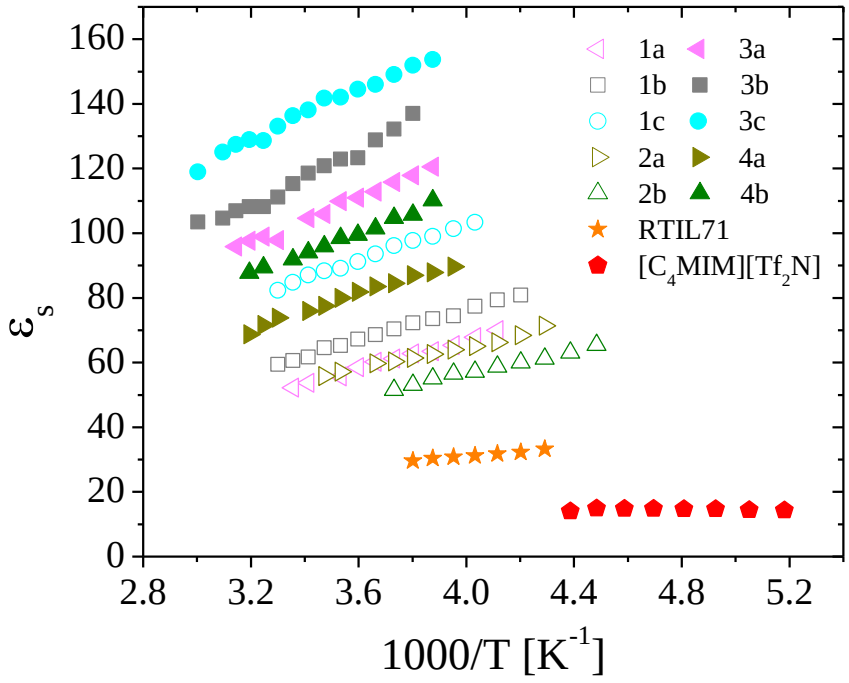


**Figure 5**| Temperature dependence of static dielectric constant for IL (**[$C_4$MIM][$Tf_2$N]** and **RTIL71**), IL monomers (**1a**, **1b**, **1c**, **2a** and **2b**) and PILs (**3a**, **3b**, **3c**, **4a** and **4b**).

Figure 5 displays $\varepsilon_s$ values for the imidazolium-based PILs, their IL monomers and the two ILs vs. inverse temperature. The neat ILs exhibit the lowest static dielectric constants at the temperatures studied. After polymerized, the $\varepsilon_s$ of the PILs are almost 2-fold higher than that of their IL monomers. Furthermore, we can observe the influence of backbone structure (acrlyate vs. methacrlyate) on the static dielectric constant. The methacrlyate monomers (**1a**, **1b** and **1c**) and their polymers (**3a**, **3b** and **3c**) exhibit higher $\varepsilon_s$ than the acrlyate monomers (**2a** and **2b**) and their polymers (**4a** and **4b**). In order to identify the origin of the difference in $\varepsilon_s$ with respect to IL monomer vs. PIL and acrylate vs. methacrylate, we have carefully explored dipolar relaxations in the dielectric loss derivative spectra

$$\varepsilon_{der} = -\frac{\pi}{2}\frac{\partial \varepsilon'(\omega)}{\partial \ln \omega},$$

elucidating the relaxation processes owing to removing the pure-loss conductivity contribution which obscures the loss peaks of interest that are due to ion motion or segmental relaxation.

Characteristic for the derivative dielectric loss curves of the ILs (**[C$_4$MIM][Tf$_2$N]** at 223 K and **RTIL71** at 243 K) is the occurrence of one main peak ($\alpha$), centered at 0.01 – 1 MHz (Fig. 6). It has been shown for the imidazolium-based ILs studied in the microwave regime that the same relaxation process, located at ~ 1 GHz, is observed at room temperature mainly due to the reorientation of the dipolar cation. In contrast to the ILs, an additional dipolar relaxation ($\alpha_2$), attributed to ions rearranging (i.e. exchanging states between isolated pairs and aggregates of pairs), in the IL monomer and PIL is observed at lower frequencies besides the $\alpha$ relaxation involving the typical characteristic of the glass transition dynamics at higher frequencies (Fig. 6).

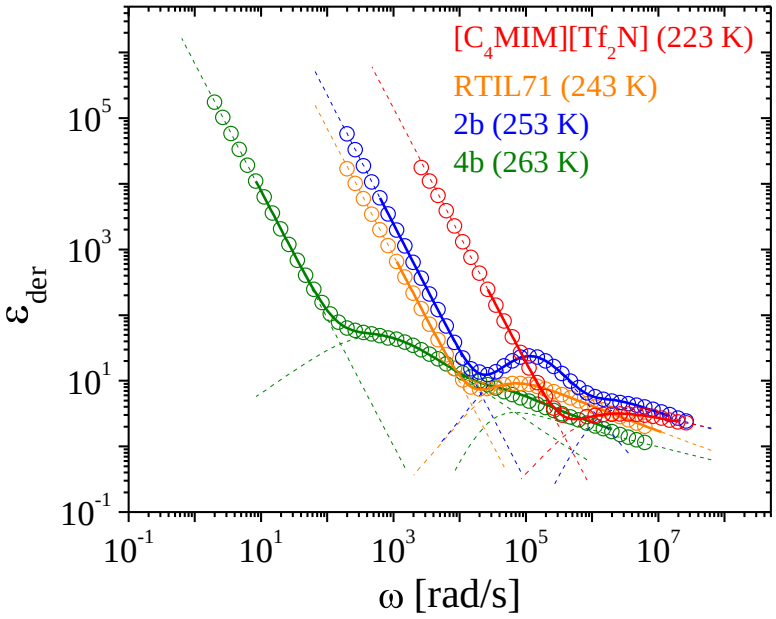


**Figure 6**| Dielectric loss derivative spectra fit (solid lines) to the sum of a power law for EP (dashed lines) and two derivative forms of the HN function of $\alpha_2$ and $\alpha$ processes (dashed lines) of the ILs (**[C$_4$MIM][Tf$_2$N]** at 223 K and **RTIL71** at 243 K) : one relaxation process ($\alpha$), and of the IL monomer (**2b** at 253 K) and the PIL (**4b** at 263 K) : two relaxation processes ($\alpha_2$ and $\alpha$).

The peak relaxation frequencies $\omega_{max}$ and strength $\Delta\varepsilon$ of the $\alpha_2$ and $\alpha$ processes can be extracted by fitting the derivative loss spectra with one power law for EP plus two Havriliak-Negami (HN) functions for those two dielectric relaxations. Such fits approximate the data quite well (Fig. 6) and give $\omega_{max}$ and $\Delta\varepsilon$ values of the $\alpha_2$ and $\alpha$ processes (Fig. 7). The peak relaxation frequencies normalized by an extrapolation of the $T_g(\alpha)$ values, which is comparable to the $T_g$ determined by DSC, follow the Vogel-Fulcher-Tammann (VFT) temperature dependence (Fig. 7a), indicating that these two relaxation processes are controlled by the glass transition temperature. This finding is

similar to the conductivity with $T_g/T$ (the inset in Figure 4a), demonstrating that conductivity is also strongly coupled with the glass transition temperature. In Figure 7b, the relaxation strength for the $\alpha_2$ process is much larger than that for the $\alpha$ process. Additionally, $\Delta\varepsilon_{\alpha_2}$ has strong temperature dependence, but $\Delta\varepsilon_{\alpha}$ has no temperature dependence with $\Delta\varepsilon_{\alpha} \approx 11$ for all IL monomers and PILs. The stronger $\alpha_2$ process involving ionic rearrangements primarily determines the temperature dependence of $\varepsilon_s$ shown in Figure 5. This can explain the fact that $\varepsilon_s$ of IL monomers and PILs exhibiting the additional $\alpha_2$ process is much higher than that of ILs exhibiting the only single $\alpha$ relaxation.

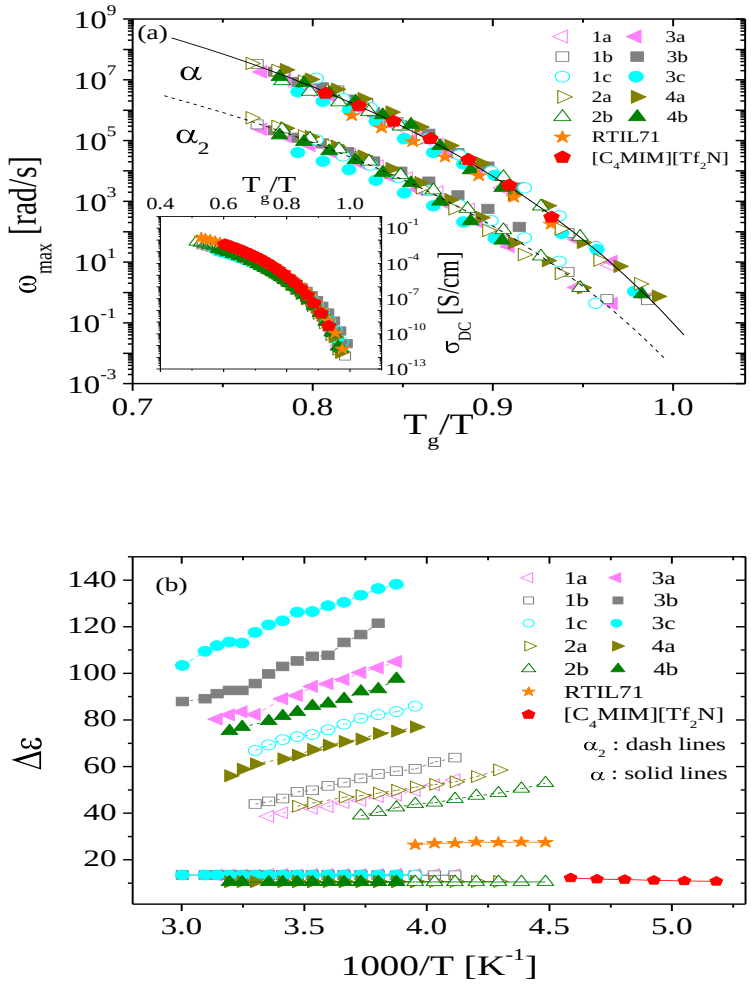


**Figure 7**| Temperature dependence of (a) relaxation frequency maxima $\omega_{max}$ (ionic conductivity $\sigma_{DC}$ in the inset) vs. $T_g/T$ and (b) relaxation strength $\Delta\varepsilon$ vs. 1000/T of the $\alpha_2$ (dash line) and $\alpha$ (solid line) processes (all ratios of $\Delta\varepsilon_{\alpha}$ of each PL and its IL monomer are identically unity).

● Viscoelastic Behavoir of Imidazolium-based Ionomers

In collaboration with Yuesheng Ye from Dr. Elabd group, I am studying the physical properties of imidazolium-based ionomers with $Tf_2N^-$ and $BF_4^-$ counterions, using rheometer.

To verify the effect of side chain length and counterion on $T_g$ and ionic aggregation in these ionomers, we study their viscoelasticity which allows one to observe the impact of associating ion pairs, or aggregates acting as physical crosslinks between chains.

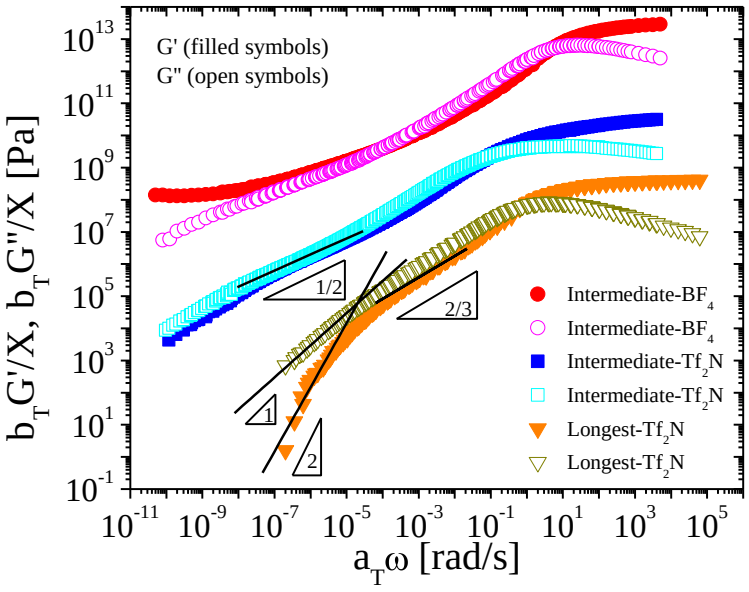


**Figure 8**| Storage ($b_T G'$, filled symbols) and loss ($b_T G''$, open symbols) moduli for imidazolium-based ionomers with $BF_4^-$ or $Tf_2N^-$ counterions. Master curves referenced to $T_g$: 358 K (**Intermediate-$BF_4$**), 288 K (**Intermediate-$Tf_2N$**) and 238 K (**Longest-$Tf_2N$**) are then divided by vertical shift factor, X for clarity.

Figure 8 shows the master curves of the storage $b_T G'$ and loss $b_T G''$ moduli on frequency $a_T \omega$ for these ionomers, constructed using time-temperature superposition (tTS) referenced at $T_g$ and using time- and modulus-scale multiplicative shift factors $a_T$ and $b_T$, respectively. tTS works well for these materials, which is consistent with an earlier finding of the success of tTS for imidazolim-based ionomers with various counteranions.[23,49] **Longest-$Tf_2N$** exhibits terminal behavior in $G'$ and $G''$ data, with a limiting slope of $\lim_{\omega \to 0}(\log G'/\log \omega) \sim 2$ and $\lim_{\omega \to 0}(\log G''/\log \omega) \sim 1$, respectively.[60] However, **Intermediate-$Tf_2N$** did not reach terminal response for frequencies nearly 5 orders of magnitude lower than **Longest-**

**$Tf_2N$**. For **Intermediate-$BF_4$**, while its $T_g$ is only 86 $^0$C, the terminal flow behavior was not observed at temperatures up to 200 $^0$C and rather the rubbery plateau appears at the low frequency. Typically, an extensive rubbery plateau is only observed in the bulk state of polymers when the molecular weight (MW) of the polymer exceeds $10^6$.[52] However, **Intermediate-$BF_4$** with a MW of 61,100 g/mol[34] exhibits viscoelastic behavior that resembles a crosslinked elastomer. Since **Intermediate-$Tf_2N$** with a similar MW of 43,080 g/mol[34] does not exhibit a plateau, this behavior is attributed to the strong ionic associations that occur in the ionomer with small counterions. These findings that terminal relaxation time increases with increasing ion content (or decreasing side chain length) and decreasing counterion radius have been observed in other ionomers. The slope of the glass-to-rubber transition region ($10^{-8} < a_T\omega < 10^{-4}$ rad/s) of $G'$ and $G''$ versus $\omega$ for **Intermediate-$Tf_2N$** is 1/2, which agrees with a Rouse model, while the slope of 2/3 for **Longest-$Tf_2N$** in the transition region ($10^{-5} < a_T\omega < 10^{-2}$ rad/s) follows a Zimm model, which is not surprising, since hydrodynamic interactions are likely to be important in the ionomer that was diluted by introducing non-ionic parts to the cation.

## TECHNOLOGY TRANSFER

### III. COLLABORATIONS

- Kraton Polymers (Long and Winey)
  J.-H. Choi, A. Kota, K. I. Winey*, *Industrial and Engineering Chemistry*, 49, 12093-12097, 2010. “Micellar morphology in sulfonated pentablock copolymer solutions.”
- Kimberly Clark Corporation (Long)
  Cationic polyelectrolytes as triggerable water-dispersible materials
- Sandia National Laboratories (Winey)
- National Institute for Standards and Technology (NIST) (Long)
  Microfluidic Devices for Polyelectrolyte Synthesis
- Army Research Laboratories (ARL) (Long)
  Graduate student exchanges (Steve June, VT/Josh Orlicki, ARL)
- NASA Glenn Research Center (Zhang and Dr. M. Yoonesi)
  Charge transport and storage in ionomers and ionic electroactive devices.

## ILEAD MURI Manuscripts (Total of 86)

## Peer Reviewed Papers - published:

1. J.-H. Choi, C. L. Willis, K. I. Winey, Effects of neutralization with $Et_3Al$ on structure and properties in sulfonated styrenic pentablock copolymers. *Journal of Membrane Science*, 428, 516-522, **2013**.

2. M. H. Allen, S. Wang, S. T. Hemp, Y. Chen, L. A. Madsen, K. I. Winey, T. E. Long, Hydroxyalkyl-containing imidazolium homopolymers: Correlation of structure with conductivity. *Macromolecules*, 46, 3037-3045, **2013**.

3. J.-H. Choi, Y. Ye, Y. A. Elabd, K. I. Winey, Network Structure and Strong Microphase Separation for High Ion Conductivity in Polymerized Ionic Liquid Block Copolymers. *Macromolecules*, 46, 5290-5300, **2013**.

4. Hemp, S. T.; Zhang, M.; Allen, M. H., Jr.; Cheng, S.; Moore, R. B.; Long, T.E., Comparing Ammonium and Phosphonium Polymerized Ionic Liquids: Thermal Analysis, Conductivity, and Morphology. *Macromolecular Chemistry and Physics* **2013**, 214(18), 2099-2107

5. Hemp, S. T.; Allen, M. H. Jr.; Smith, A. E.; Long, T. E., Synthesis and Properties of Sulfonium Polyelectrolytes for Biological Applications. *ACS Macro Letters* **2013**, 2(8), 731-735.

6. Gao, R.; Zhang, M.; Wang, S.; Moore, R. B.; Colby, R. H.; Long, T. E., Polyurethanes Containing an Imidazolium Diol-Based Ionic-Liquid Chain Extender for Incorporation of Ionic-Liquid Electrolytes. *Macromolecular Chemistry and Physics* **2013**, 214(9), 1027-1036.

7. Allen, M. H.; Day, K. N.; Hemp, S. T.; Long, T. E., Synthesis of Folic Acid-Containing Imidazolium Copolymers for Potential Gene Delivery Applications. *Macromolecular Chemistry and Physics* **2013**, 214(7), 797-805.

8. Allen, M. H., Jr.; Wang, S.; Hemp, S. T.; Chen, Y.; Madsen, L. A.; Winey, K. I.; Long, T.E., Hydroxyalkyl-Containing Imidazolium Homopolymers: Correlation of Structure with Conductivity. *Macromolecules* **2013**, 46(8), 3037-3045.

9. Gao, R.; Ramirez, S. M.; Inglefield, D. L.; Bodnar, R. J.; Long, T. E., The preparation of cation-functionalized multi-wall carbon nanotube/sulfonated polyurethane composites. *Carbon* **2013**, (54), 133-142.

*10.* Allen, M. H.; Hemp, S. T.; Zhang, M.; Zhang, M.; Smith, A. E.; Moore, R. B.; Long, T. E., Synthesis and characterization of 4-vinylimidazole ABA triblock copolymers utilizing a difunctional RAFT chain transfer agent. *Polymer Chemistry* **2013,** 4*(*7), *2333-2341.*

11. A. A. Lee, R. H. Colby and A. A. Kornyshev, Statics and Dynamics of Electroactuation with Single-Charge-Carrier Ionomers, *J. Phys.: Condens. Matt*. 25, 082203 (**2013**).

12. A. A. Lee, R. H. Colby and A. A. Kornyshev, Electroactuation with Single Charge Carrier Ionomers: the roles of Electrostatic Pressure and Steric Strain, *Soft Matter* 9, 3767 (**2013**)

13. Y. Liu, C. Lu, S. Twigg, M. Ghaffari, J. Lin, N. Winograd, Q. M. Zhang, Direct Observation of Ion Distributions near Electrodes in Ionic Polymer Actuators Containing Ionic Liquids. *Scientific Reports*, 3, 973 (**2013**)

14. Price, S.C.; Ren, X.; Jackson, A.C.; Ye, Y.; Elabd, Y.A.; Beyer, F.L. Bicontinuous Alkaline Fuel Cell Membranes from Strongly Self-Segregating Block Copolymers. *Macromolecules* **2013**, *46*, 7332-7340.

15. Choi, J.-H.; Ye, Y.; Elabd, Y.A.; Winey, K.I. Network Structure and Strong Microphase Separation for High Ion Conductivity in Polymerized Ionic Liquid Block Copolymers. *Macromolecules* **2013**, *46*, 5290-5300.

16. Choi, U H.; Mittal, A.; Price, T. L., Jr.; Gibson, H. W.; Runt, J.; Colby, R. H. Polymerized Ionic Liquids with Enhanced Static Dielectric Constant, *Macromolecules* **2013**, *46,* 1175-1186.

17. Ye, Y.; Wang, S.; Davis, E.M.; Winey, K.I.; Elabd Y.A. High Hydroxide Conductivity in Polymerized Ionic Liquid Block Copolymers. *ACS Macro Letters* **2013**, *2*, 575-580.

18. Ye, Y.; Stokes, K.K.; Beyer, F.L.; Elabd, Y.A. Development of Phosphonium-based Bicarbonate Anion Exchange Polymer Membranes. *J. Membrane Sci.* **2013**, *443*, 93-99.

19. J. Lin, Y. Liu, Q.M. Zhang, Influence of the Ionic Polymer Membrane Thickness on Charge dynamics of Ionic Liquids in Ionic Polymer Actuators. *Macromolecules*, 45, 2050 (**2012**)

20. Y. Liu, R. Zhao, J. Lin, S. Liu, Q. M. Zhang, H. Cebeci, R. Guzmán de Villoria, B. Wardle, R. Montazami, D. Wang, J. R. Heflin. Equivalent Circuit Modeling of Ionomer and Ionic Polymer Conductive network Composite Actuators Containing Ionic Liquids. *Sensors and Actuators*. A 181, (**2012**)

21. G. Hatipoglu, Y. Liu, R. Zhao, M. Yoonessi, D.M. Tigelaar, S. Tadigadapa, Q. M. Zhang, A Highly Aromatic and Sulfonated Ionomer for High Elastic Modulus Ionic Polymer Membrane Micro-actuators. *Smart Mater & Struct,* 21, 055015 (**2012**)

22. Y. Liu, R. Zhao, M. Ghaffari, J. Lin, M. Lin and Q. M. Zhang. Enhanced Electro-mechanical Responses of P(VDF-CTFE) based Actuators. DOI: 10.1021/ma300591a *Macromolecules* (**2012**)

23. Ye, Y.; Choi, J.-H.; Winey, K.I.; Elabd, Y.A. Polymerized Ionic Liquid Block and Random Copolymers: Effect of Weak Microphase Separation on Ion Transport. *Macromolecules* **2012**, *45*, 7027-7035.

24. Salas-de la Cruz, D.; Green, M.D.; Ye, Y.; Elabd, Y.A.; Long, T.E.; Winey, K.I. Correlating Backbone-to-Backbone Distance to Ionic Conductivity in Amorphous Polymerized Ionic Liquids. *J. Polym. Sci.: Part B: Pol. Phys.* **2012**, *50*, 338-346.

25. R. Montazami, D. Wang, J.R. Heflin, Influence of Conductive Network Composite Structure on the Electromechanical Performance of Ionic Electroactive Polymer Actuators, *International Journal of Smart and Nano Materials* 3, 204-213 (**2012**)

26. D. Salas-de la Cruz, J. G. Denis, M. D. Griffith, D. R. King, P. A. Heiney, K. I. Winey, Environmental chamber for *in situ* dynamic control of temperature and relative humidity during X-ray scattering, *Review of Scientific Instruments*, 83, 025112, **2012**.

27. K. Sinha, W. Wang, K. I. Winey, J. K. Maranas, Dynamic patterning in PEO based single ion conductors for Li ion batteries." *Macromolecules*, 45, 4354 - 4362, **2012.**

28. Y. Ye, J.-H. Choi, K. I. Winey, Y. A. Elabd, Polymerized ionic liquid block and random copolymers: Effect of weak microphase separation on ion transport *Macromolecules*, 45, 7027 - 7035, **2012**.

29. Wu, T.; Wang, D.; Zhang, M.; Heflin, J. R.; Moore, R. B.; Long, T. E., RAFT Synthesis of ABA Triblock Copolymers as Ionic Liquid-Containing Electroactive Membranes. *Applied Materials & Interfaces* **2012**, 4(12), 6552-6559.

30. Green, M. D.; Wang, D.; Hemp, S.T.; Choi, J-H.; Winey, K. I.; Heflin, J. R.; Long, T. E., Synthesis of imidazolium ABA triblock copolymers for electromechanical transducers. *Polymer* **2012**, 53(17), 3677-3686.

31. Gao, R.; Wang, D.; Heflin, J. R.; Long, T. E., Imidazolium sulfonate-containing pentablock copolymer-ionic liquid membranes for electroactive actuators. *Journal of Materials Chemistry* **2012**, 22(27), 13473-13476.

32. Hemp, S. T.; Smith, A. E.; Bryson, J. M.; Allen, M. H.; Long, T. E., Phosphonium-Containing Diblock Copolymers for Enhanced Colloidal Stability and Efficient Nucleic Acid Delivery. *Biomacromolecules* **2012**, 13(8), 2439-2445.

33. Green, M. D.; Choi, J-H.; Winey, K. I.; Long, T. E., Synthesis of Imidazolium-Containing ABA Triblock Copolymers: Role of Charge Placement, Charge Density, and Ionic Liquid Incorporation. *Macromolecules* **2012**, 45(11), 4749-4757.

34. Allen, M. H.; Hemp, S. T.; Smith, A. E.; Long, T. E., Controlled Radical Polymerization of 4-Vinylimidazole. *Macromolecules* **2012**, 45(9), 3669-3676.

35. Tamami, M.; Salas-de la Cruz, D.; Winey, K. I.; Long, T. E., Structure-Property Relationships of Water-Soluble Ammonium-Ionene Copolymers. *Macromolecular Chemistry and Physics* **2012**, 213(9), 965-972.

36. Suga, T.; Hunley, M. T.; Long, T. E.; Nishide, H., Electrospinning of radical polymers: redox-active fibrous membrane formation. *Polymer Journal* **2012**, 44(3), 264-268.

37. Hemp, S. T.; Hunley, M. T.; Cheng, S.; DeMella, K. C.; Long, T. E., Synthesis and solution rheology of adenine-containing polyelectrolytes for electrospinning. *Polymer* **2012**, 53(7), 1437-1443.

38. Salas-de la Cruz, D.; Green, M. D.; Ye, Y.; Elabd, Y. A.; Long, T. E.; Winey, K. I., Correlating backbone-to-backbone distance to ionic conductivity in amorphous polymerized ionic liquids. *Journal of Polymer Science, Part B: Polymer* Physics **2012**, 50(5), 338-346.

39. Hemp, S. T.; Allen, M. H.; Green, M. D.; Long, T. E., Phosphonium-containing polyelectrolytes for nonviral gene delivery. *Biomacromolecules* **2012**, 13(1), 231-238.

40. Aitken, B. S.; Buitrago, C. F.; Heffley, J. D.; Lee, M.; Gibson, H. W. Winey, K. I.; Wagener, K. B. Precision Ionomers: Synthesis and Thermal/Mechanical Characterization, *Macromolecules* **2012**, *45,* 681–687.

41. Choi, U-H.; Lee, M.; Wang, S.; Liu, W.; Winey, K. I.; Gibson, H. W.; Colby, R. H. Ionic Conduction and Dielectric Response of Poly(imidazolium acrylate) Ionomers, *Macromolecules* **2012**, *45,* 3974–3985.

42. C. Daengngam, M. Hofmann, Z. Liu, A. Wang, J.R. Heflin, Y. Xu Demonstration of a Cylindrically-Symmetric Second-Order Nonlinear Fiber with Self-Assembled Organic Surface Layers, **2011,** *Optics Express* 19, 10326-10335.

43. R. Montazami, S. Liu, Y. Liu, D. Wang, Q. Zhang, J.R. Heflin Thickness Dependence of Curvature, Strain, and Response Time in Ionic Electroactive Polymer Actuators Fabricated via Layer-by-Layer Assembly, **2011** *J. Appl. Phys.* 109, 104301:1-5.

44. K.G. Wilmsmeyer, X. Zhang, and L.A. Madsen, Switchable bistable ordering and real-time alignment dynamics in wormlike micelles, *Soft Matter* **2011** 8, 57-60.

45. Green, M. D., Schreiner, C., Long, T. E., Thermal, Rheological, and Ion-Transport Properties of Phosphonium-Based Ionic Liquids. *Journal of Physical Chemistry A*, **2011**, 115(47), 13829-13835.

*46.* Green, M. D.; Salas-de la Cruz, D.; Ye, Y.; Layman, J. M.; Elabd, Y. A.; Winey, K. I; Long, T. E. Alkyl-Substituted N-Vinylimidazolium Polymerized Ionic Liquids: Thermal Properties and Ionic Conductivities. *Macromol Chem Phys* **2011** *212* (23), 2522-2528.

47. Green, M.D.; Allen, Jr., M.H.; Dennis, J. M.; Salas-de la Cruz, D.; Gao, R.; Winey, K. I.; Long, T. E. Tailoring Macromolecular Architecture with Imidazole Functionality: A Perspective for Controlled Polymerization Processes. *European Polymer Journal* 2011. 47(4), 486-496.

48. Weber, R.L.; Ye, Y.; Banik, S.M.; Elabd, Y.A.; Hickner, M.A.; Mahanthappa, M.K. Thermal and Ion Transport Properties of Hydrophilic and Hydrophobic Polymerized Styrenic Imidazolium Ionic Liquids. *J. Polym. Sci.: Part B: Pol. Phys.* **2011**, *49*, 1287-1296.

49. Weber, R. L.; Ye, Y.; Schmitt, A. L.; Banik, S. M.; Elabd, Y. A.; Mahanthappa, M. K. Effect of Nanoscale Morphology on the Conductivity of Polymerized Ionic Liquid Block Copolymers. *Macromolecules* **2011**, *44*, 5727-5735.

50. Allen Michael H. Jr.; Green Matthew D.; Getaneh Hiwote K.; et al. Tailoring Charge Density and Hydrogen Bonding of Imidazolium Copolymers for Efficient Gene Delivery *Biomacromolecules* **2011**. (12)6. 2243-2250

51. Weber Ryan L.; Ye Yuesheng; Schmitt Andrew L.; et al. Effect of Nanoscale Morphology on the Conductivity of Polymerized Ionic Liquid Block Copolymers. *Macromolecules* **2011** 44(14); 5727-5735 .

52. Reza Montazami, Sheng Liu, Yang Liu, Dong Wang, Qiming Zhang, and James R. Heflin Thickness dependence of curvature, strain, and response time in ionic electroactive polymer actuators fabricated via layer-by-layer assembly. *Journal of Applied Physics* **2011** (109) 104301:1-5.

53. Tudryn Gregory J.; Liu Wenjuan; Wang Shih-Wa; et al. Counterion Dynamics in Polyester-Sulfonate Ionomers with Ionic Liquid Counterions. *Macromolecules* **2011** (44) 9; 3572-3582.

54. X. Chen, Y. Zhang, H. Wang, S-W. Wang, S. Liang and R.H. Colby, "Solution rheology of cellulose in 1-butyl-3-methyl imidazolium chloride" *J Rheol* **2011**, 55(3), 485-494.

55. X. Chen, S. Liang, S-W. Wang, Y. Zhang, H. Wang and R.H. Colby, "Solution rheology of cellulose in 1-butyl-3-methyl imidazolium chloride and 1-ethyl-3-methyl imidazolium methylphosphonate" *Polymeric Materials: Science & Engineering* **2011**, 104, 586-588

56. S-W. Wang, W.J. Liu, and R.H. Colby, "Counterion dynamics in polyurethane-carboxylate ionomers with ionic liquid counterions" *Chem Mater* **2011**, 23, 1862-1873.

57. Lee Minjae; Choi U. Hyeok; Colby Ralph H.; et al. Ion Conduction in Imidazolium Acrylate Ionic Liquids and their Polymers. *Chemistry Of Materials* **2011** (22) 5814-5822.

58. Lee, M.; Choi, U-H.; Salas-de la Cruz, D.; Winey, K. I.; Colby, R. H.; Gibson, H. W., Imidazolium Polyesters, *Adv. Funct. Mater.* **2011**, *20,* 708-717.

59. Lee, M.; Wi, S.; Slebodnick, C.; Gibson, H. W. 1,2-Bis[N-(N'-alkylimidazolium)]ethane Salts as a New Class of Organic Ionic Plastic Crystals, *J. Mater. Chem. (21)* **2011**.

60. J. K. Park, J. Li, G. Divoux, L. A. Madsen, and R. B. Moore , Oriented Morphology and Anisotropic Transport in Uniaxially Stretched Perfluorosulfonate Ionomer Membranes.. *Macromolecules* **2011** (44), 5701–5710.

61. J. Hou, Z. Zhang, and L. A. Madsen , Cation/Anion Associations in Ionic Liquids Modulated by Hydration and Ionic Medium. *Journal of Physical Chemistry B* 115, 4576-4582 (**2011**).

62. J. Li, J. K. Park, R. B. Moore, and L. A. Madsen, Linear coupling of alignment with transport in a polymer electrolyte membrane. *Nature Materials* 10, 507-511 (**2011**).

63. Allen, Michael H., Jr.; Green, Matthew D.; Getaneh, Hiwote K.; Miller, Kevin M.; Long, Timothy E. Tailoring Charge Density and Hydrogen Bonding of Imidazolium Copolymers for Efficient Gene Delivery. *Biomacromolecules* **2011**, *12*, 2243-2250.

64. Ye, Y.; Elabd, Y. A. Anion Exchanged Polymerized Ionic Liquids: High Free Volume Single Ion Conductors. *Polymer* **2011**, (52), 1309-1317.

65. Junhong Lin, Yang Liu, Q. M. Zhang. Charge Dynamics and Bending Actuation in Aquivion Membrane Swelled with Ionic Liquids. *Polymer* 52, 540 (**2011**).

66. Green Matthew D.; Allen Michael H. Jr.; Dennis Joseph M.; et al. Tailoring macromolecular architecture with imidazole functionality: A perspective for controlled polymerization processes. *European Polymer Journal*. **2010.** Volume: (47)4; SI 486-496.

67. Hunley Matthew T.; England Jeneffer P.; Long Timothy E. Influence of Counteranion on the Thermal and Solution Behavior of Poly(2-(dimethylamino)ethyl methacrylate)-Based Polyelectrolytes. *Macromolecules* **2010,** (43)23. 9998-10005

68. Brown, R. H.; Duncan, A. J.; Choi, J.; Park, J. K.; Wu, T.; Leo, D. J.; Winey, K. I.; Moore, R. B.; Long, T. E., Effect of Ionic Liquid on Mechanical Properties and Morphology of Zwitterionic Copolymer Membranes. *Macromolecules* **2010,** *43* (2), 790-796.

69. Williams, S. R.; Salas-de la Cruz, D.; Winey, K. I.; Long, T. E., Ionene segmented block copolymers containing imidazolium cations: Structure-property relationships as a function of hard segment content. *Polymer* **2010,** *51* (6), 1252-1257.

70. Duncan, A. J.; Layman, J. M.; Cashion, M. P.; Leo, D. J.; Long, T. E., Oligomeric A(2) + B-3 synthesis of highly branched polysulfone ionomers: novel candidates for ionic polymer transducers. *Polymer International* **2010,** *59* (1), 25-35.

71. Das, S.; Goff, J. D.; Williams, S.; Salas-de la Cruz, D.; Riffle, J. S.; Long, T. E.; Winey, K. I.; Wilkes, G. L., Synthesis and Characterization of Novel Segmented Polyionenes Based on Polydimethylsiloxane Soft Segments. *Journal of Macromolecular Science Part A: Pure and Applied Chemistry* **2010,** *47* (3), 215-224.

72. Gwee Liang; Choi Jae-Hong; Winey Karen I.; et al. Block copolymer/ionic liquid films: The effect of ionic liquid composition on morphology and ion conduction *Polymer* **2010** 51(23) 5516-5524.

73. Colby Ralph H. Structure and linear viscoelasticity of flexible polymer solutions: comparison of polyelectrolyte and neutral polymer solutions. *Rheologica Acta* **2010** (49)5. SI 425-442 .

74. Aitken, B. S.; Lee, M.; Hunley, M.; Gibson, H. W.; Wagener, K. B. Synthesis Of Precision Ionic Polyolefins Derived From Ionic Liquids, *Macromolecules* **2010**, *43,* 1699-1701.

75. Lee Minjae; Choi U. Hyeok; Salas-de la Cruz David; et al. Imidazolium Polyesters: Structure-Property Relationships in Thermal Behavior, Ionic Conductivity, and Morphology *Advanced Functional* **2010.** (21)4. 708-717.

76. Lee, M.; Niu, Z.; Slebodnick, C.; Gibson, H. W. Structure and Properties of N,N-Alkylene Bis(N'-alkylimidazolium) Salts, *J. Phys. Chem. B* **2010**, *114*, 7312-7319.

77. Lee, M.; Niu, Z.; Schoonover, D.; Slebodnick, C; Gibson, H. W. 1,2-Bis[N-(N'-alkylimidazolium)]ethane Salts as New Guests for Crown Ethers and Cryptands, *Tetrahedron* **2010**, *66,* 7077-7082.

78. Lee, M.; Choi, U-H.; Colby, R. H.; Gibson, H. W. Structure-Property Relationships: Ion Conduction in Polymerizable Ionic Liquid Acrylates and Their Polymers, *Chem. Mater.* **2010**, *22,* 5814-5822.

79. Gwee, L.; Choi, J.-H.; Winey, K.I.; Elabd, Y.A. Block Copolymer/Ionic Liquid Films: The Effect of Ionic Liquid Composition on Morphology and Ion Conduction. *Polymer*, 51, 5516-5524 (**2010**).

80. Dong, B.; Gwee, L.; Salas-de la Cruz, D.; Winey, K.I. Elabd, Y.A. Super Proton Conductive High Purity Nafion Nanofibers. *Nano Letters*. **2010**, *10*, 3785–3790.

81. Sheng Liu, Yang Liu, Hülya Cebeci, Roberto Guzmán de Villoria, Jun-Hong Lin, Brian L. Wardle and Q. M. Zhang. High Electromechanical Response of Ionic Polymer Actuators with Controlled-Morphology Aligned Carbon Nanotube/Nafion Nanocomposite Electrodes. *Adv. Funct. Mater.* **2010**, 3266.

82. S. Liu, R. Montazami, Y. Liu, V. Jain, M. Lin, X. Zhou, J.R. Heflin, Q.M. Zhang. Influence of the Conductor Network Composites on the Electromechanical Performance of Ionic Polymer Conductor Network Composite Actuators, *Sensors and Actuators* A 157, 267-275 **(2010).**

83. Ion Transport and Storage of Ionic Liquids in Ionic Polymer Conductor Network Composites. Y. Liu, S. Liu, J. Lin, D. Wang, V. Jain, R. Montazami, J.R. Heflin, J. Li, L. Madsen, and Q.M. Zhang, *Appl. Phys. Lett*. 96, 223503:1-3 (**2010**).

84. High Contrast Asymmetric Solid State Electrochromic Devices Based on Layer-by-Layer Deposition of Polyaniline and Poly(aniline sulfonic acid). R. Montazami, V. Jain, J.R. Heflin, *Electrochimica Acta* **56**, 990-994 (**2010**).

85. Williams, Sharlene R.; Wang, Wenqin; Winey, Karen I.; Long, Timothy E. Synthesis and Morphology of Segmented Poly(tetramethylene oxide)-Based Polyurethanes Containing Phosphonium Salts. Macromolecules, 41, 9072 (**2008**).

86. Williams, Sharlene R.; Borgerding, Erika M.; Layman, John M.; Wang, Wenqin; Winey, Karen I.; Long, Timothy E. Synthesis and Characterization of Well-Defined 12,12-Ammonium Ionenes: Evaluating Mechanical Properties as a Function of Molecular Weight. *Macromolecules*, 41, 5216 (**2008**).

**2013 UPDATES**

**Technical Highlights & Accomplishments**

*Karen I. Winey*

Correlating backbone-to-backbone distance to ionic conductivity in amorphous polymerized ionic liquids. D. Salas de la Cruz, M. D.Green., Y. Ye, Y. A. Elabd, T. E. Long, and K. I. Winey*, *J. Polym. Sci. B Polym. Phys.,* **50**, 338-346, 2012.

`

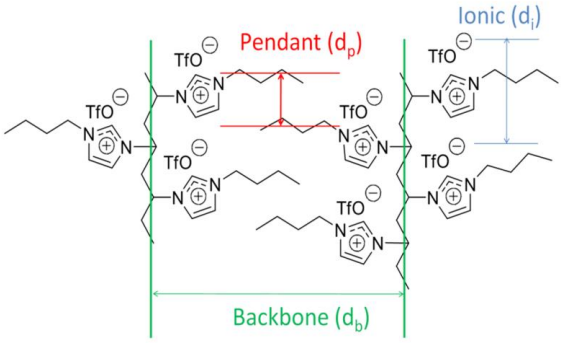


The morphology and ionic conductivity of poly(1-n-alkyl-3-vinylimidazolium)-based homopolymers polymerized from ionic liquids were investigated as a function of the alkyl chain length and counterion type. In general, X-ray scattering showed three features: (i) backbone-to-backbone, (ii) anion-to-anion and (iii) pendant-to-pendant characteristic distances. As the alkyl chain length increases, the backbone-to-backbone separation increases. As the size of counterion increases, the anion-to-anion scattering peak becomes apparent and its correlation length increases. The X-ray scattering features shift to lower angles as the temperature increases due to thermal expansion. The ionic conductivity results show that the glass transition temperature (Tg) is a dominant, but not exclusive, parameter in determining ion transport. The Tg-independent ionic conductivity decreases as the backbone-to-backbone spacing increases. Further interpretation of the ionic conductivity using the Vogel-Fulcher-Tammann (VFT) equation enabled the correlation between polymer morphology and ionic conductivity, which highlights the importance of anion hoping between adjacent polymer backbones.

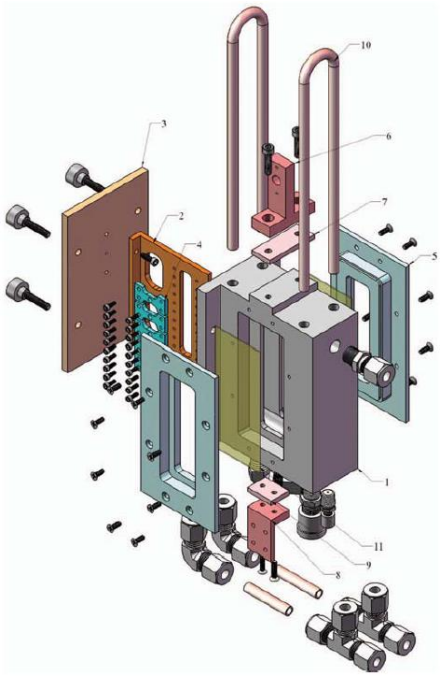

<u>Environmental chamber for *in situ* dynamic control of temperature and relative humidity during X-ray scattering.</u> D. Salas-de la Cruz, J. G. Denis, M. D. Griffith, D. R. King, P. A. Heiney, K. I. Winey*, *Review of Scientific Instruments*, **83**, 025112, 2012.

We have designed, constructed, and evaluated an Environmental Chamber that has in situ dynamic control of temperature (25 to 90 oC) and relative humidity (0 to 95%). The compact specimen chamber is designed for X-ray scattering in transmission with a horizontal escape angle of 2□ = ±30 degrees. The chamber is compatible with evacuated flight paths, as is typically used with sealed tube or rotating anode X-ray sources, but is also compatible with synchrotron X-ray sources. Minor modification would adapt the chamber for in situ neutron scattering. When attached to a linear motor, the environmental chamber can access multiple sample positions. The temperature and relative humidity inside the specimen chamber are controlled by passing a mixture of dry and saturated gas through the chamber and by heating the chamber walls. Alternatively, the chamber can be used to control the gaseous environment without humidity. To illustrate the value of this apparatus, we have probed morphology transformations in Nafion® membranes and a polymerized ionic liquid as a function of relative humidity in nitrogen. Our design was licensed and is now sold by JJX-ray of Denmark.

Effects of neutralization with $Et_3Al$ on structure and properties in sulfonated styrenic pentablock copolymers. J.-H. Choi, C. L. Willis, K. I. Winey*, *Journal of Membrane Science*, **428**, 516-522, 2013.

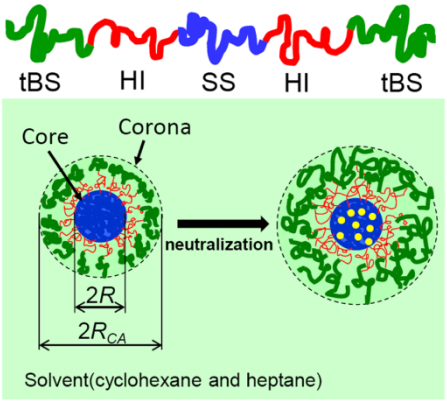


The effect of neutralization with Et3Al on morphologies in a sulfonated pentablock copolymer solution and cast membrane was investigated using small-angle X-ray scattering (SAXS) and transmission electron microscopy (TEM). The sulfonated pentablock copolymer in a non-polar solvent mixture (cyclohexane/heptane) persists as spherical micelles after neutralization where the micelle core of sulfonated polystyrene (SS) incorporates Al (3+) ions and the corona is solvated hydrogenated isoprene (HI) and t-butylstyrene (tBS). Membranes cast from this micellar solution exhibit a bicontinuous microphase separated morphology with interconnected SS microdomains. The aluminum-neutralized membrane with a continuous transport channel shows excellent water vapor transport rate (WVTR) (22 kg/(m2day)), which is comparable to the WVTR of membranes in the sulfonic acid form. The strong interaction between Al(3+) ions and the sulfonic acid group in the aluminum-

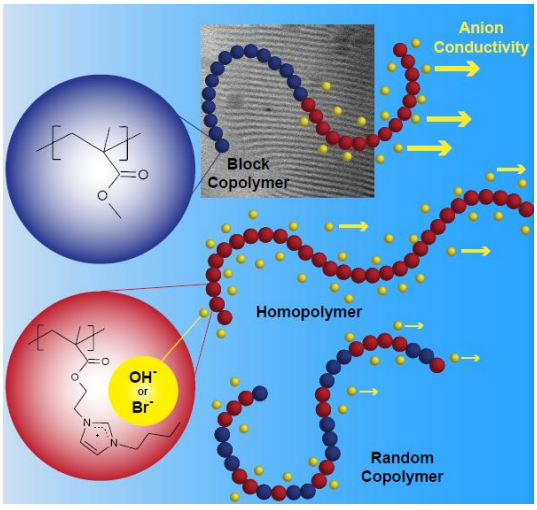

neutralized membrane results in significantly lower water uptake (~30 % wt) that provides much-improved mechanical stability in the wet state.

High hydroxide conductivity in polymerized ionic liquid block copolymers. Y. Ye, S. Wang, E. M. Davis, K. I. Winey*, Y. A. Elabd*, *ACS Macro Letters*, **2**, 575-580, 2013.

Herein, we report a polymerized ionic liquid diblock copolymer with high hydroxide conductivity and nanoscale morphology. Surprisingly, the conductivity is not only higher (over an order of magnitude) than its random copolymer analog at the same ion and water content, but also higher than its homopolymer analog, which has a higher ion and water content than the block copolymer. These results should have a significant impact on low-cost (platinum-free) long-lasting solid-state alkaline fuel cells. The environmental chamber for the multiple-angle X-ray scattering instrument made it possible to probe the morphology at the same temperature and relative humidity at the electrochemical impedance spectroscopy measurements.

Network Structure and Strong Microphase Separation for High Ion Conductivity in Polymerized Ionic Liquid Block Copolymers. J.-H. Choi, Y. Ye, Y. A. Elabd, K. I. Winey*, *Macromolecules*, **46**, 5290-5300, 2013.

A series of strongly microphase-separated polymerized ionic liquid (PIL) diblock copolymers, poly(styrene-b-1-((2-acryloyloxy)ethyl)-3-butylimidazolium bis(trifluoromethanesulfonyl)imide) (poly(S-b-AEBIm-TFSI)), were synthesized to explore relationships between morphology and ionic conductivity. Using small-angle X-ray scattering and transmission electron microscopy, a variety of self-assembled nanostructures including hexagonally packed cylinders, lamellae, and coexisting lamellae and network morphologies were observed by varying PIL composition (6.6 – 23.6 PIL mol %). At comparable PIL composition, this acrylate-based PIL block copolymer with strong microphase separation exhibited ~1.5-2 orders of magnitude higher ionic conductivity than a methacrylate-based PIL block copolymer with weak microphase separation. Remarkably, we achieved high ionic conductivity (0.88 mS cm-1 at 150 ºC) and a morphology factor (normalized ionic conductivity, f) of ~ 1 through the morphological transition from lamellar to a coexistence of lamellar and three-dimensional network morphologies with increasing PIL composition in anhydrous single-ion conducting PIL block copolymers, which highlights a good agreement with the model

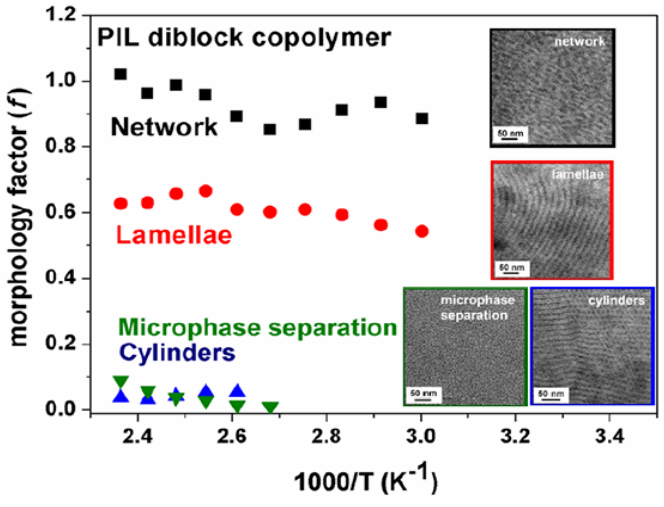

predictions. In addition to strong microphase separation and the connectivity of conducting microdomains, the orientation of conducting microdomains and the compatibility between polymer backbone and IL moiety of PIL also significantly affect the ionic conductivity. This study provides avenues to controlling the extent of microphase separation, morphology and ion transport properties in PIL block copolymers for energy conversion and storage applications.

**Project Title #1:** High Hydroxide Conductivity in Polymerized Ionic Liquid Block Copolymers

**Personnel:** Yuesheng Ye (Advisor: Y.A. Elabd)

**Collaborators:** Sharon Sharick (Advisor: K.I. Winey)

**Published in:** ACS Macro Letters

Herein, we report a polymerized ionic liquid diblock copolymer with high hydroxide conductivity and nanoscale morphology. Surprisingly, the conductivity is not only higher (over an order of magnitude) than its random copolymer analog at the same ion and water content, but also higher than its homopolymer analog, which has a higher ion and water content than the block copolymer. These results should have a significant impact on low-cost (platinum-free) long-lasting solid-state alkaline fuel cells.

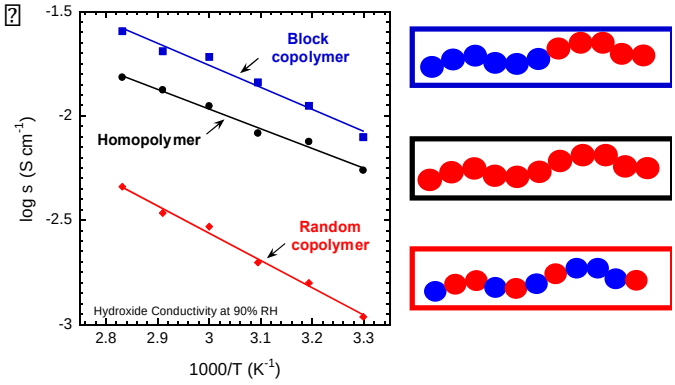


**Project Title #2:** Network Structure and Strong Microphase Separation for High Ion Conductivity in Polymerized Ionic Liquid Block Copolymers

**Personnel:** Yuesheng Ye (Advisor: Y.A. Elabd)

**Collaborators:** Jae-Hong Choi (Advisor: K.I. Winey)

**Published in:** Macromolecules

A series of strongly microphase-separated polymerized ionic liquid (PIL) diblock copolymers, poly(styrene-*b*-1-((2-acryloyloxy)ethyl)-3-butylimidazolium bis(trifluoromethanesulfonyl)imide) (poly(S-*b*-AEBIm-TFSI)), were synthesized to explore relationships between morphology and ionic conductivity. Using small-angle X-ray scattering and transmission electron microscopy, a variety of self-assembled nanostructures including hexagonally packed cylinders, lamellae, and coexisting lamellae and network morphologies were observed by varying PIL composition (6.6 – 23.6 PIL mol %). At comparable PIL composition, this acrylate-based PIL block copolymer with strong microphase separation exhibited ~1.5-2 orders of magnitude higher ionic conductivity than a methacrylate-based PIL block copolymer with weak microphase separation. Remarkably, we achieved high ionic conductivity (0.88 mS $cm^{-1}$ at 150 ºC) and a morphology factor (normalized ionic conductivity, *f*) of ~ 1 through the morphological transition from lamellar to a coexistence of lamellar and three-dimensional network morphologies with increasing PIL composition in anhydrous single-ion conducting PIL block copolymers, which highlights a good agreement with the model predictions. In addition to strong microphase separation and the connectivity of conducting microdomains, the orientation of conducting microdomains and the compatibility between polymer backbone and IL moiety of PIL also significantly affect the ionic conductivity. This study provides avenues to controlling the extent of microphase separation, morphology and ion transport properties in PIL block copolymers for energy conversion and storage applications.

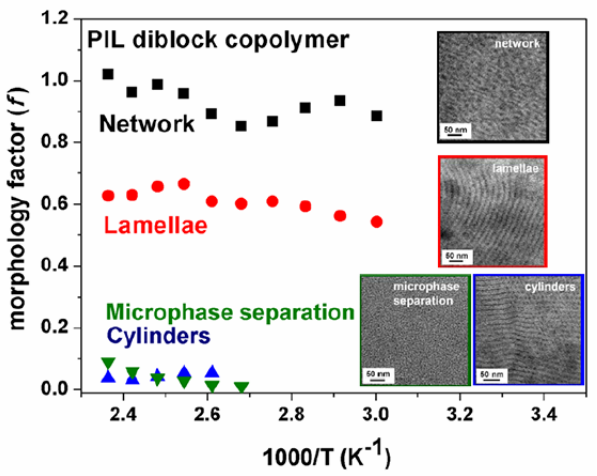


**Project Title #3:** Polymerized Ionic Liquid Block and Random Copolymers: Effect of Weak Microphase Separation on Ion Transport

**Personnel:** Yuesheng Ye (Advisor: Y.A. Elabd)

**Collaborators:** Jae-Hong Choi (Advisor: K.I. Winey)

**Published in:** Macromolecules

A series of polymerized ionic liquid (PIL) block and random copolymers were synthesized from an ionic liquid monomer, 1-[(2-methacryloyloxy)ethyl]-3-butylimidazolium bis(trifluoromethanesulfonyl)imide (MEBIm-TFSI), and a non-ionic monomer, methyl methacrylate (MMA), at various PIL compositions with the goal of understanding the influence of morphology on ion transport. For the diblock copolymers, the partial affinity between the PIL and PMMA blocks resulted in a weakly microphase-separated morphology with no evident long-range periodic structure across the PIL composition range studied, while the random copolymers revealed no microphase separation. These morphologies were identified with a combination of techniques, including differential scanning calorimetry, small angle X-ray scattering, and transmission electron microscopy. Surprisingly, at similar PIL compositions, the ionic conductivity of the block copolymers were ca. 2 orders of magnitude higher than the random copolymers despite the weak microphase-separated morphology evidenced in the block copolymers. We attribute the higher conductivity in the block copolymers to its microphase-separated morphology, since significant differences in conductivity are still observed even when differences in glass transition temperature are considered. This work demonstrates that local confinement and connectivity of conducting ions in nanoscale ionic domains in PIL block copolymers can accelerate ion transport significantly.

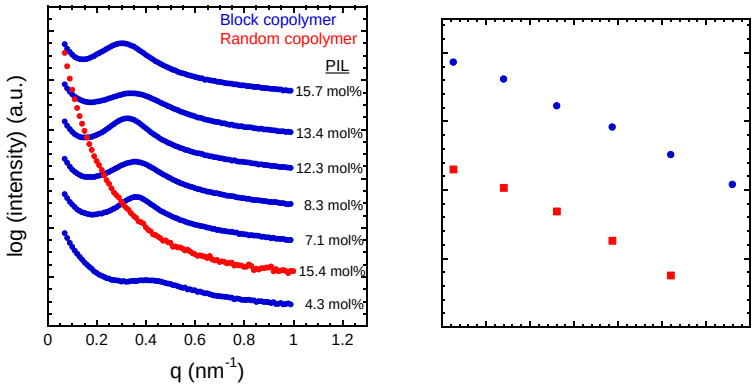


**Project Title #4:** Relative Chemical Stability of Imidazolium-Based Alkaline Anion Exchange Polymerized Ionic Liquids

**Personnel:** Yuesheng Ye (Advisor: Y.A. Elabd)

**Published in:** Macromolecules

In this study, we thoroughly investigate and quantify the chemical stability of an imidazolium-based alkaline anion exchange polymerized ionic liquid (PIL), poly(1-[(2-methacryloyloxy)ethyl]-3-butylimidazolium hydroxide) (poly(MEBIm-OH), over a broad

range of humidities, temperatures, and alkaline concentrations using the combined techniques of electrochemical impedance spectroscopy and nuclear magnetic resonance spectroscopy. High chemical stability was observed under dry conditions (10% RH) at 30 °C, humid and saturated conditions up to 80 °C, and even in mild alkaline conditions ([KOH] < 1 M) at 25 °C. Degradation was only observed under more vigorous conditions: dry conditions (10% RH) at 80 °C or at higher alkaline concentrations ([KOH] > 1 M). Under these conditions, we suggest an imidazolium ring-opening mechanism as the primary degradation pathway, based on a detailed analysis of the $^{1}$H NMR spectra. Similar to poly(MEBIm-OH), other alkaline anion (carbonate ($CO_3^{2-}$) and bicarbonate ($HCO_3^{-}$)) exchange PILs were also synthesized in this study via salt metathesis of the PIL precursor, poly(1-[(2-methacryloyloxy)ethyl]-3-butylimidazolium bromide) (poly(MEBIm-Br)). The thermal and ion conductive properties of each PIL in this study were characterized. The ionic conductivity of the hydroxide conducting PIL, poly(MEBIm-OH), was the highest of these PILs investigated at 9.6 mS·cm$^{-1}$ at 90% RH and 30 °C with an Arrhenius activation energy of 17.1 kJ·mol$^{-1}$ at 90% RH.

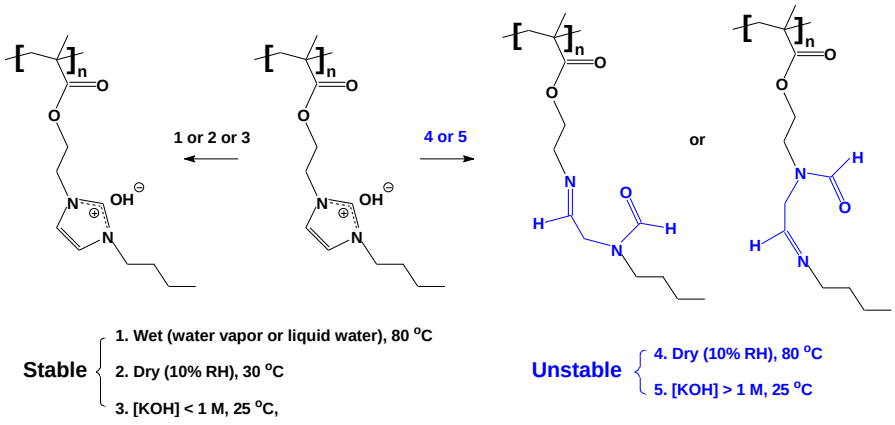


**Project Title #5:** Block Copolymer/Ionic Liquid Films: The Effect of Ionic Liquid Composition on Morphology and Ion Conduction

**Personnel:** Gwee Liang (Advisor: Y.A. Elabd)

**Collaborators:** Jae-Hong Choi (Advisor: K.I. Winey)

**Published in:** Polymer

The effect of morphology on ion transport in ionic liquid-based solid-state films was investigated. In this study, mixtures of a block copolymer, poly(styrene-*b*-methyl methacrylate) (SbMMA), and an ionic liquid (IL), 1-ethyl-3-methylimidazolium bis (trifluoromethylsulfonyl)imide (EMIm-TFSI), were prepared as clear solid-state films at various IL compositions (0-50 wt%) by solution casting from a volatile co-solvent. The IL

was preferentially miscible with the MMA block as evidenced by visual inspection and differential scanning calorimetry. Both equilibrium and non-equilibrium morphologies were identified with X-ray scattering and transmission electron microscopy and the morphology varied with MMA/IL volume fraction. The morphology and microdomain orientation had a significant impact on ionic conductivity. Higher through-plane conductivities were observed in morphologies with a three-dimensionally continuous conducting path (e.g., non-conducting S cylinders) compared to morphologies with a non-continuous conducting path (e.g., lamellae). When the lamellae were oriented in the plane, the through-plane conductivity was significantly lower than the in-plane conductivity, while the conductivity was direction-independent when the morphologies have a continuous conductive path. Also, a significant increase in conductivity was observed with increasing IL content at the glass transition of the conductive (MMA/IL) microdomain. Finally, significantly higher ionic conductivities can be achieved in a block copolymer/IL solid-state film compared to a homopolymer/IL film at the same IL content (wt%), because the non-conductive microdomain excludes IL, which produces a higher local IL concentration in the conductive phase.

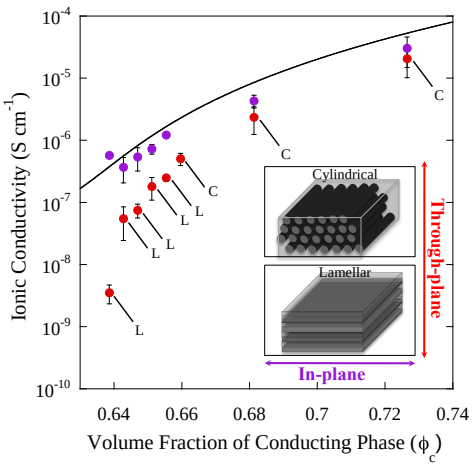


**Project Title #6:** Polymerized Ionic Liquids: The Effect of Random Copolymer Composition on Ion Conduction
**Personnel:** Hong Chen (Advisor: Y.A. Elabd)

**Collaborators:** Jae-Hong Choi, David Salas-de la Cruz (Advisor: K.I. Winey)

**Published in:** Macromolecules

Ionic conductivity in new polymerized ionic liquids is of great interest as it applies to solid-state electrolytes for electrochemical and electromechanical applications. In this study, an ionic liquid monomer was synthesized and polymerized into random copolymers and their ionic conductivity and structure were investigated as a function of

copolymer composition. Both nonionic-ionic and ionic-ionic copolymers were synthesized, where the nonionic and ionic monomers were hexyl methacrylate (HMA) and a methacrylate-based imidizolium neutralized with tetrafluoroborate ($BF_4$) or bis(trifluoromethane sulfonyl)imide (TFSI). In the nonionic-ionic copolymer, the ionic conductivity increased by over an order of magnitude with increasing HMA composition, even though the overall charge content decreased, because the additional of HMA significantly lowered the glass transition temperature. The ionic conductivity also increased by more than an order of magnitude in the ionic-ionic copolymer with increasing TFSI content, even though there was no change in the overall charge content, because substituting the larger anion TFSI for $BF_4$ resulted in weaker ionic interactions and also significantly lowered the glass transition temperature. In both types of copolymers, the temperature dependence of the ionic conductivity was well described by both Arrhenius and Vogel-Tamman-Fulcher models. An important difference between the two classes of random copolymers was that the nonionic-ionic copolymer exhibited microphase separation in X-ray scattering that correlated with a discontinuity in the increasing ionic conductivity with increasing HMA content suggesting that structure can also play a significant role in ion transport in polymerized ionic liquids.

*Qiming Zhang*

Ion transport and storage in porous electrodes are of great importance for various energy storage and conversion materials and devices, including batteries, supercapacitors, fuel cells, and ionic electroactive polymer (*i*-EAP) actuators. Deeper understanding of electrical responses of ILs under the operation voltage (~ 2-5 V) of these ionic devices, especially the excess ion distribution at electrodes, becomes crucial in guiding the application of ILs and the design of these ionic electroactive devices. It has been well established that the excess ion distribution of a dilute solution (ion concentration $C < 10^{-5}$ M) near a charged wall can be modeled by Poisson-Nernst-Planck (PNP) equations, Poisson-Boltzmann (PB) equations, and Gouy-Chapman-Stern (GCS) model, particularly, under the condition of a low applied voltage φ ($\varphi < k_BT/e$, where $k_B$ is the Boltzmann constant, T is temperature, and e is electron change. $k_BT/e$ at room temperature is ~25 mV). Different from dilute solutions, ILs possess high

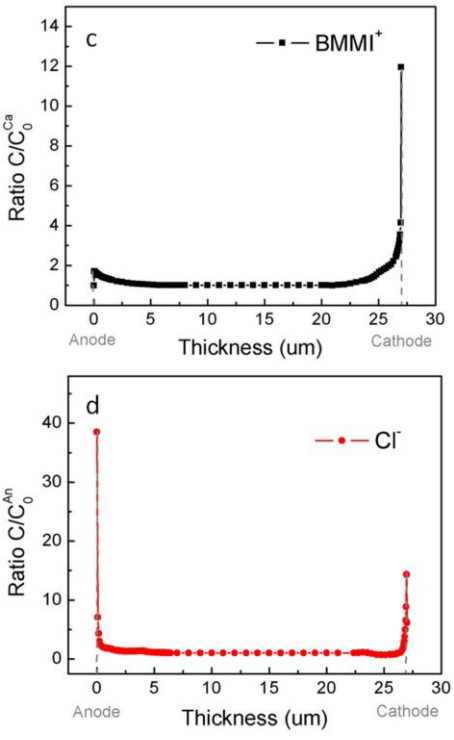


Fig. 1. Directly measured ion distribution at the anode and cathode of a membrane actuator with IL of BMMI-Cl.

ion concentration (C ~ 3-7 M), which is attractive for ionic electroactive devices but also poses a challenge to understand their non-linear response under device working voltages (V ~ 2-5 V, > 100 $k_BT/e$) and operation conditions which are likely in non-equilibrium in these electroactive ionic devices.

Since ToF-SIMS with $C_{60}^+$ cluster ion beam allows etching organic materials without damaging their chemical integrity, the ion depth-profile information can be probed directly. This unique feature makes it possible to study the electrode-electrolyte interaction in *i*-EAP actuators and ionic based energy storage devices, such as supercaoacitors and Li-polymer batteries. In this MURI program, utilizing ToF-SIMS, we characterized the excess cation and anion profiles at both cathode and anode for an ionic electroactive polymer actuator, consisting of Aquivion® membrane with IL of BMMI-Cl and planar electrodes. Such a Metal-Ionic conductor-Metal (MIM) structure, i.e., an ionic conductor with ILs sandwiched between two planar metal electrodes, is widely used as model systems to study ion transport and storage in ionic electroactive devices.

Presented in Figure 1 is directly measured ion profiles at both the cathode and anode for the Aquivion ionomer membrane (27 □m thick) with [BMMI][Cl] ionic liquid after application of 2.5 V. Based on the data in Figure 1, the relative excess ion (cation and anion) distribution at the two electrodes are presented in Figure 2, which shows that

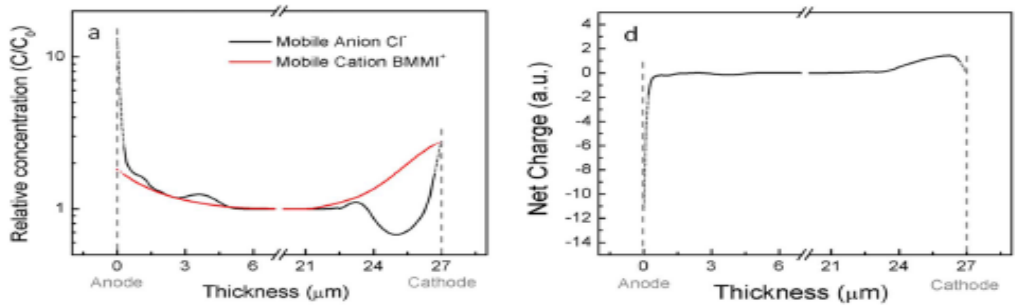


Fig. 2. (a) Relative mobile ion distributions of cation and anion at the two electrodes, and (d) the net charge distribution at the cathode and anode.

both cations and anions are present at the two electrodes. Although the excess cation concentration at the cathode is much higher (> 50% higher) than that at the anode, there are still substantial amount of excess cations present at anode. At both electrodes, the excess cation concentration decays monotonically with distance away from the electrodes. For anions, the data reveal quite interesting results: (i) Right near the cathode, there are high concentration excess anions. However, different from cations, the excess anion concentration becomes negative (anion deficiency) and also displays weak oscillation, which is much beyond the experimental error, till around 5 □m away from the cathode. (ii) ) At a narrow region near anode (d < 0.5 □m) there is a very high concentration of anions, which results in a higher capacitance at anode than that at cathode. The concentration of anions is always above the average and decays with the distance away from the anode. The decrease of the excess anion concentration with

distance from the cathode is not monotonic and also exhibits oscillation. The observed asymmetric excess ion concentration profiles between the two electrodes are likely caused by the large difference in ion size between cation and anion.

The results here also demonstrate that ToF-SIMS is a powerful tool to directly characterize the carrier profiles in ionic energy storage and conversion devices, which provides great insights on the electroactive responses in these devices.

*James R. Heflin, Dong Wang*

We have utilized the layer-by-layer (LbL) self-assembly technique to deposit conductive network composite (CNC) layers consisting of gold nanoparticles (Au NPs, 3 nm in diameter) on both sides of the ionic conductive polymer membranes to fabricate ionic liquid (IL) contained electromechanical ionic polymer-metal composite (IPMC) bending actuators. The transportation and accumulation of the ions from the IL soaked in the actuator result in bending. The high conductivity and porosity of the CNC imparted by the Au NPs can not only increase the IL uptake but is also highly beneficial for the ion transportation and accumulation in the actuator and thus largely improves the overall bending performance. We have been performing a detailed examination of the key factors influencing the magnitude and speed of the response in these actuators and, in collaboration with the group of Prof. Long, examining the properties and performance of novel ionic liquid-derived polymer membranes as alternatives to Nafion®.

As the most commonly used ion conductive polymer, the Nafion® membrane is an iconic example of good balance between the ionic conductivity, mechanical robustness, and flexibility, which makes it an ideal understructure for IPMC actuator fabrication. Primarily collaborating with Prof. Zhang's group at PSU within this MURI, we studied the bending performance of Nafion® based IPMC actuators [1], proposed an equivalent electric model to mimic the bi-directional bending behavior caused by the transport of both cations and anions from the IL [2], and investigated the dependence of the bending performance on the thickness of CNC [3].

More recently, the effect of IL uptake and CNC coatings on the bending performance of the IPMC actuator was further investigated [4]. We fabricated and tested Nafion® based actuators with/without CNC coating and with different IL uptake. The bending curves were fitted with the equivalent circuit model and the theoretical maximum curvatures due to the cation and anion accumulation were obtained as shown in Table 1 and Table 2.

**Table 1. Fitted maximum cationic and anionic curvature of actuators made of Nafion® coated with 40 nm thick Au NPs CNC.**

| ILs weight uptake | 0.0% | 17.3% | 30.1% | 35.0% |
|---|---|---|---|---|
| $K_c$ ($mm^{-1}$) | **0.04** | **0.7** | **3.3** | **4.7** |
| $K_a$ ($mm^{-1}$) | **0.4** | **1.2** | **4.7** | **5.6** |

**Table 2. Fitted maximum curvature of the actuators made of neat Nafion®.**

| ILs weight uptake | 0.0% | 3.6% | 9.0% | 21.0% | 29.5% |
|---|---|---|---|---|---|
| $K_c$ ($mm^{-1}$) | **0.22** | **0.14** | **1.45** | **1.64** | **1.44** |
| $K_a$ ($mm^{-1}$) | **0.3** | **0.7** | **1.92** | **2.22** | **2.02** |

It can be seen that the maximum curvatures (both cationic and anionic) are significantly increased for the actuators with increased IL uptake (up to 35% wt.) and for actuators with CNC compared to those without. This is expected since more IL provides more ions for the accumulation to enhance the bending. However, as shown in Table II, the performance improvement of actuators without CNC layers saturates when the IL uptake reaches around 10% wt. This demonstrates the role of the CNC layers to provide a porous reservoir for ions. This increases the device capacitance and can thus accommodate the accumulation of more ions near the electrodes, which in turn boosts the overall bending curvature of the actuator.

In order to obtain a more complete picture of the ion transport and accumulation of the IPMC actuator, we studied their electrical properties during the charging (bending) and discharging (relaxing) procedure. The IPMC actuators used in this study have a Nafion® membrane as the backbone and EMI-Tf IL as the working electrolyte. It was found that the charging current through the actuator after a DC voltage was applied agrees somewhat with the equivalent circuit model proposed before [2]. However, the actual current does not eventually fall to zero as it should according to that model. Instead, a steady current was observed after the bending of the actuator reaches equilibrium and this current maintains its magnitude for an extended time (hours) even though there was no more bending motion of the actuator. This thus excludes the ion accumulation as the reason. Moreover, we found the steady-state current closely relates to the relative humidity of the environment in which the testing was performed. For these reasons, we concluded that this steady-state current is caused by the electrolysis of the water adsorbed from the environment by the actuator. Right after a DC voltage is applied on the IPMC actuator, the charging current is mainly determined by the ion transport of the IL. Once the IL transport and accumulation is complete, i.e. the bending reaches a steady point, the charging current is only determined by the electrolysis of water in the actuator. The dynamic balance between the adsorption of water vapor and the

consumption of water during the electrolysis results in the steady current which depends on the relative humidity. So, we have proposed a modified equivalent circuit model to better simulate the electrical property of the IPMC actuator, as shown in Figure 1.

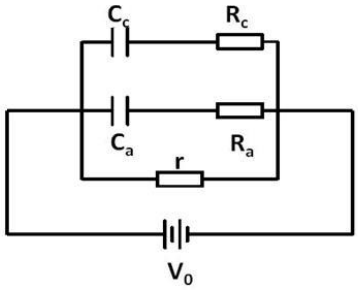


**Fig. 1 Equivalent circuit model for the IPMC actuator. $R_c$: resistance exerted on the cations during migration, $C_c$: capacitance relating to the cation accumulation, $R_a$: resistance exerted on the anions during migration, $C_a$: capacitance relating to the anion accumulation, $V_0$: applied voltage, r: internal resistance of the system.**

This model includes a "leakage" resistor "r" to represent the equivalent resistance of the water electrolysis process. Based on this model, the charging current through the IPMC actuator under a DC voltage can be expressed as:

$$I = V_0[\frac{1}{R_c}e^{-t/\tau_c} + \frac{1}{R_a}e^{-t/\tau_a} + \frac{1}{r}] \quad (1)$$

where the RC time constants $\tau_c = R_c C_c$, $\tau_a = R_a C_a$. The meanings of the parameters are explained in the caption of Figure 1.

The leftover voltage across the actuator when it is disconnected from the power supply after being fully charged can be deduced and the final expression is:

$$V = rV_0[\frac{C_c}{t_c}e^{-t/t_c} + \frac{C_a}{t_a}e^{-t/t_a}] \quad (2)$$

where $t_c = \frac{\tau_c + \tau_a + r(C_c + C_a) + \sqrt{[\tau_c - \tau_a + r(C_c - C_a)]^2 + 4r^2 C_c C_a}}{2}$, and

$$t_a = \frac{\tau_c + \tau_a + r(C_c + C_a) - \sqrt{[\tau_c - \tau_a + r(C_c - C_a)]^2 + 4r^2 C_c C_a}}{2}$$

To test this modified circuit model, two identical Au NPs CNC coated Nafion® actuators were soaked with different amounts of EMI-Tf IL (19.4%, 28.2% wt. uptake) and their charging current and discharging voltage were measured and fitted according to the proposed model. By comparing the key parameters $C_c$ and $C_a$ obtained from two

fittings, we can see a general agreement of the fitting data for charging and discharging, as shown in Table 3.

**Table 3. The comparison of capacitances in the circuit model (Figure 1) obtained by fitting the charging and discharging behavior of the IMPC actuator.**

| **$C_c$ (μF)** | **19.4%** | **28.2%** |
|---|---|---|
| Charging | 14.42 | 21.39 |
| Discharging | 6.08 | 20.66 |
| **$C_a$ (μF)** | **19.4%** | **28.2%** |
| Charging | 553.76 | 694.97 |
| Discharging | 1432.98 | 1316.71 |

The general agreement shows the validity of this model to a certain extent. The differences between the parameters obtained from fitting the charging and discharging behavior could result from the different ionic conducting channels in the Nafion® membrane with/without external electric field. A paper with more detailed study on this model is under preparation.

Although Nafion® has been a favorable ion conductive membrane for IPMC actuator applications, this commercially available membrane has significant disadvantages of the lack of control over several key parameters. Recently, instead of using Nafion®, we fabricated and tested IPMC actuators based on the novel ion conductive imidazolium pentablock [5] and triblock [6] copolymer membranes, as well as DMAEA containing ABA triblock copolymer membrane [7], all of which were synthesized by Prof. Long's group at Virginia Tech. These polymer membranes exhibit both good storage moduli and reasonable ionic conductivity, and expand the class of multiphase copolymers that are suitable for electromechanical IPMC actuator applications.

Because of their high ionic conductivity, acceptable affinity to ionic liquids, and tailored structures and morphologies, imidazolium-containing polymers are a promising candidate for the fabrication of electromechanical actuators. By utilizing the commercially available sulfonated pentablock copolymer as a precursor, Gao et al. [5] neutralized the sulfonic acid sites with various *N*-alkyl imidazoles. This modified pentablock copolymer contains a hydrophilic, imidazolium polystyrene sulfonate central block that enables the incorporation of IL, and hydrogenated polyisoprene blocks that impart membrane flexibility and elasticity, as well as the hydrophobic poly(*tert*-butyl styrene) outer blocks acting as the physical crosslink to provide mechanical strength in the presence of IL. The synthesized copolymer membrane was then soaked with EMI-Tf IL and subjected to LbL assembly of Au NPs CNC to be fabricated into an IPMC actuator. Comparable bending behavior as compared to the reference Nafion® actuator was obtained (see Fig. 4 in Ref [5]) was this membrane.

Another novel imidazolium-containing polymer was synthsized by Green et al. [6]. By applying nitroxide-mediated polymerization, they synthesized the poly(sty-*b*-[EVBIm][$Tf_2N$]]-*b*-sty) and casted it into an ionic conductive polymer membrane for IPMC actuator fabrication. The charged, low $T_g$ imidazolium central block imparts the electrochemical stability and high ion conductivity, while polystyrene outer blocks offer mechanically reinforcing phases for suitable mechanical properties. It is noteworthy that this was the first time to apply a cationic triblock copolymer ($Tf_2N^-$ is the counter ion) for the electromechanical actuator. Unlike the anionic Nafion®, the actuator made of this cationic polymer membrane bends toward the cathode only under a DC input due to the accumulation of the anionic counter ion on the anode side of the actuator, as shown in Fig. 6 in Ref [6].

Besides the imidazolium-containing family, Wu et al. [7] successfully synthesized high-molecular-weight poly(sty-*b*-(*n*BA-*co*-SBDMAEA)-*b*-sty) triblock copolymer as the ion conductive membrane by employing RAFT polymerization. The presence of the tertiary amine functionality in the central block of this triblock copolymer afforded tunable polarity toward polar guest molecules, such as IL. This results in a good affinity toward EMI-Tf IL, which is desirable for better actuation performance. The IPMC actuators fabricated from this copolymer membrane can take up to 58 wt.% EMI-Tf IL (as compared to max. 40 wt.% uptake for Nafion® actuator) and clearly shows bi-directional bending behavior. Similar to those obtained from the Nafion® actuators, the bending curves could be perfectly fitted with the equivalent circuit model (Fig. 10 in Ref [7]).


[1] S. Liu, R. Montazami, Y. Liu, V. Jain, M. Lin, X. Zhou, J.R. Heflin, Q.M. Zhang, Sensors and Actuators A: Physical 157 (2010) 267.

[2] Y. Liu, S. Liu, J. Lin, D. Wang, V. Jain, R. Montazami, J.R. Heflin, J. Li, L. Madsen, Q.M. Zhang, Applied Physics Letters 96 (2010).

[3] R. Montazami, S. Liu, Y. Liu, D. Wang, Q.M. Zhang, J.R. Heflin, Journal of Applied Physics 109 (2011).

[4] D. Wang, R. Montazami, J.R. Heflin, MRS Online Proceedings Library 1575 (2013).

[5] R. Gao, D. Wang, J.R. Heflin, T.E. Long, Journal of Materials Chemistry 22 (2012) 13473.

[6] M.D. Green, D. Wang, S.T. Hemp, J.-H. Choi, K.I. Winey, J.R. Heflin, T.E. Long, Polymer 53 (2012) 3677.

[7] T. Wu, D. Wang, M. Zhang, J.R. Heflin, R.B. Moore, T.E. Long, Acs Applied Materials & Interfaces 4 (2012) 6552.

**1a. Bisimidazolium Salts**

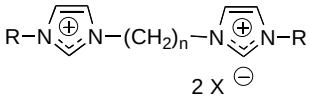

A series of 19 compounds was prepared with various R groups, n values and counterions. [3] The $Br^-$ and $PF_6^-$ salts were crystalline or plastic crystalline materials, while the $NO_3^-$, $BF_4^-$ and $TFSI^-$ salts were ionic liquids. [3] X-ray crystal structures were obtained for two of the $PF_6$ compounds, revealing the hydrogen-bond like interactions between all of the imidazolium protons and the counterions. While a number of highly conductive plastic crystalline phases are known, these new plastic crystals, which possess up to four reversible crystalline phases, did not display high ionic conductivities; the maximum values were $10^{-6}$ S/cm at 150 $^oC$. [7] Some deuterium NMR studies were carried out by Prof. Sungsool Wi at VT to elucidate their behavior. [7] Later the dynamics of one of the novel plastic crystals were studied in more detail in the Madsen laboratory at VT, indicating that ion transport occurs at grain boundaries. [11]

These imidazolium salts were shown to be suitable guests for complexation with crown ethers and cryptands. [4]

**1b. Imidazolium Polyesters:**

Polyesters were prepared from imidazolium diols and sebacoyl chloride; we varied the spacer lengths x and y (6 or 11) and counterion ($PF_6^-$ or $TFSI^-$). $PF_6^-$ polymers tended to be semicrystalline, but the $TFSI^-$ analogs were amorphous. [7] $T_g$s

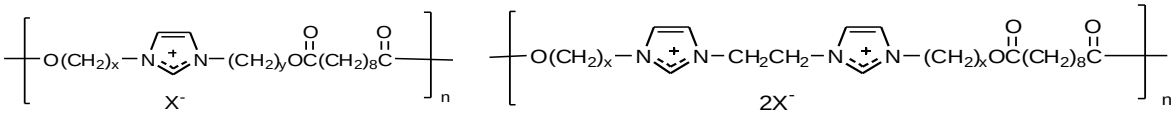

as low as -63 $^oC$ were observed. Room temperature ionic conductivities of the mono-imidazolium polyesters (4 x $10^{-6}$ to 3 x $10^{-5}$ S/cm) were higher than those of the corresponding bis-imidazolium polyesters (4 × $10^{-9}$ to 8 × $10^{-6}$ S/cm), even though the bis-imidazolium polyesters had higher ion concentrations. Counterions affected ionic conduction significantly; all polymers with $TFSI^-$ counterions had higher ionic conductivities than the $PF_6^-$ analogs. Interestingly, the $PF_6^-$ bisimidazolium polyester with x=11 displayed ~400-fold higher room temperature ionic conductivity (2 × $10^{-6}$ S/cm) than the x=6 analog (4 × $10^{-9}$ S/cm), attributable to the differences in the semicrystalline nature of the former, indicating that semicrystalline polymers can result in high ionic conductivity in the soft (low $T_g$) amorphous phase and good mechanical properties of the crystalline phase. [7]

## 1c. Polycaprolactones:

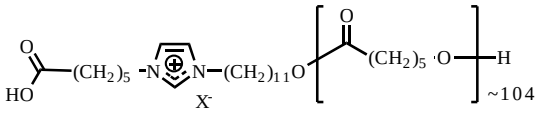

(X = Br or TFSI)

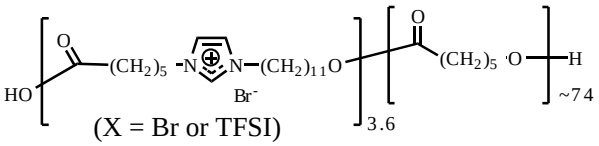

(X = Br or TFSI)

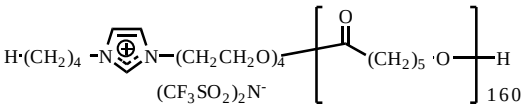

Two monomeric imidazolium alcohols, one an ionic liquid, were successfully utilized as initiators for ROP of CL, yielding corresponding end-functionalized polycaprolactones. [12] Use of an imidazolium oligoester as an initiator provided a block copolymer. [12] By anion exchange, polymers with $Br^-$ counterions were converted to $TFSI^-$ analogs. The end-functional polymers and the block copolymers displayed melting ($T_m$) and crystallization ($T_c$) transitions typical of PCL and glass transitions ($T_g$) corresponding to both PCL and the imidazolium component. At the observed phase transitions, the temperature dependence of ionic conductivity was discontinuous (changed slope). The single-ion conductivities of the PCL block copolymers were higher than those of the PCL homopolymers, despite the similar $T_g$, because of their higher ionic content. The PCL polymers with larger $TFSI^-$ counterions possessed lower $T_g$s, resulting in higher mobility and ionic conductivity, compared to the polymers with smaller $Br^-$ counterions. For polymers with the same counterion, mobilities increased with ionic content. The static dielectric constant ($\varepsilon_s$) increased linearly with ion content; the PCL block copolymers had much higher $\varepsilon_s$ than the PCL homopolymers and even the oligoester at any temperature above $T_c$. These results demonstrate clearly that with proper design, block copolymers have the potential to provide high single-ion conductivities combined with good mechanical strength, key attributes for application of these materials in mechanical actuators.

## 1d. Vinyl Terminated Imidazolium Salts and Their ADMET Polymers:

A series of monomers was prepared with varied x and y values, all with $PF_6^-$ counterions. Some of these were subjected to Acyclic Diene Methathesis Polymerization (ADMET) in Prof. Ken Wagener's laboratory at the U of Florida. [2, 8] Unfortunately these materials were extremely difficult to work with because of their high

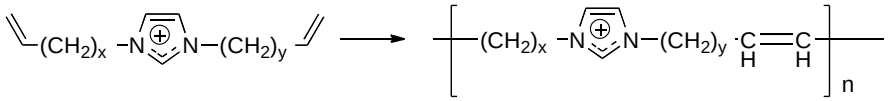

viscosity and surfactant-like natures; as a result no conductivity measurements were carried out on them.

**1e. Poly(meth)acrylate-based imidazolium Salts:**

A series of acrylates and methacrylates with variable length spacers X and Y, terminal N-substituents Z and counterions was prepared. [5, 9, 10] These monomers were polymerized by classical AIBN initiation. The resultant polymers exhibited low $T_g$s (down to -50 $^oC$) and high room temperature ionic conductivities (up to 8 x $10^{-5}$ S/cm). Ionomers with an *n*-butyl tail (Z) exhibit much larger static dielectric constants than those with *n*-dodecyl tails. Based on analysis of the static dielectric constant using

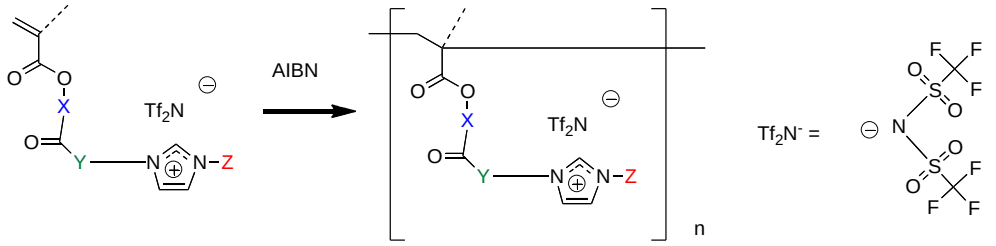


Onsager theory, there was more ionic aggregation in ionomers with the *n*-dodecyl tails than in those with the *n*-butyl tails, consistent with X-ray scattering, which revealed a much stronger ionic aggregate peak for the ionomers with dodecyl tails. [9] Based on analysis of the static dielectric constants using the Kirkwood g correlation factor, the dipoles in conventional (small) ionic liquids prefer antiparallel alignment ($g \approx 0.1$), lowering $\varepsilon_s$ values (≤30), because their polarizability volumes $V_p$ strongly overlap, whereas the dipoles in the larger ionic liquid monomers display $g \sim 1$ and $50 \leq \varepsilon_s \leq 110$. Longer spacers lead to higher static dielectric constants, owing to significant increases in the relaxation strength of the $\alpha_2$ process, which is directly reflected through an unanticipated increase of the static dielectric constant with ionic liquid molecular volume $V_m$. The glass transition temperature of polymerized imidazolium ionic liquids with various counterions was also shown to simply be a monotonically decreasing function of $V_m$. Furthermore, the ionomers consistently exhibited 1.5−2.3 times higher static dielectric constants ($\varepsilon_s$ up to ∼140 at room temperature) than the monomers from which they were synthesized, suggesting that polymerization encourages the observed synergistic dipole alignment ($g > 1$). [10]

Unfortunately these monomers are quite prone to auto-polymerization, thus making them difficult to work with and to use in controlled radical polymerizations for preparation of the block copolymers needed for actuator application of these soft materials.

**1f. Poly(oxa)norbornenes via Ring Opening Metathesis Polymerization (ROMP):**

In order to avoid the autopolymerization problem encountered with (meth)acrylates, we synthesized a variety of oxanorbornenes and norbornenes with one

or two imidazolium moieties connected via oligoethyleneoxy units and terminated with either butyl or oligoethyleneoxy units.

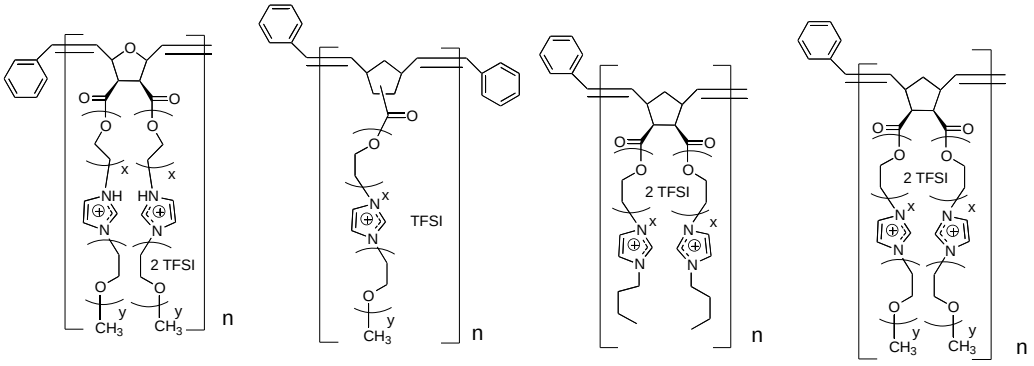


These monomers were thermally stable and could be stored for indefinite periods. ROMP was readily accomplished with a Grubbs catalyst at room temperature in a living process, allowing molecular weight control and block copolymerization. These polymers possessed $T_g$s as low as -65 $^oC$ and room temperature ionic conductivities ranging up to $10^{-4}$ S/cm.

To prepare block copolymers as potentially useful actuator materials we chose to incorporate an oxanorbornene imide as the hard A segment of an ABA triblock system. Two of these triblock copolymers were prepared. Thermal analysis and preliminary X-ray scattering results indicated that a substantial amount of phase mixing occurred, lowering the $T_g$ of the hard blocks and raising that of the soft block; this was attributed to interaction of the imide's aryl moiety with the imidazolium groups in the soft block. To avoid this, N-alkyl imides were prepared, but the resulting systems have not been evaluated, since funding expired.

A film of one of the ABA triblock copolymers (x=2, y=3, a=58, b=29; mass ratios 21:58:21; total $M_n$ 65.3 kDa) exhibited an electromechanical actuator response as a single ion conductor without a low molar mass dopant. However, the deflection was relatively small and speed was relatively slow. This may be the result of: a) unoptimized phase separation as noted above, b) too high a modulus from the imide. Use of N-alkyl imide analogs is expected to improve the performance of the resulting triblock systems.

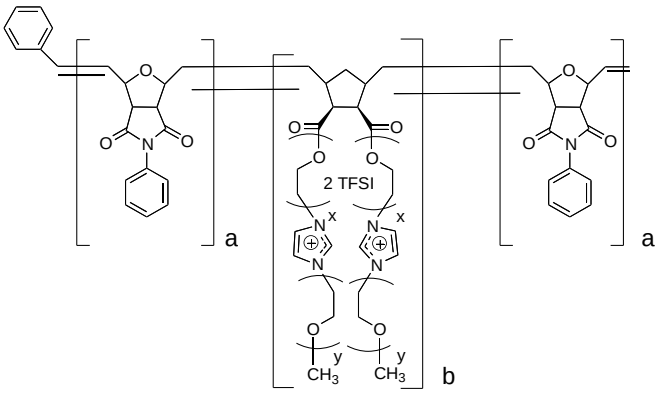


These results will be included in several manuscripts to be constructed in the near future.

*Timothy E. Long*

**Anionic Polymerization and Post-Alkylation of 4-Vinylbenzyl piperidine (Alison R. Schultz and Timothy E. Long)**

Synthetic protocols for controlled radical polymerization processes typically require elevated temperatures, bulk concentrations, and extensive reaction times. These conditions are also prerequisite for thermal autopolymerization requirements for styrenic monomers, which often limits polymerization control. Traditional anionic living polymerization strategies provide an alternative solution, and promote linear chain propagation in polar or nonpolar environments, at ambient temperatures, and for short reaction times. Living anionic polymerization of 4-vinylbenzyl piperidine (VBP) provided a viable strategy for achieving a novel series of piperidinyl homopolymers and block copolymers. This study reports piperidinyl-containing macromolecules as a relatively unexplored site for subsequent alkylation and production of novel piperidinium polymers for ionomer and polyelectrolyte applications.

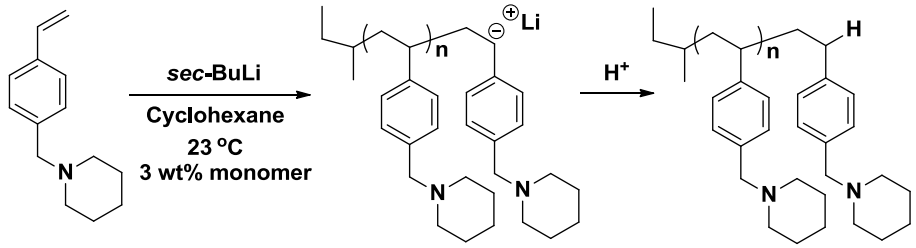


**Scheme 1.** General reaction scheme for the anionic polymerization of 4-vinylbenzyl piperdine

**Scheme 1** depicts the anionic polymerization strategy for synthesizing poly(vinylbenzyl piperidine). *In situ* fourier transform infrared spectroscopy (FTIR) monitored the polymerization and revealed complete monomer consumption within approximately 30 min. Tracking the monomer concentration over time provided a pseudo-first-order kinetics plot which led to the calculated propagation rate $k_p$ of 2.7 L mol$^{-1}$ s$^{-1}$ (**Figure 1**). This experimental value agreed with previously reported rate constants for styrene (2.0 L mol$^{-1}$ s$^{-1}$) and isoprene (1.5 L mol$^{-1}$ s$^{-1}$),[14] which demonstrated the suitability for anionic polymerization conditions.

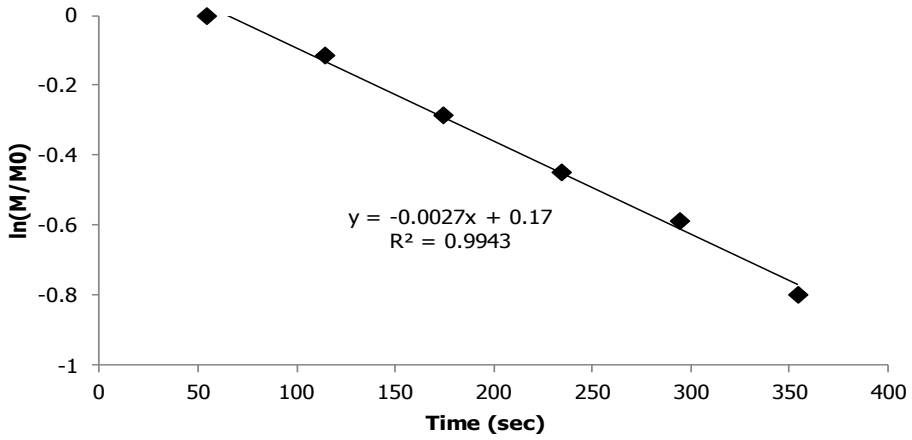


**Figure 1.** Pseudo-first-order kinetic plot for 4-vinylbenzyl piperidine anionic polymerization

Elucidating the anionic polymerization kinetics allowed controlled polymerizations studies to proceed, leading to a series of increasing molecular weight homopolymers. $^{1}$H-NMR confirmed the polymer structure (**Figure 2**) and SEC verified that the target molecular weights were achieved with well-defined molecular weight distribution (**Figure 3 and Table 1**). Controlled anionic polymerization was successful and enabled to the production piperidinyl containing homopolymers for post alkylation.

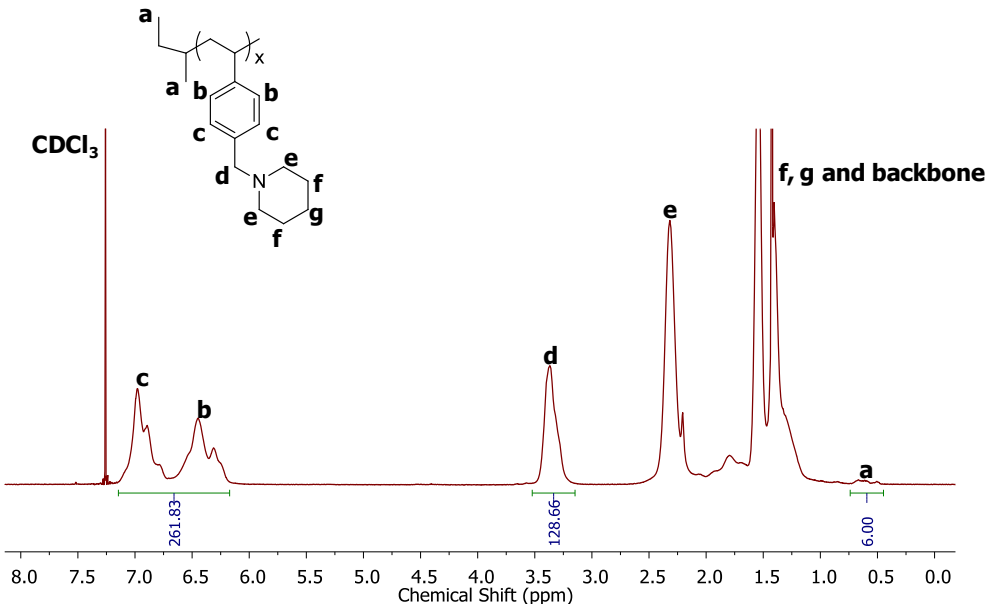


**Figure 2.** $^{1}$H-NMR characterization of poly(VBP). 400 MHz, $CDCl_3$, 22 $^{o}$C

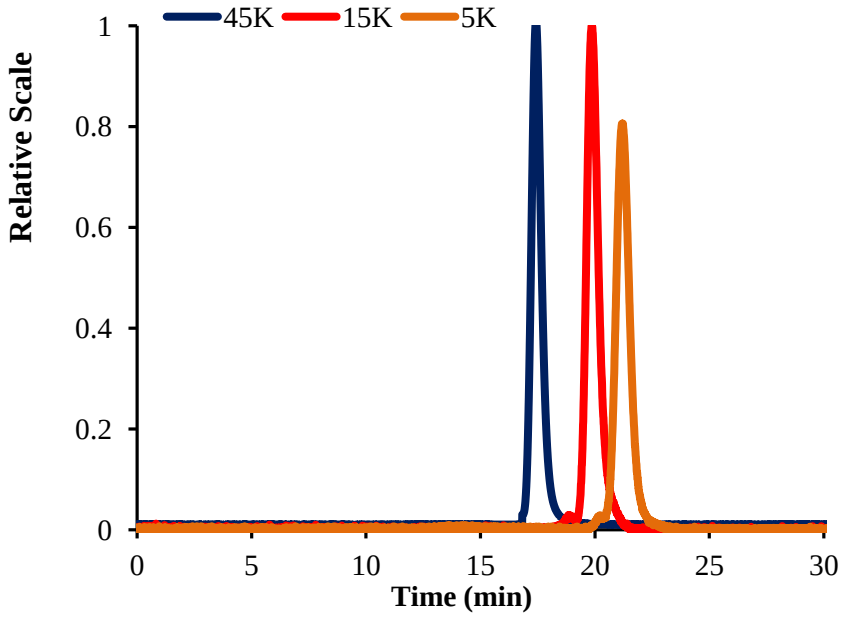


**Figure 3.** SEC characterization of poly(VBP). 400 MHz, $CDCl_3$, 22 $^oC$

**Table 1.** SEC characterization for the controlled anionic polymerization of VBP

| Target $M_n$ g/mol x $10^{-3}$ | SEC $M_n$ g/mol x $10^{-3}$ | $M_w/M_n$ |
|---|---|---|
| 5.0 | 6.2 | 1.03 |
| 15.0 | 13.4 | 1.05 |
| 45.0 | 42.3 | 1.04 |

Post-polymerization alkylation achieved novel piperidinium-containing polymers.[1,2] **Scheme 4** depicts the general alkylation reaction on poly(VBP) for achieving novel poly(piperidinium)s. This method is applicable for any bromoalkane. Modification with 4-(bromomethyl)-benzyltriphenylphosphonium bromide (TPhPBr) demonstrated the versatile alkylation method. Ammonium and phosphonium containing polymers are highly recognized for their antibacterial properties.[3-10] Recent studies now show structures containing both salts exhibit even better bacterial resistance.[11,12] This feature is ideal for applications in water purification[13,14] and gene delivery.[11,15]

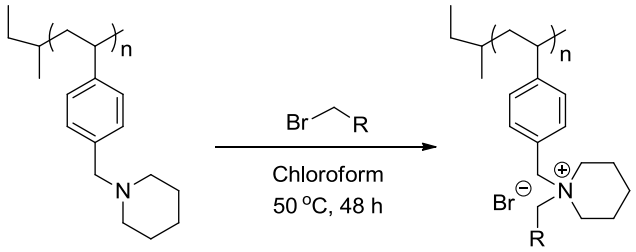


**Scheme 4.** Alkylating Poly(VBP) with bromoalkanes to develop a new class of ammonium containing charged polymers

$^1$H NMR revealed quantitative alkylation with TPhPBr. Thermogravimetric analysis (TGA) and differential scanning calorimetry (DSC) probed the thermomechanical properties of both polymers (**Table 2**). Figure 10 highlights the TGA transitions for both polymers, revealing high thermal degradation and indicating a slight decrease in stability for Poly(VBP-TPhPBr)$^+$. DSC analysis showed an increase in glass transition ($T_g$) temperature values. The increase in $T_g$ is rationalized by the incorporation of charged species and bulky phenyl substituents.

**Table 2.** Thermomechanical properties for polyVBP and poly(VBP-TPhPBr)$^+$

| Sample | $T_{d1}$ | $T_{d2}$ | $T_g$ |
|---|---|---|---|
| polyVBP | 373 | ----- | 82 |
| Poly(VBP-TPhPBr) | 311 | 447 | 176 |

Overall, living anionic polymerization provided an efficient route to overcome thermal autopolymerization challenges, and enabled the first reported controlled polymerization of 4-vinylbenzyl piperidine. Post alkylation successfully produced novel piperidinium based polymers to introduce a new series of charged polymers for expanding ionomer and polyelectrolyte applications.

## References

(1) Tomoi, M.; Hosokawa, Y.; Kakiuchi, H. *J. Polym. Sci., Polym. Chem. Ed.* **1984**, *22*, 1243.
(2) Parent, J. S.; Penciu, A.; Guillen-Castellanos, S. A.; Liskova, A.; Whitney, R. A. *Macromolecules* **2004**, *37*, 7477.
(3) Popa, A.; Ilia, G.; Iliescu, S.; Dehelean, G.; Pascariu, A.; Bora, A.; Davidescu, C. M. *Mol. Cryst. Liq. Cryst.* **2004**, *418*, 195.
(4) Beyth, N.; Yudovin-Farber, I.; Bahir, R.; Domb, A. J.; Weiss, E. I. *Biomaterials* **2006**, *27*, 3995.
(5) Harney, M. B.; Pant, R. R.; Fulmer, P. A.; Wynne, J. H. *ACS Appl. Mater. Interfaces* **2009**, *1*, 39.
(6) Kim, Y. H.; Sun, G. *Text. Res. J.* **2000**, *70*, 728.

(7) Sheldon, B. G.; Wingard, R. E., Jr.; Weinshenker, N. M.; Dawson, D. J.; Dynapol, USA . 1983, p 30 pp.
(8) Takai, K.; Ohtsuka, T.; Senda, Y.; Nakao, M.; Yamamoto, K.; Matsuoka, J.; Hirai, Y. *Microbiol. Immunol.* **2002**, *46*, 75.
(9) Kanazawa, A.; Ikeda, T.; Endo, T. *J. Polym. Sci., Part A: Polym. Chem.* **1993**, *31*, 1467.
(10) Tashiro, T. *Macromol. Mater. Eng.* **2001**, *286*, 63.
(11) Kenawy, E.-R.; Abdel-Hay, F. I.; El-Shanshoury, A. E.-R. R.; El-Newehy, M. H. *J. Polym. Sci., Part A: Polym. Chem.* **2002**, *40*, 2384.
(12) Kenawy, E.-R.; Abdel-Hay, F. I.; El-Shanshoury, A. E.-R. R.; El-Newehy, M. H. *J. Controlled Release* **1998**, *50*, 145.
(13) Sagle, A. C. *Journal of membrane science* **2009**, *340*, 92.
(14) Hatakeyama, E. S.; Ju, H.; Gabriel, C. J.; Lohr, J. L.; Bara, J. E.; Noble, R. D.; Freeman, B. D.; Gin, D. L. *Journal of membrane science* **2009**, *330*, 104.
(15) Hemp, S. T.; Smith, A. E.; Bryson, J. M.; Allen, M. H.; Long, T. E. *Biomacromolecules* **2012**, *13*, 2439.

**Well-Defined Imidazolium ABA Triblock Copolymers as Ionic-Liquid Containing Electroactive Membranes (Chainika Jangu and Timothy E. Long)**

Nitroxide-mediated polymerization (NMP) afforded the synthesis of well-defined ABA triblock copolymers with polystyrene external blocks and a charged poly(1-methyl-3-(4-vinylbenzyl)imidazolium bis(trifluoromethane sulfonyl)imide central block. Aqueous SEC and $^{1}$H NMR spectroscopic studies confirmed the control of the composition and block lengths for both central and external blocks. Dynamic mechanical analysis (DMA) revealed a room temperature modulus suitable for fabricating these triblock copolymers into electroactive devices in the presence of added ionic liquid. Dielectric relaxation spectroscopy (DRS) elucidated the ion-transport properties of the ABA triblock copolymers with varied compositions. Ionic conductivity in these single-ion conductors exhibited Vogel-Fulcher-Tammann (VFT) and Arrhenius temperature dependence, and electrode polarization (EP) analysis determined the number density of simultaneously conducting ions and their mobility

Ionic conductivity in single-ion conductors strongly depends on frequency and temperature. The value of DC conductivity presented is defined as the in-phase component of the conductivity, which is independent of frequency in a roughly three-decade frequency range. Poly[$Sty_{40}$-*b*-$(MVBIm\text{-}Tf_2N)_{35}$-*b*-$Sty_{40}$], which has the lowest weight percent of the ion-conducting blocks, exhibited the highest ionic conductivity and the lowest $T_g$ of the ion conducting block. Ionic conductivity decreased with increasing weight percent of the imidazolium ion-containing block and correlated closely with the $T_g$ of the ion-containing block except for poly[$Sty_{10}$-*b*-$(MVBIm\text{-}Tf_2N)_{80}$-*b*-$Sty_{10}$], where an

unusual Arrhenius temperature dependence of ionic conductivity was observed and DMA suggested incorporation of polystyrene into the ion-conducting phase.

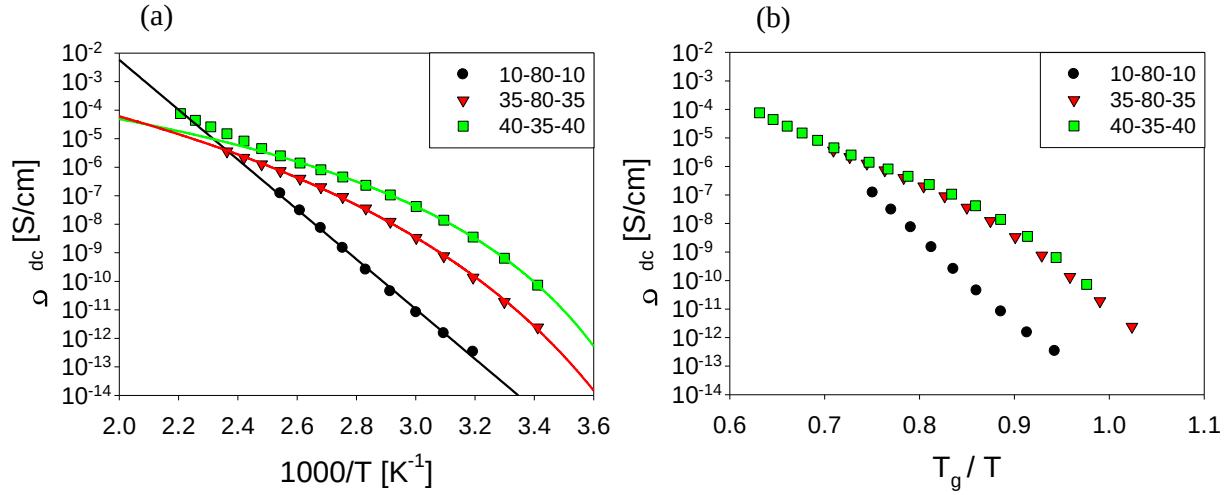


**Figure 1. (a)** Temperature dependence of ionic conductivity for poly[Sty-*b*-(MVBIm-$Tf_2N$)-*b*-Sty] having different weight percent of the styrene external blocks. **(b)** Ionic conductivity with respect to inverse temperature normalized by $T_{g1}$.

The actuation performance of these triblock copolymers without ionic liquid was previously reported in the literature and showed ion migration and accumulation at one electrode.[11] In the present study, triblock copolymer poly($Sty_{35}$-*b*-(MVBIm-$Tf_2N$)$_{80}$-*b*-$Sty_{35}$) casted with 32 wt.% ionic liquid was fabricated into electromechanical actuators. A cast-with method ensured uniform incorporation of the IL throughout the triblock copolymer.[10] In the evaluation, a 4V DC step input was applied to the actuator at ambient conditions (20 ˚C and ~ 43% RH) and a high definition camera for further analysis recorded the induced electromechanical actuation. The analysis demonstrated electromechanical actuation upon application of low voltages, which is the first time these triblock copolymers have demonstrated actuation. A common feature for electroactive devices is ion saturation, and the polarity of the device is subsequently reversed and the device relaxes in opposite direction. These triblock copolymers exhibited electrochemically stability between +4 V and -4 V observed through cyclic voltammetry.

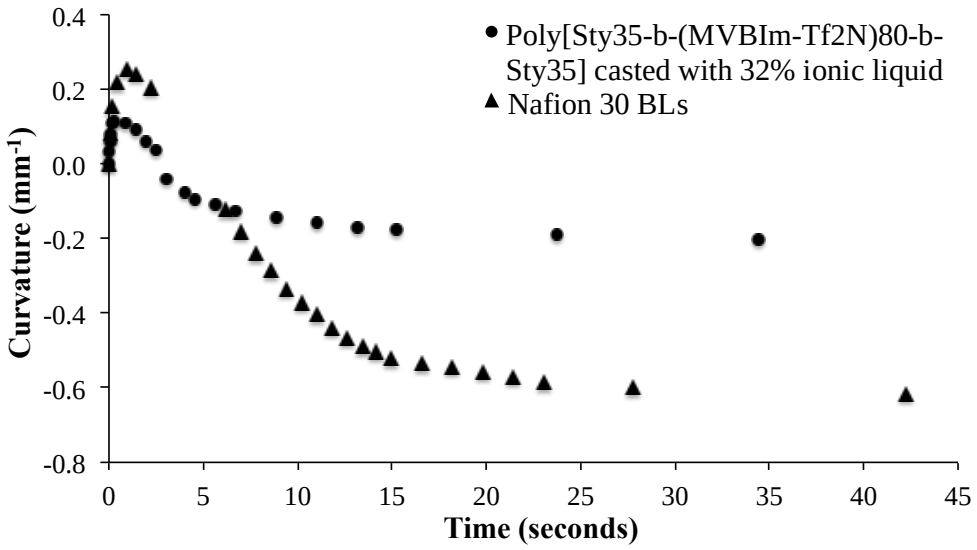


**Figure 2.** Curvature observed under a 4 V applied voltage for electromechanical actuators made from poly($Sty_{35}$-*b*-(MVBIm-$Tf_2N)_{80}$-*b*-$Sty_{35}$) triblock copolymer casted with 32% of ionic liquid and Nafion® membrane swollen with 34% ionic liquid.

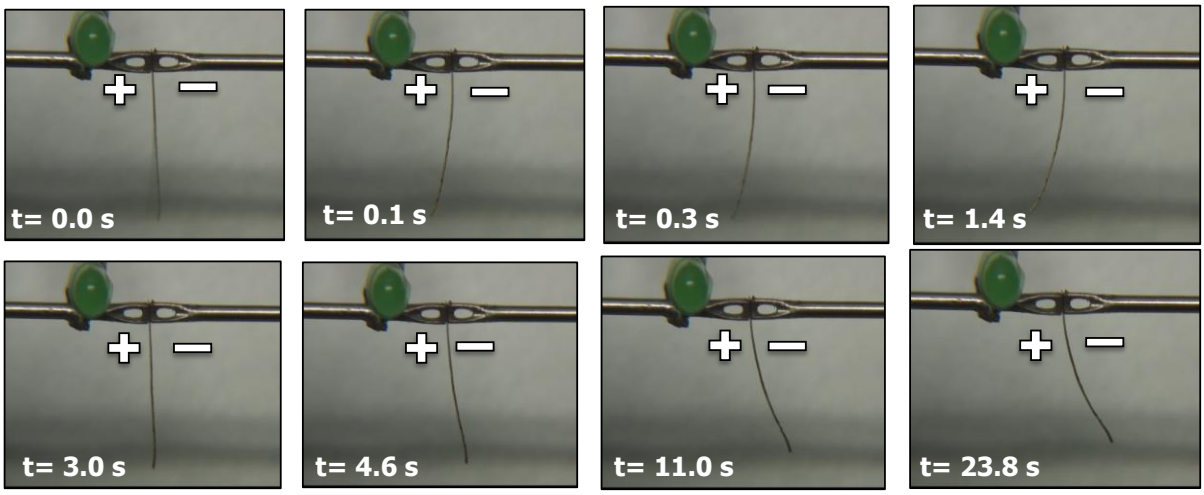


**Figure 3.** Still images of electromechanical transducer fabricated from poly[$Sty_{35}$-*b*-(MVBIm-$Tf_2N)_{80}$-$Sty_{35}$] film casted with 32 wt.% ionic liquid [EMIm] [TfO] under applied potential of 4V.

The bending performance of the actuator of the poly($Sty_{35}$-*b*-(MVBIm-$Tf_2N)_{80}$-*b*-$Sty_{35}$) triblock copolymer membrane, and a Nafion® membrane swollen with 32% ionic liquid as control are shown in Figure 11. Due the difference size and migration speed of the cation and anion of IL in the actuator, the triblock copolymer actuator experienced the same bi-directional bending behavior as the Nafion® actuator[30] under the 4V DC applied voltage. Although the triblock copolymer actuator showed smaller bending

curvature as compared to Nafion®, the actuation speed was fairly rapid comparable to the Nafion® actuator. The fast actuation speed indicated the triblock copolymer had good ion conductivity, while the smaller bending curvature was presumably due to lower IL uptake.

**ILEAD MURI Publicaitons (Manuscripts, Reprints and Conference Proceedings)**

The main avenue of disseminating research results from the ILEAD MURI efforts relies on publications, including manuscripts, reprints, and conference proceedings. During the 2012-2013 year the ILEAD MURI team submitted 3 manuscripts, published 42 reprints, presented 19 presentations at Conferences, Universities, and Industrial Companies.

**Peer Reviewed Papers – submitted or in press (manuscripts):**

1. Anuj Mittal, U Hyeok Choi, Terry L. Price, Jr., James Runt, Ralph H. Colby, and Harry W. Gibson, Imidazolium-based Ionic Liquids & Analogs as Initiators in Ring Opening Polymerization of ε-Caprolactone: End-Functional Polymers and Block Copolymers

2. U Hyeok Choi, Yuesheng Ye, David Salas de la Cruz, Wenjuan Liu, Karen I. Winey, Yossef A. Elabd, James Runt and Ralph H. Colby, Dielectric and Viscoelastic Behavior of Imidazolium-based Ionomers with Different Counterions and Side Chain Lengths

3. Kidd, B. E.; Lingwood, M. D.; Lee, M.; Gibson, H. W; Madsen, L. A. Cation and Anion Transport in a Dicationic Imidazolium-Based Plastic Crystal Ion Conductor, *J. Phys. Chem. B*

**Peer Reviewed Papers – published (new reprints):**

1. Junhong Lin, Yang Liu, Q.M. Zhang, Influence of the Ionic Polymer Membrane Thickness on Charge dynamics of Ionic Liquids in Ionic Polymer Actuators. *Macromolecules* 45, 2050 (**2012**).

2. Yang Liu, Ran Zhao, Junhong Lin, Sheng Liu, Q. M. Zhang, Hülya Cebeci, Roberto Guzmán de Villoria, Brian Wardle, Reza Montazami, Dong Wang, James R. Heflin. Equivalent Circuit Modeling of Ionomer and Ionic Polymer Conductive network Composite Actuators Containing Ionic Liquids. *Sensors and Actuators*. A 181, 70 (**2012**).

3. Gokhan Hatipoglu*,* Yang Liu*,* Ran Zhao*,* Mitra Yoonessi*,* Dean M. Tigelaar*,* Srinivas Tadigadapa *and* Q. M. Zhang, A Highly Aromatic and Sulfonated Ionomer for High Elastic Modulus Ionic Polymer Membrane Micro-actuators. *Smart Mater & Struct,* 21, 055015 (**2012**).

4. Yang Liu, Ran Zhao, Mehdi Ghaffari, Jun-Hong Lin, Minren Lin and Q. M. Zhang. Enhanced Electro-mechanical Responses of P(VDF-CTFE) based Actuators. DOI: 10.1021/ma300591a *Macromolecules* (**2012**).

5. Yang Liu, Caiyan Lu, Stephen Twigg, Mehdi Ghaffari, Junhong Lin, Nicholas Winograd, Q. M. Zhang, Direct Observation of Ion Distributions near Electrodes in Ionic Polymer Actuators Containing Ionic Liquids. *Scientific Reports*, 3, 973 (**2013**).

6. Price, S.C.; Ren, X.; Jackson, A.C.; Ye, Y.; Elabd, Y.A.; Beyer, F.L. Bicontinuous Alkaline Fuel Cell Membranes from Strongly Self-Segregating Block Copolymers. *Macromolecules* **2013**, *46*, 7332-7340.

7. Choi, J.-H.; Ye, Y.; Elabd, Y.A.; Winey, K.I. Network Structure and Strong Microphase Separation for High Ion Conductivity in Polymerized Ionic Liquid Block Copolymers. *Macromolecules* **2013**, *46*, 5290-5300.

8. Ye, Y.; Wang, S.; Davis, E.M.; Winey, K.I.; Elabd Y.A. High Hydroxide Conductivity in Polymerized Ionic Liquid Block Copolymers. *ACS Macro Letters* **2013**, *2*, 575-580.

9. Ye, Y.; Stokes, K.K.; Beyer, F.L.; Elabd, Y.A. Development of Phosphonium-based Bicarbonate Anion Exchange Polymer Membranes. *J. Membrane Sci.* **2013**, *443*, 93-99.

10. Ye, Y.; Choi, J.-H.; Winey, K.I.; Elabd, Y.A. Polymerized Ionic Liquid Block and Random Copolymers: Effect of Weak Microphase Separation on Ion Transport. *Macromolecules* **2012**, *45*, 7027-7035.

11. Salas-de la Cruz, D.; Green, M.D.; Ye, Y.; Elabd, Y.A.; Long, T.E.; Winey, K.I. Correlating Backbone-to-Backbone Distance to Ionic Conductivity in Amorphous Polymerized Ionic Liquids. *J. Polym. Sci.: Part B: Pol. Phys.* **2012**, *50*, 338-346.

12. "Influence of Conductive Network Composite Structure on the Electromechanical Performance of Ionic Electroactive Polymer Actuators," R.Montazami, D. Wang, J.R. Heflin, International Journal of Smart and Nano Materials 3, 204-213 (**2012**)

13. "The Effect of Ionic Liquid Uptake and Self-Assembled Conductive Network Composite Layers on Nafion-Based Ionic Polymer Metal Composite Electromechanical Bending Actuators," D. Wang, R. Montazami, J.R. Heflin, MRS Online Proceedings Library 1575 (**2013**)

14. A. A. Lee, R. H. Colby and A. A. Kornyshev, Statics and Dynamics of Electroactuation with Single-Charge-Carrier Ionomers, *J. Phys.: Condens. Matt*. 25, 082203 (**2013**).

15. A. A. Lee, R. H. Colby and A. A. Kornyshev, Electroactuation with Single Charge Carrier Ionomers: the roles of Electrostatic Pressure and Steric Strain, *Soft Matter* 9, 3767 (**2013**).

16. D. Salas-de la Cruz, J. G. Denis, M. D. Griffith, D. R. King, P. A. Heiney, K. I. Winey, *Review of Scientific Instruments*, 83, 025112, **2012**. “Environmental chamber for *in situ* dynamic control of temperature and relative humidity during X-ray scattering.”

17. K. Sinha, W. Wang, K. I. Winey. J. K. Maranas* *Macromolecules*, 45, 4354 - 4362, **2012.** “Dynamic patterning in PEO based single ion conductors for Li ion batteries.”

18. Y. Ye, J.-H. Choi, K. I. Winey*, Y. A. Elabd*, *Macromolecules*, 45, 7027 - 7035, **2012**. “Polymerized ionic liquid block and random copolymers: Effect of weak microphase separation on ion transport.”

19. J.-H. Choi, C. L. Willis, K. I. Winey, *Journal of Membrane Science*, 428, 516-522, **2013**. “Effects of neutralization with $Et_3Al$ on structure and properties in sulfonated styrenic pentablock copolymers.”

20. M. H. Allen, S. Wang, S. T. Hemp, Y. Chen, L. A. Madsen, K. I. Winey, T. E. Long, *Macromolecules*, 46, 3037-3045, **2013**."Hydroxyalkyl-containing imidazolium homopolymers: Correlation of structure with conductivity."

21. J.-H. Choi, Y. Ye, Y. A. Elabd, K. I. Winey, *Macromolecules*, 46, 5290-5300, **2013**. "Network Structure and Strong Microphase Separation for High Ion Conductivity in Polymerized Ionic Liquid Block Copolymers."

22. Hemp, S. T.; Zhang, M.; Allen, M. H., Jr.; Cheng, S.; Moore, R. B.; Long, T.E., Comparing Ammonium and Phosphonium Polymerized Ionic Liquids: Thermal Analysis, Conductivity, and Morphology. *Macromolecular Chemistry and Physics* **2013**, 214(18), 2099-2107

23. Hemp, S. T.; Allen, M. H. Jr.; Smith, A. E.; Long, T. E., Synthesis and Properties of Sulfonium Polyelectrolytes for Biological Applications. *ACS Macro Letters* **2013**, 2(8), 731-735.

24. Gao, R.; Zhang, M.; Wang, S.; Moore, R. B.; Colby, R. H.; Long, T. E., Polyurethanes Containing an Imidazolium Diol-Based Ionic-Liquid Chain Extender for Incorporation of Ionic-Liquid Electrolytes. *Macromolecular Chemistry and Physics* **2013**, 214(9), 1027-1036.

25. Allen, M. H.; Day, K. N.; Hemp, S. T.; Long, T. E., Synthesis of Folic Acid-Containing Imidazolium Copolymers for Potential Gene Delivery Applications. *Macromolecular Chemistry and Physics* **2013**, 214(7), 797-805.

26. Allen, M. H., Jr.; Wang, S.; Hemp, S. T.; Chen, Y.; Madsen, L. A.; Winey, K. I.; Long, T.E., Hydroxyalkyl-Containing Imidazolium Homopolymers: Correlation of Structure with Conductivity. *Macromolecules* **2013**, 46(8), 3037-3045.

27. Gao, R.; Ramirez, S. M.; Inglefield, D. L.; Bodnar, R. J.; Long, T. E., The preparation of cation-functionalized multi-wall carbon nanotube/sulfonated polyurethane composites. *Carbon* **2013**, (54), 133-142.

*28.* Allen, M. H.; Hemp, S. T.; Zhang, M.; Zhang, M.; Smith, A. E.; Moore, R. B.; Long, T. E., Synthesis and characterization of 4-vinylimidazole ABA triblock copolymers utilizing a difunctional RAFT chain transfer agent. *Polymer Chemistry* **2013,** 4*(7*), *2333-2341.*

29. Wu, T.; Wang, D.; Zhang, M.; Heflin, J. R.; Moore, R. B.; Long, T. E., RAFT Synthesis of ABA Triblock Copolymers as Ionic Liquid-Containing Electroactive Membranes. *Applied Materials & Interfaces* **2012**, 4(12), 6552-6559.

30. Green, M. D.; Wang, D.; Hemp, S.T.; Choi, J-H.; Winey, K. I.; Heflin, J. R.; Long, T. E., Synthesis of imidazolium ABA triblock copolymers for electromechanical transducers. *Polymer* **2012**, 53(17), 3677-3686.

31. Gao, R.; Wang, D.; Heflin, J. R.; Long, T. E., Imidazolium sulfonate-containing pentablock copolymer-ionic liquid membranes for electroactive actuators. *Journal of Materials Chemistry* **2012**, 22(27), 13473-13476.

32. Hemp, S. T.; Smith, A. E.; Bryson, J. M.; Allen, M. H.; Long, T. E., Phosphonium-Containing Diblock Copolymers for Enhanced Colloidal Stability and Efficient Nucleic Acid Delivery. *Biomacromolecules* **2012**, 13(8), 2439-2445.

33. Green, M. D.; Choi, J-H.; Winey, K. I.; Long, T. E., Synthesis of Imidazolium-Containing ABA Triblock Copolymers: Role of Charge Placement, Charge Density, and Ionic Liquid Incorporation. *Macromolecules* **2012**, 45(11), 4749-4757.

34. Allen, M. H.; Hemp, S. T.; Smith, A. E.; Long, T. E., Controlled Radical Polymerization of 4-Vinylimidazole. *Macromolecules* **2012**, 45(9), 3669-3676.

35. Tamami, M.; Salas-de la Cruz, D.; Winey, K. I.; Long, T. E., Structure-Property Relationships of Water-Soluble Ammonium-Ionene Copolymers. *Macromolecular Chemistry and Physics* **2012**, 213(9), 965-972.

36. Suga, T.; Hunley, M. T.; Long, T. E.; Nishide, H., Electrospinning of radical polymers: redox-active fibrous membrane formation. *Polymer Journal* **2012**, 44(3), 264-268.

37. Hemp, S. T.; Hunley, M. T.; Cheng, S.; DeMella, K. C.; Long, T. E., Synthesis and solution rheology of adenine-containing polyelectrolytes for electrospinning. Polymer **2012**, 53(7), 1437-1443.

38. Salas-de la Cruz, D.; Green, M. D.; Ye, Y.; Elabd, Y. A.; Long, T. E.; Winey, K. I., Correlating backbone-to-backbone distance to ionic conductivity in amorphous polymerized ionic liquids. *Journal of Polymer Science, Part B: Polymer* Physics **2012**, 50(5), 338-346.

39. Hemp, S. T.; Allen, M. H.; Green, M. D.; Long, T. E., Phosphonium-containing polyelectrolytes for nonviral gene delivery. *Biomacromolecules* **2012**, 13(1), 231-238.

40. Aitken, B. S.; Buitrago, C. F.; Heffley, J. D.; Lee, M.; Gibson, H. W. Winey, K. I.; Wagener, K. B. Precision Ionomers: Synthesis and Thermal/Mechanical Characterization, *Macromolecules* **2012**, *45,* 681–687.

41. Choi, U-H.; Lee, M.; Wang, S.; Liu, W.; Winey, K. I.; Gibson, H. W.; Colby, R. H. Ionic Conduction and Dielectric Response of Poly(imidazolium acrylate) Ionomers, *Macromolecules* **2012**, *45,* 3974–3985.

42. Choi, U H.; Mittal, A.; Price, T. L., Jr.; Gibson, H. W.; Runt, J.; Colby, R. H. Polymerized Ionic Liquids with Enhanced Static Dielectric Constant, *Macromolecules* **2013**, *46,* 1175-1186.

**Papers presented at meetings, but not published in conference proceedings:**

1. D. Wang, R. Montazami, J.R. Heflin; "The Effect of Ionic Liquid Uptake and Self-Assembled Conductive Network Composite Layers on Nafion-Based Ionic Polymer Metal Composite Electromechanical Bending Actuators," *2013 Materials Research Society Spring Meeting* (San Francisco, CA, 4 April, **2013**).

2. Winey, K.I.; Materials Science and Engineering, University of Michigan (March, **2013**) Ann Arbor, MI "Recent Progress in the Morphology of Precise Copolymers, Ionic Conductivity in Ionomers, and Electrical Conductivity in Polymer Nanocomposites"

3. Wang, S.; Ye, Y.; Elabd, Y.A.; Winey, K.I. Morphologies and Ionic Conductivity in Polymerized Ionic Liquid Block Copolymers. Materials Research Society Meeting, San Francisco, CA, April **2013**.

4. Elabd, Y.A. Fuel Cell Membranes. Short course on Membranes for Clean Water and Energy. American Physical Society Meeting, Baltimore, MD, March 2013. Invited Speaker

5. Beyer, F.L.; Price, S.; Jackson, A.; Ren, X.; Chu, D.; Ye, Y.; Elabd, Y.A. Anion Exchange Membranes Based on Reactive Block Copolymers. American Physical Society Meeting, Baltimore, MD, March **2013.**

6. Wang, S.; Ye, Y.; Elabd, Y.A.; Winey, K.I. Ordered and Disordered Polymerized Ionic Liquid Block Copolymers: Morphology and Ion Conductivity. American Physical Society Meeting, Baltimore, MD, March **2013**.

7. Choi, J.-H.; Ye, Y.; Elabd, Y.A.; Winey, K.I. Effect of Morphology on Ion Transport in Polymerized Ionic Liquid Block Copolymers. American Physical Society Meeting, Baltimore, MD, March **2013**.

8. Elabd, Y.A. Block Copolymers in Fuel Cells. Advanced in Materials for Proton Exchange Membrane Fuel Cells Systems Meeting, sponsored by The Division of Polymer Chemistry (POLY) of the American Chemical Society, Asilomar, CA, February **2013**. Invited Speaker

9. Ye, Y.; Choi, J.; Wang, S.; Winey, K.I.; Elabd, Y.A. Hydroxide Conducting Polymerized Ionic Liquid Block Copolymers for Alkaline Fuel Cells. Annual Meeting of the American Institute of Chemical Engineers, Pittsburgh, PA October **2012**. Invited Speaker

10. Ionically Conductive Polymers Incorporating Imidazolium Moieties, H. W. Gibson, M. Lee, A. Mittal, D. V. Schoonover, T. L. Price, Jr., A. Murugan, U-H. Choi, D. Salas-de la Cruz, R. H. Colby and K. I. Winey, XXI International Materials Research Congress, Cancun, Mexico, August 12-17, **2012**. (Invited)

11. Design, Synthesis and Evaluation of Ion Conducting Imidazolium Polymers for Use as Actuators, H. W. Gibson, M. Lee, A. Mittal, T. L. Price, Jr., A. Murugan, D. V. Schoonover, U-H. Choi, R. H. Colby, D. Salas de la Cruz, K. I. Winey, Materials Engineering and Science Department, Penn State University, University Park, PA, March 12, **2013**. (Invited)

12. Transport Dynamics in a Bis-Imidazolium-Based Organic Ionic Plastic Crystal, B. E. Kidd, M. D. Lingwood, M. Lee, H. W. Gibson, L. A. Madsen, 245th National Meeting of the American Chemical Society, New Orleans, LA, April 9, **2013**.

13. Design and Synthesis of ROMP Imidazolium Polymers for Use as Actuators, T. L. Price, Jr.; U H. Choi, D. Wang, A. Murugan, D. V. Schoonover, M. Zhang, R. H. Colby, J. R.

Heflin, R. B. Moore, H. W. Gibson, 245th National Meeting of the American Chemical Society, New Orleans, LA, April 11, **2013**.

14. Design and Synthesis of ROMP Imidazolium Polymers for Use as Actuators, T. L. Price, Jr.; U H. Choi, D. Wang, A. Murugan, D. V. Schoonover, M. Zhang, R. H. Colby, J. R. Heflin, R. B. Moore, H. W. Gibson, Virginia Academy of Sciences 91st Annual Meeting, Virginia Tech, Blacksburg, VA, May 23, **2013**.

15. Long, T. E. Gordon Research Conference, Adhesives, Charged Polymers as Interfacial Adhesives, July **2013**.

16. Long, T.E. ACS Polymer Division Workshop, Polycondensation 2012, Engineering Thermoplastics Containing Charged Units, September **2012**.

17. Long, T.E. BASF Research Seminar (invited), Germany, New Directions in Polymer Synthesis: Strategies and Structure, September **2012**.

18. Long, T.E. SABIC Corporation (invited), Charged Polymers Enabling New Technologies, October **2012**.

19. Long, T.E. LORD Corporation (invited), Block Copolymer Design, April **2013**.